(NASA-CR-156123) UNSTEADY LOADS DUE TO PROPULSIVE LIFT CONFIGURATIONS. PART D: THE DEVELOPMENT OF AN EXPERIMENTAL FACILITY FOR THE INVESTIGATION OF SCALING EFFECTS ON PROPULSIVE LIFT CONFIGURATIONS (Virginia

N78-20070

G3/02

Unclas
11881

RESEARCH LABORATORIES FOR THE ENGINEERING SCIENCES

SCHOOL OF ENGINEERING AND APPLIED SCIENCE

University of Virginia

Charlottesville, Virginia 22901

Technical Report

UNSTEADY LOADS DUE TO PROPULSIVE LIFT CONFIGURATIONS PART D - THE DEVELOPMENT OF AN EXPERIMENTAL FACILITY FOR THE INVESTIGATION OF SCALING EFFECTS ON PROPULSIVE LIFT CONFIGURATIONS

Submitted to:

NASA Scientific and Technical Information Facility
P. O. Box 8757
Baltimore/Washington International Airport
Maryland 21240

Submitted by:

J. K. Haviland
Professor

William W. Herling

Report No. UVA/528095/MAE78/114

March 1978

RESEARCH LABORATORIES FOR THE ENGINEERING SCIENCES

Members of the faculty who teach at the undergraduate and graduate levels and a number of professional engineers and scientists whose primary activity is research generate and conduct the investigations that make up the school's research program. The School of Engineering and Applied Science of the University of Virginia believes that research goes hand in hand with teaching. Early in the development of its graduate training program, the School recognized that men and women engaged in research should be as free as possible of the administrative duties involved in sponsored research. In 1959, therefore, the Research Laboratories for the Engineering Sciences (RLES) was established and assigned the administrative responsibility for such research within the School.

The director of RLES—himself a faculty member and researcher—maintains familiarity with the support requirements of the research under way. He is aided by an Academic Advisory Committee made up of a faculty representative from each academic department of the School. This Committee serves to inform RLES of the needs and perspectives of the research program.

In addition to administrative support, RLES is charged with providing certain technical assistance. Because it is not practical for each department to become self-sufficient in all phases of the supporting technology essential to present-day research, RLES makes services available through the following support groups: Machine Shop, Instrumentation, Facilities Services, Publications (including photographic facilities), and Computer Terminal Maintenance.

Technical Report

UNSTEADY LOADS DUE TO PROPULSIVE LIFT CONFIGURATIONS PART D - THE DEVELOPMENT OF AN EXPERIMENTAL FACILITY FOR THE INVESTIGATION OF SCALING EFFECTS ON PROPULSIVE LIFT CONFIGURATIONS

Submitted to:

NASA Scientific and Technical Information Facility
P. O. Box 8757
Baltimore/Washington International Airport
Maryland 21240

Submitted by:

J. K. Haviland
Professor

William W. Herling

Department of Mechanical and Aerospace Engineering
RESEARCH LABORATORIES FOR THE ENGINEERING SCIENCES
SCHOOL OF ENGINEERING AND APPLIED SCIENCE
UNIVERSITY OF VIRIGINIA
CHARLOTTESVILLE, VIRGINIA

Report No. UVA/528095/MAE78/114 Copy No. ____

March 1978

ABSTRACT

The design and construction of an experimental facility for the investigation of scaling effects in propulsive lift configurations is described. The facility was modeled after an existing full size facility at NASA - Langley which consisted of a coaxial turbofan jet engine with a rectangular nozzle in a blown surface configuration. The flow field of the model facility was examined with and without a simulated wing surface in place at several locations downstream of the nozzle exit plane.

Emphasis was placed on obtaining pressure measurements which were made with static probes and surface pressure ports connected via plastic tubing to condenser microphones for fluctuating measurements. The microphone signals were processed to obtain rms levels, frequency spectra, and auto- and cross-correlations. The auto- and cross-correlations were additionally processed by computer computations utilizing a Fast Fourier Transform algorithm to obtain power spectral densities, phase lags, and coherences of the pressure signals. Several pressure spectra were compared with those obtained from the NASA facility, and were used in a preliminary evaluation of scaling laws.

TABLE OF CONTENTS

LIST OF FIGURES

LIST OF FIGURES (continued)

LIST OF FIGURES (continued)

LIST OF TABLES

LIST OF SYMBOLS

A	Area
B	Bypass ratio
$B.W.$	Third octave bandwidth
d	Dimension
d_{eff}	Effective nozzle diameter
d_{equiv}	Equivalent nozzle diameter
d_h	Hydraulic diameter
D	Circular nozzle diameter
f	Frequency
H	Total head
M	Mach number
P	Nozzle perimeter
P_2	Average static pressure
P_{rms}	Rms static pressure
q	Dynamic pressure
R_{11}, R_{22}	Auto - correlation functions of rms static pressure
R_{12}	Cross - correlation function of rms static pressure
S_t	Strouhal number
T	Static temperature
U,V	Average velocities
U_c	Convection velocity

LIST OF SYMBOLS (continued)

U_j	Jet exit velocity
x, y, z	Position coordinates
θ	Lateral probe adjustment angle
λ	Vortex spacing
ρ	Density
ρ_{12}	Rms static pressure cross - correlation coefficient
ϕ	Vertical probe adjustment angle
ω	Phase lag

Chapter 1 Introduction

Recent interest in providing jet aircraft with STOL (short takeoff or landing) capabilities has generated research into the nature of jet flows and of their interaction with bounding surfaces. In particular, interest has been strong in two configurations which provide STOL capabilities known as upper surface blown and externally blown flaps. Each of these configurations generates propulsive lift (as opposed to lift due to the forward motion of the vehicle) through the interaction of the engine exhaust flow and a wing-flap combination. The blown surface configuration has the engines mounted atop of the wing with the exhaust directed over the wing surface by "D" shaped nozzles, which spread the flow over a larger area of the wing surface than is obtained with more conventional circular nozzles. On the other hand, in externally blown flap configuration where the engines are hung under the wing the engine exhaust impinges directly on the flap which deflects the flow down.

The nature of the turbulent exhaust flow and of the resulting dynamic loads on airfoil surfaces is relatively unknown. Consequently, flap hinges on these type aircraft would have to be designed with a large safety margin to accommodate large fluctuating loads. In order for these aircraft to operate efficiently and economically their weight must be kept to a minimum. To accomplish this task it is necessary to be able to predict accurately structural loads due to propulsive lift configurations.

The pressure loads experienced by the wing-flap surface are the results of a combination of steady and fluctuating pressures. Methods for predicting steady loads are relatively well developed and will not be discussed in this paper. Several approaches are being taken in the development of prediction capabilities to deal with fluctuating

loads. These range from full scale testing of aircraft to cold, model jets scaled to a full size configuration. Investigations using scaled flows have included circular, rectangular, and "D" shaped nozzles.

Through NASA funding, a facility was developed at the University of Virginia to study fluctuating loads which dealt exclusively with a rectangular nozzle in an upper surface blown configuration. This facility is a one-quarter scale model of a test configuration at the NASA Langley Research Center. The scale facility, like its NASA counterpart, is easily adapted to both different nozzle shapes and different engine-wing-flap arrangements. However, whereas the NASA facility uses a turbofan jet engine, the scale facility uses room temperature air at a maximum of 670 Pa (5 mmHg) total head.

It is the goal of the research project under which the facility was developed to demonstrate scaling laws for propulsive lift configurations, and thus to enable accurate prediction of fluctuating pressure loads. The project was initiated in January 1974, with earlier work concentrating on circular jets and development of instrumentation.

This thesis will present a summary of relevant literature concerning coherent structures and associated scaling laws in circular jets. This will include a brief discussion of rectangular jets. The development of the scale facility will be described in detail. Results of a preliminary survey of the flow field and a limited number of comparisons with data from the NASA facility (the 'beach' facility) will be presented.

Chapter 2 Background

A detailed review of the literature on circular jets will not be presented in this paper. The interested reader is referred to work done by Schroeder (ref. 1) and Catalano (ref. 2) where ample background on circular jets is provided. Each of these works contains an extensive bibliogrpphy on circular jets. Interest in the circular jet, so far as this paper is concerned arises from flow mechanisms that have been found in circular jets which may be common to those in rectangular jets. With this in mind a brief review of circular jet theory follows.

As regards the work done by the author the primary concern with circular jets has been with the nature of pressure fluctuations within the first few nozzle diameters of the exit plane. It is within this region that airfoil surfaces typical of jet STOL aircraft would be placed. There is much evidence that, within this region, the pressure or velocity fluctuations are in a large part due to the presence of coherent turbulence structures (ref. 3-5). These coherent structures are the basis of the vortex model of a circular jet which is depicted in Figure 2.1. In this model, vortices are believed to result from roll-up of the vortex tube which is extruded from the lip of the nozzle. It is the convection of these vortices that is responsible for producing the Strouhal number (fD/U) dependent spectra characteristic of circular jets. This Strouhal dependence is in the form of peaks in velocity and pressure spectra at a Strouhal number of between 0.3 to 0.5. In addition, auto and cross-correlation studies have indicated that the pressure field is influenced over a large area by the passage of the vortex rings. The implication is that a surface subjected to this type of flow might experience relatively severe fluctuating pressure loads with similar spectra.

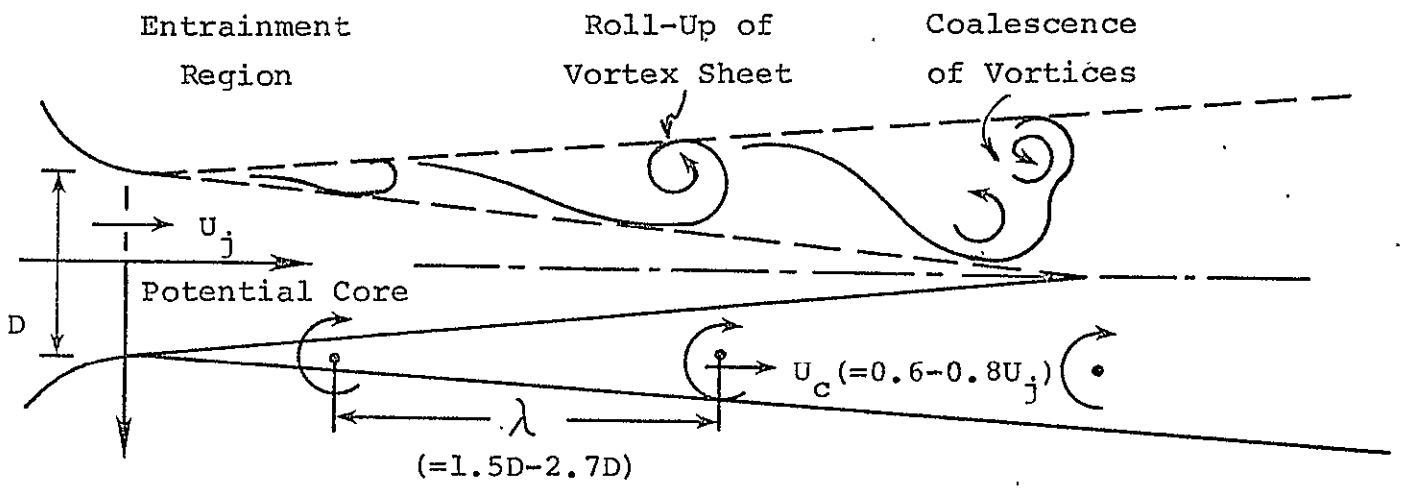

U_j = Jet Exit Velocity

U_c = Vortex Convection Velocity

Figure 2.1 Vortex Model of a Circular Jet

The evidence supporting the vortex model of a circular jet is sufficiently well documented to warrant serious consideration. The main point, however, is that frequency spectra determined at points early in the downstream development of a circular jet (within the first five diameters) are characterized by peaks which scale according to jet velocity and nozzle diameter.

The question arises then as to just how well do pressure spectra scale. As mentioned the spectra tend to peak according to Strouhal number. However, conflicting evidence exists as to exactly what Strouhal number is preferred. There appears to be a range of Strouhal numbers at which peaks will occur in the spectra depending on the particular equipment used to generate the jet. Crow and Champagne (ref. 5) did a detailed investigation of coherent structures in circular jets. Using an unheated jet operating at a Reynolds number of between 10^4-10^5 they observed two kinds of axisymmetric structure. These were small wavelength surface ripples on the vortex tube near the nozzle lip and larger "vortex puffs" which develop one to two diameters downstream. The former scale on the laminar boundary layer thickness leaving the nozzle lip while the latter scale on the diameter of the nozzle. Further investigation into the nature of the larger vortex structure was accomplished by introducing a pressure surge at controlled frequencies into the boundary conditions of the jet. This was accomplished by placing a loud speaker in the settling chamber of their apparatus. Response curves of the jet's reaction to this stimulus were determined by measuring the amplitudes of the velocity fluctuations along the jet axis relative to the values at the exit plane. They determined that for small excitations the response was linear but that a saturation point was reached where large increases in excitation pro-

duced little or no increase in response. They also found that the jet was most sensitive to excitation frequencies corresponding to a Strouhal number of 0.3. In addition an unforced jet will produce spectra that peak between Strouhal numbers of 0.3 to 0.5. The above findings not only explain some of the differences as to peak Strouhal number found in the literature but also have some important ramifications for scaling flows from turbofan engines. Spectral peaks in these flows may be the result of internal engine noise. Thus in order to produce accurately scaled flows it may be necessary to excite these flows with scaled internal noise spectra of the turbofan engine.

Further discussion of scaling laws for circular jets can be found in Schroeder's work (ref. 1). As mentioned earlier, however, the present thesis is concerned with rectangular nozzles in an upper surface blown configuration. At present it is uncertain as to how scaling laws from circular jets will apply to rectangular jets. Little work has been published on model rectangular or D-shaped jets in blown surface configurations. There has been some work done on large scale facilities where turbofan engines are in a static configuration set up for externally blown flaps and upper surface blowing (ref. 6-8) (such as NASA Langely's 'Beach' facility). There has been an indication that overall fluctuating pressure levels encountered in full scale jets vary slightly with Mach number. Mach number effects may present some difficulties in scaling model flows but as yet nothing definitive has been established.

In his work on far field jet noise, Stone (ref. 9) has suggested an effective diameter for rectangular nozzles for scaling noise spectra. This diameter is given by

$$d_{eff} = (d_{equiv})^{0.6} (d_h)^{0.4}$$

where d_{equiv} and d_h are given by

$$d_{equiv} = \sqrt{\frac{4A}{\pi}}$$

$$d_h = \frac{4A}{P}$$

where A and P are, respectively, the area and perimeter of the nozzle. The effective diameter as a scaling dimension for pressure spectra from the present study will be discussed in chapter 4.

Chapter 3 Development of the Experimental Facility

3.0 Design Process

As stated earlier, it is the goal of the present work to develop accurate scaling laws for pressure fluctuations encountered by wing and flap structures as the result of impingement of flow from the exhaust of a jet engine. Towards this end it was decided to construct a test facility capable of producing model flows in propulsive lift configurations. Beyond this requirement, it was also desired that the facility be as versatile as possible while remaining within the framework of the primary objective (i.e., provide the capability to study either blown flap or blown surface configurations with a choice of nozzle geometries).

Economic considerations dictated the use of locally available air supplies as well as much of the materials and construction techniques. Thus much of the design was fixed by the above requirements or restrictions. For example, the use of a heated air supply was ruled out for economic reasons. This left a choice between the laboratory's compressed air supply or some small unit centrifugal blowers that were available. The blowers were selected on the basis of their higher continuous flow rates and greater versatility than the compressed air supply.

One final criterion was established for the design. It was decided that the facility should be scaled geometrically to an existing facility at NASA Langley herein referred to as the "Beach" facility. The philosophy behind this decision was that a ready supply of data would be available from this full size facility with which to compare results from the model to be constructed.

3.0.1 Theoretical Predictions of Model and "Beach" Facility Performance

Dimensions and configuration of the "Beach" facility are presented in Figure 3.1 (ref. 8). This facility consists of a Pratt and Whitney JT15D-1 turbofan engine mounted in a static test stand. The engine is fitted with a rectangular outer or secondary nozzle 15.6 x 94.0 cm. The primary nozzle provided by the manufacturer was replaced with an elliptical nozzle. To simulate an upper surface blown arrangement a steel "boiler plate" airfoil is mounted above the engine to represent a wing flap surface.

Information on the performance parameters of the JT15D-1 engine was limited. The limited amount of data available on the exit plane conditions was used with isentropic relations to determine other parameters of interest such as velocity and mass flow ratios at the exit plane of primary and secondary nozzles. This method provided a rough approximation of full scale flow conditions to which possible model flow conditions were compared, the object being to determine what flow quantities in the "Beach" facility could be scaled by the model.

The major assumptions used in the analysis of the full scale flow were: no mixing between core and bypass flow; densities same as air (density variations due to unburnt fuel and products of combustion were ignored); and, as mentioned above, isentropic flow. These assumptions were judged to be consistent with the degree of accuracy needed for the initial design study. Data from reference 8 was used to estimate average velocity of core and bypass air in the exit plane of the secondary nozzle. This data has been reproduced in Figure 3.2. The values used were as follows:

average core velocity, V_3=424 m/s
average bypass velocity, V_3'=280 m/s,

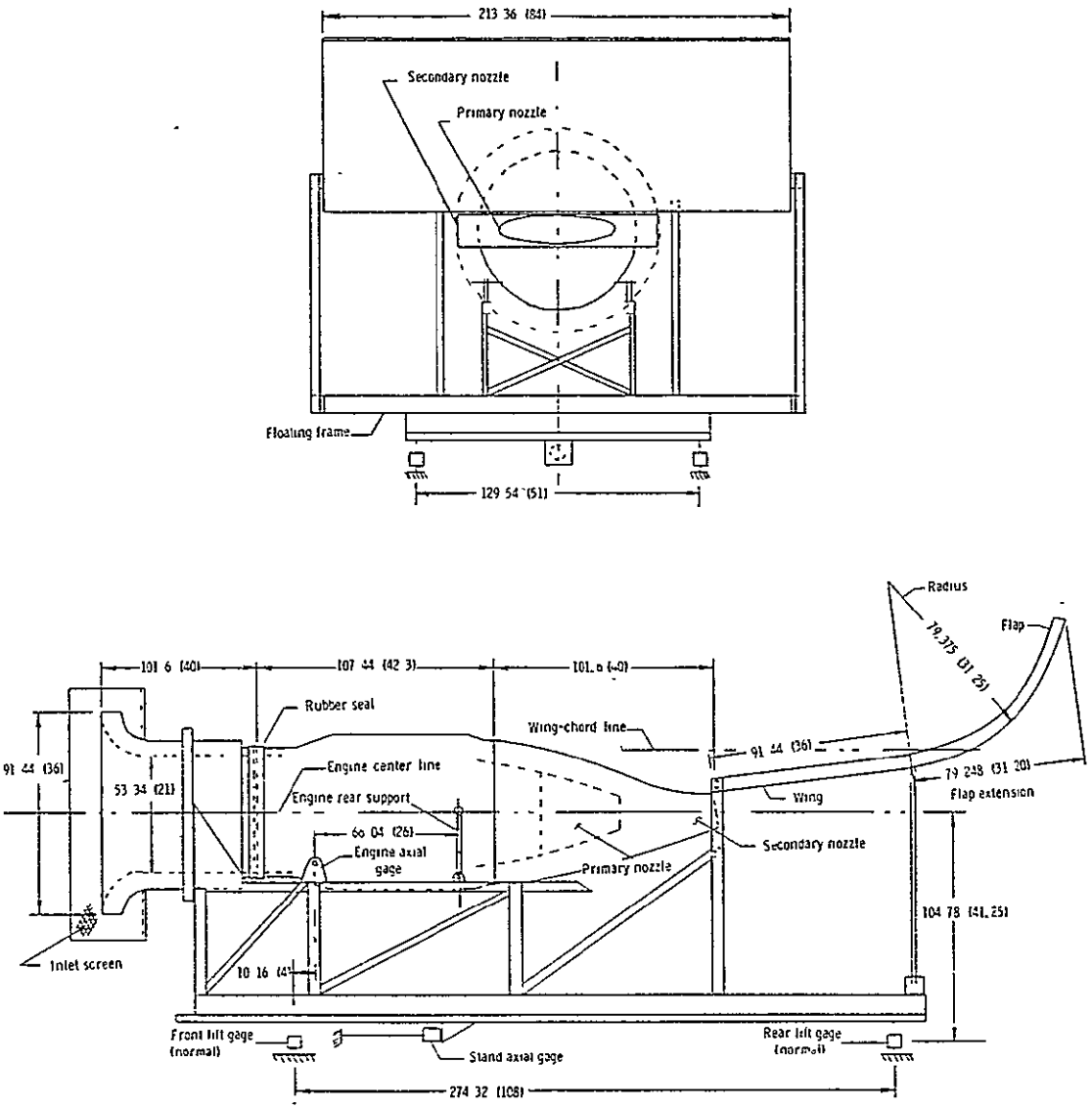

Dimensions in Centimeters (Inches)

Figure 3.1 NASA "Beach" Facility

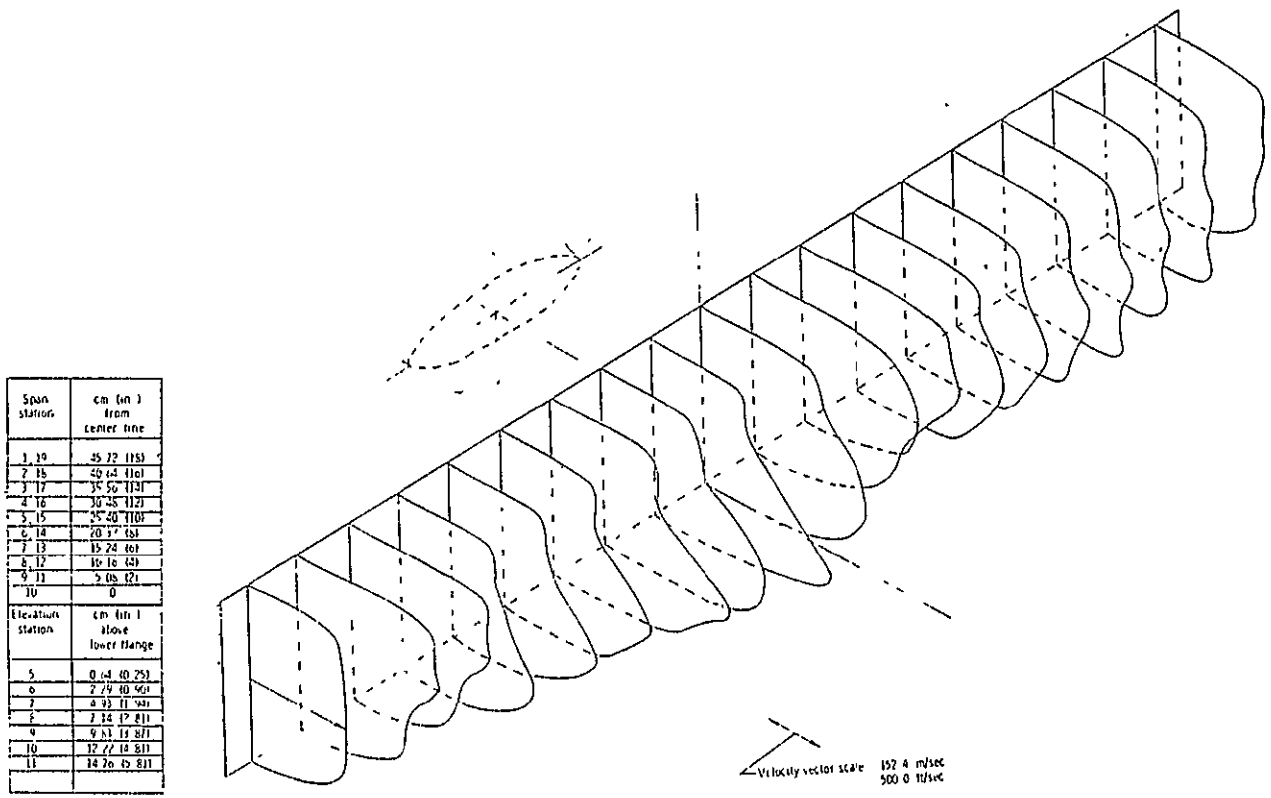

Figure 3.2 Velocity Profiles - Secondary Nozzle Exit Plane - NASA "Beach" Facility

where the prime indicates bypass conditions.

Using the known values of bypass to primary exit area ratio (A_2'/A_2=1.29) total area of the secondary exit plane (A_{3T}=0.148 m^2), bypass ratio (B=3.34), and an assumed value for the temperature of bypass air (T_3'=21.1 C=294.1 K), the remaining parameters of interest were determined via an iteration procedure using the isentropic gas tables. The parameters of interest were velocity ratios (core:bypass) at the primary exit plane (V_2/V_2') and at the secondary exit plane (V_3/V_3'), volume flow rate ratio at the primary exit plane ($V_2'A_2'/V_2A_2$), Mach numbers at the exit plane, and dynamic pressure ratio at the secondary exit plane (q_3/q_3'). All of these ratios would be scaled in a hot jet facility, however, this is impossible when core air is drawn from a cold plenum chamber.

As of this writing it is not known which if any of the above quantities is most essential to provide the most accurate scaling of pressure fluctuations. However, it is clear that, if perfect mixing could be obtained in full scale engines, achievement of these ratios would be unimportant. It was also obvious from the beginning that it would be impractical to achieve Mach numbers or Reynolds numbers in the model equivalent to those in the "Beach" facility.

For the purposes of the initial design study, analysis was to be based on a 1/4 scale coaxial model. The initial choice of the scale was somewhat arbitrary. However, the results of the analysis indicated that reasonable velocities could be obtained with a 1/4 scale configuration, so this was chosen as the scale to be used.

The analysis of the model was based on the assumption of no mixing of core and by pass air and was accomplished with the use of the incompressible continuity and Bernoulli

equations. The relations used are as follows

$$H_1 = \tfrac{1}{2}\rho V_2^2 + P_2 = \tfrac{1}{2}\rho V_3^2$$
$$H_1' = \tfrac{1}{2}\rho V_2'^2 + P_2 = \tfrac{1}{2}\rho V_3'^2$$

$$P_2 = P_2$$

no mixing: $$V_2 A_2 = V_3 A_3$$
$$V_2' A_2' = V_3' A_3'$$

where the subscript indicates the station number (Figure 3.3 is a side view of the initial design) and the prime denotes bypass conditions. The velocity ratio in the exit plane of the secondary nozzle, V_3/V_3', was fixed at 1.51 (same as the full scale) and a total head, H_1, was selected that was well within the operating range of the blowers (H_1 = 746 Pa). The results of this and the full scale analysis are presented in Table 1. These ratios, other than the exit velocity ratios, do not scale because of temperature differences between the two flows.

It is possible to achieve some variation in the ratios given in Table 1 by changing the exit area of the core nozzle from the true scale value. A kinematic scaling would then be possible whereby velocity ratios in the exit plane and volume flow rates would scale. It is believed this would correctly scale convection velocities and Strouhal numbers of vortices. Alternatively, a dynamic scaling could be achieved by scaling dynamic pressures and mass flow ratios while sacrificing kinematic scaling. Thus a cold model facility is capable of simulating only two of the full scale ratios at a time. In light of this, it was decided to provide a true geometric scaling of both primary (core) and secondary (bypass) nozzles for the initial facility.

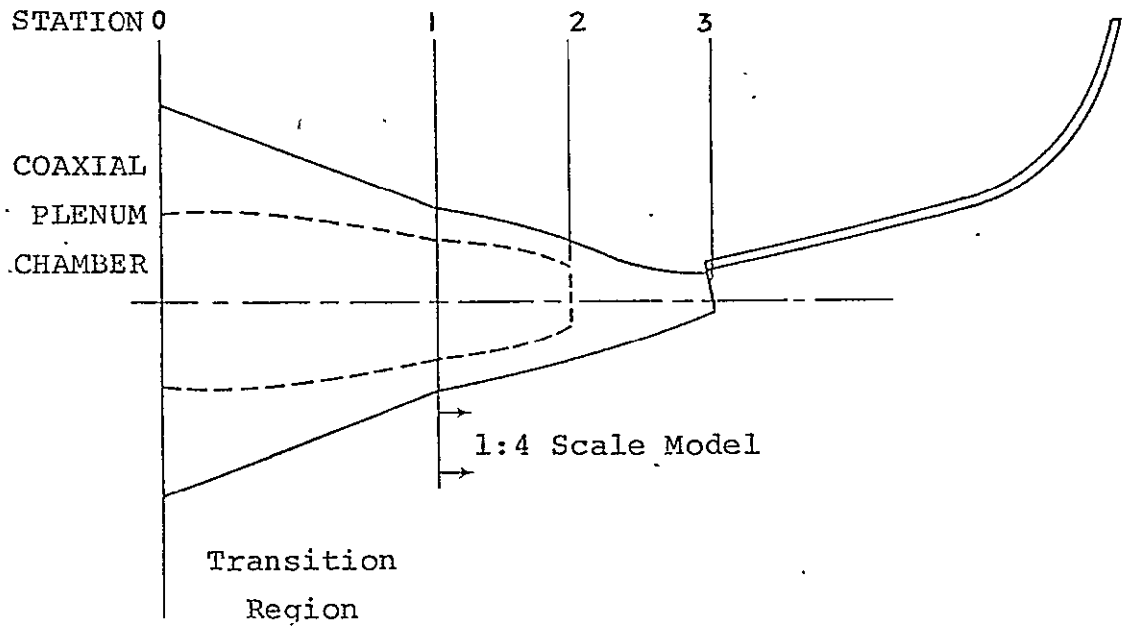

Figure 3.3 Initial Design Study Configuration

TABLE 3.1

Characteristics of a Scaled Nozzle Design

	V_2/V_2'	V_3/V_3'	$V_2'A_2'/V_2A_2$	M_3	M_3'	q_3/q_3'
Full Scale Engine	2.33	1.51	1.86	0.91	0.81	1.26
1/4 Scale Model	2.81	1.51	1.52	0.10	0.068	2.28

Prime Indicates Bypass Air

Unprimed Indicates Core Air

3.1 Description of the Experimental Facility

The model consists of a 1:4 scale of the sections aft of the fan casing of a JT15D-1 turbofan engine as modified for NASA Langley's "Beach" facility. Figures 3.4 and 3.5 represent the inside contours of the primary and secondary nozzles with the dimensions being those of the model. However, to date no measurements have been made with the primary nozzle installed. Contours of the primary nozzle have been included for completeness. A decision was reached to postpone installation of the primary nozzle until an evaluation of the effectiveness of secondary nozzle flow as a scaled flow could be completed. Chapter four is a presentation of the initial phase of that evaluation. The remainder of this paper will be concerned with the facility set up with the secondary nozzle only.

The secondary nozzle was connected to an aluminum plenum chamber via an adjustment cone contoured for smooth transition into the secondary nozzle (see Figure 3.5). The nozzles and adjustment cone were constructed of fiberglass on wooden molds which were made by glueing sections together that were roughly the shape of the cross section of the nozzle, and then sanding them to the desired contour. The wood was then treated with a wood sealer, wax, and mold release after which the fiberglass was laid up on the mold. Due to asymmetries in the primary and secondary nozzles, the fiberglass could not be removed from the mold in one piece. Therefore, metal fins were inserted into the secondary nozzle mold which allowed the fiberglass to be removed in two pieces while fiberglass was removed from the primary nozzle mold by cutting the nozzle into two halves. After removal from the mold, inside surfaces of the nozzle and adjustment cone were sanded smooth and painted. Figure 3.6 shows photographs of the secondary nozzle and adjustment

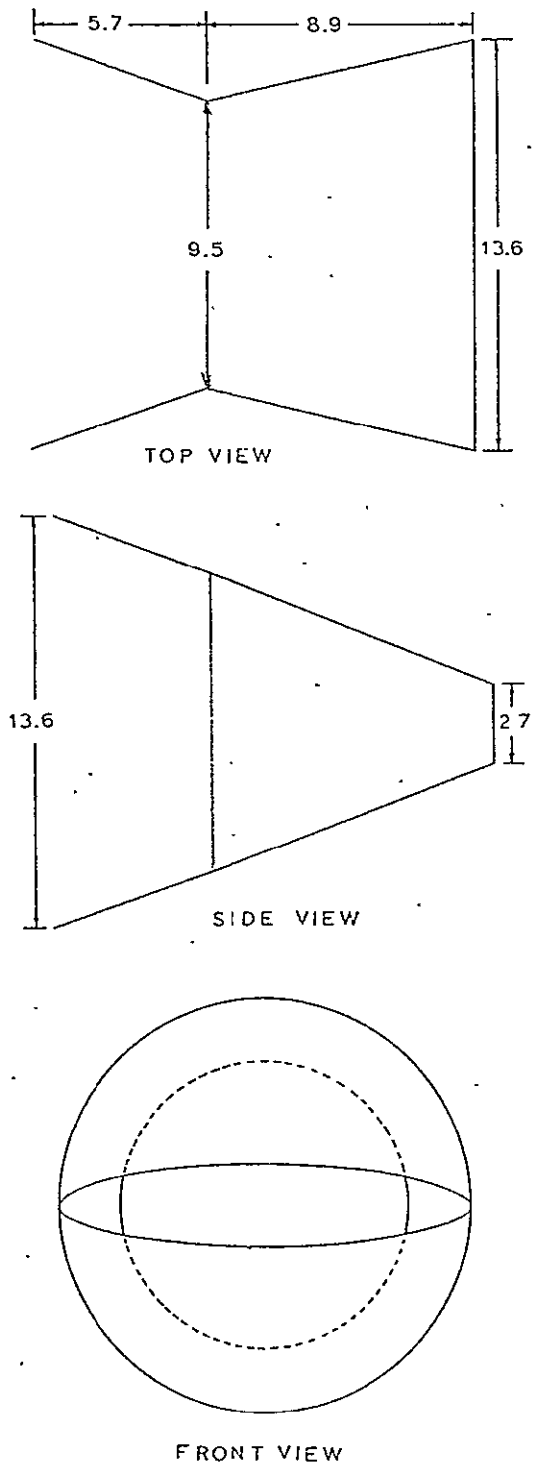

Figure 3.4 Primary Nozzle - Dimensions in Centimeters

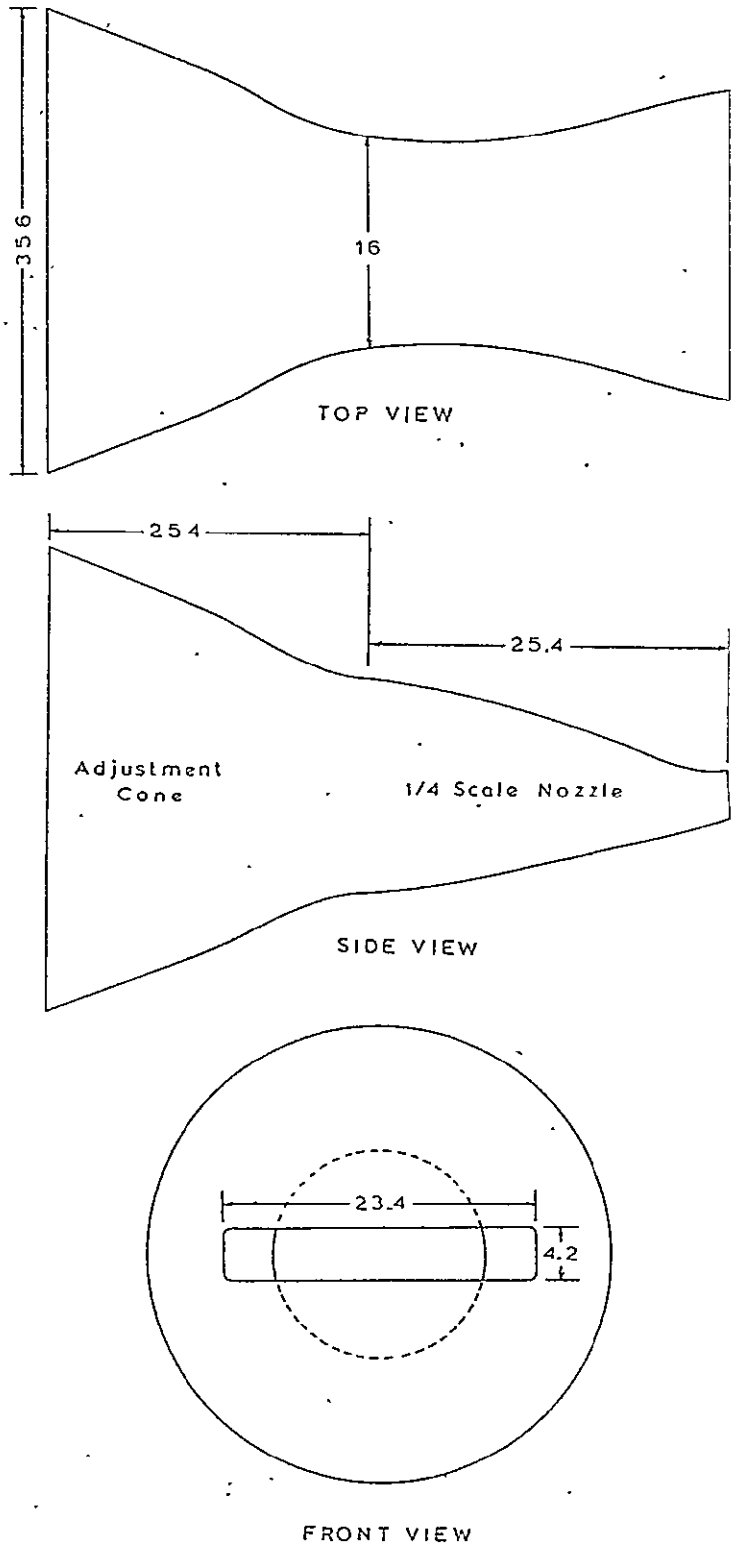

Figure 3.5 Secondary Nozzle and Adjustment Cone - Dimensions in Centimeters

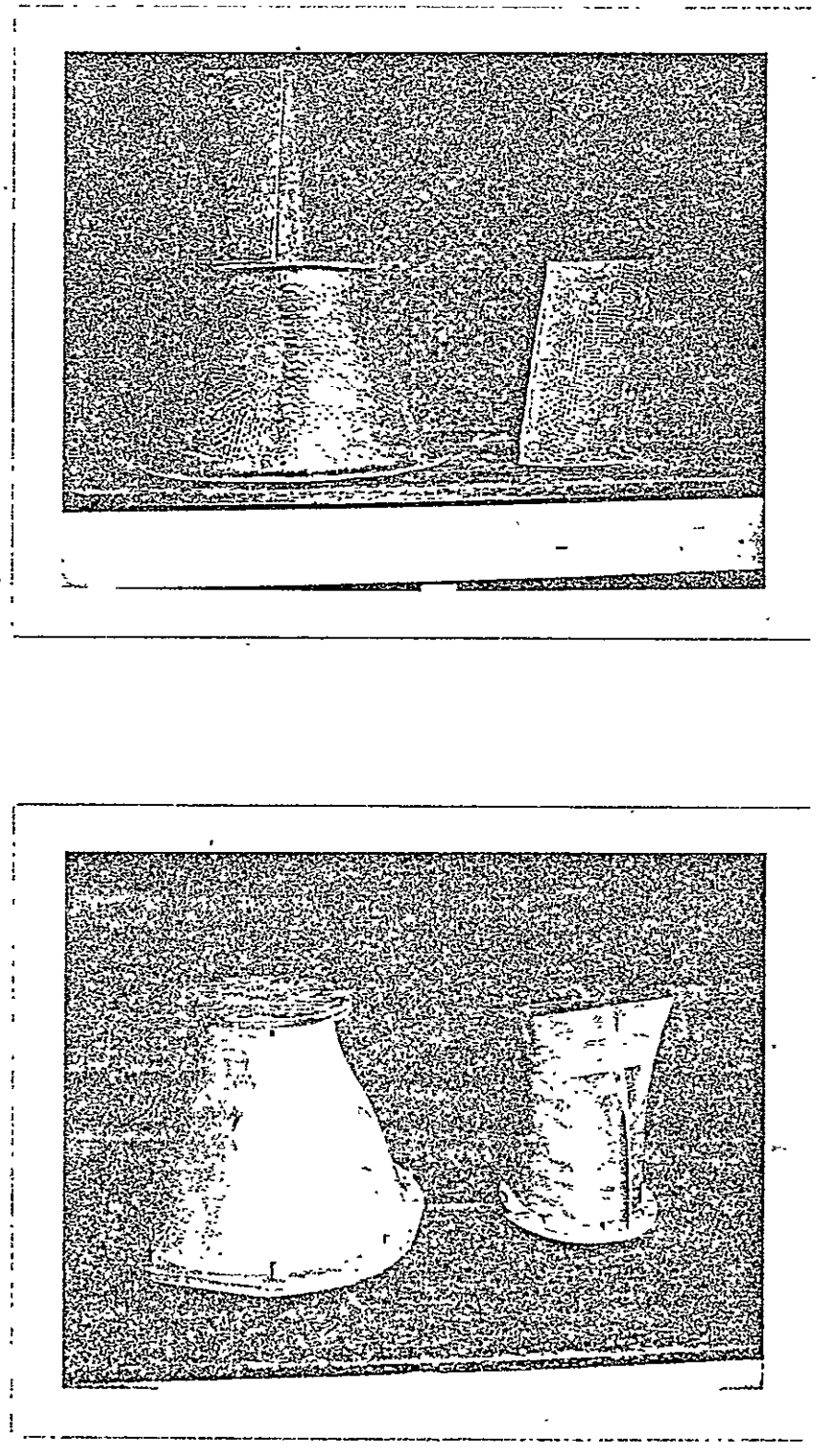

Figure 3.6 Secondary Nozzle and Adjustment Cone and Molds

cone under construction together with the molds used.

The plenum chamber was 38.1 cm (15 in.) by 38.1 cm (15 in.) by 50.8 cm (20 in.). Flow straightening was provided by a simulated honeycomb made of soda straws packed tight along the axis of the facility. Wire screens were placed on both ends of the soda straws for turbulence reduction. Two Rototron centrifugal blowers were mounted at the rear and side of the chamber. The entire structure was supported by a steel and plywood table which was mounted on a 3.65 m (12 ft.) lathe bed. Figure 3.7 is a layout drawing of the original configuration of the experimental facility. This configuration was later modified (see section 3.3 Muffler Design). However, the majority of the measurements were made on the facility as it is shown in Figure 3.7. A removable wing section (Figure 3.8) completes the simulation of the "Beach" facility. The wing is made of mahogany sections glued together and sanded to form a smooth surface.

3.2 Instrumentation and Data Analysis Capabilities

With minor exceptions instrumentation and data analysis techniques used in this work were identical to those used by Schroeder (ref. 1). A detailed description of the computer analyses used has been provided by Schroeder and will not be repeated here. Briefly, two basic types of spectral analyses were used. The first was a third octave analysis of pressure signals provided by a B & K 2113 Audio Frequency Spectrometer. Alternatively, power spectral densities were obtained via Fourier transforms of auto-correlations. Auto-correlations (and cross-correlations) were obtained from a Federal Scientific Model UC202-B Ubiquitous Correlator whose digital output is linked to a teletype, and thence via telephone to a CDC 6400 computer. Alternatively, paper tapes

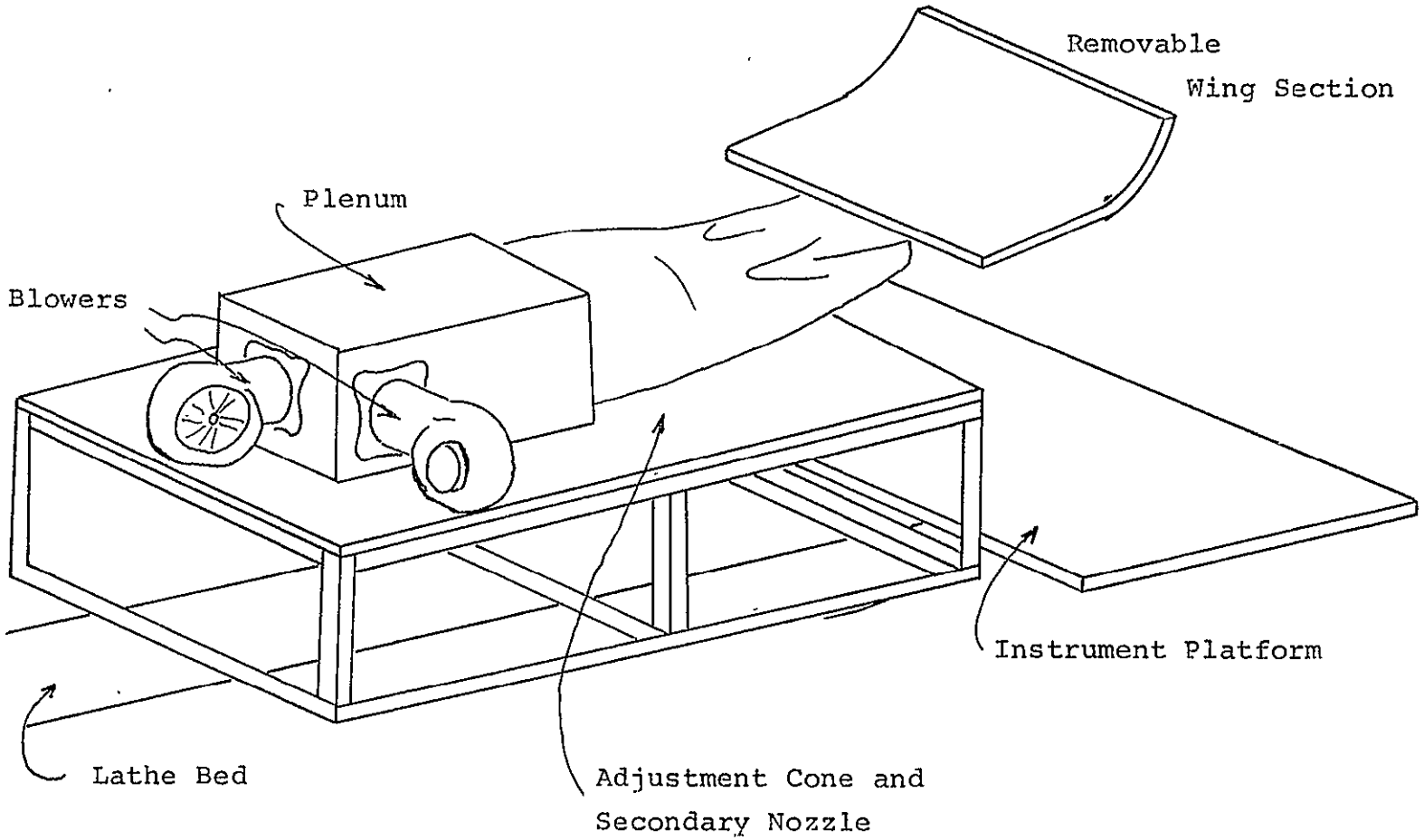

Figure 3.7 The Initial Facility

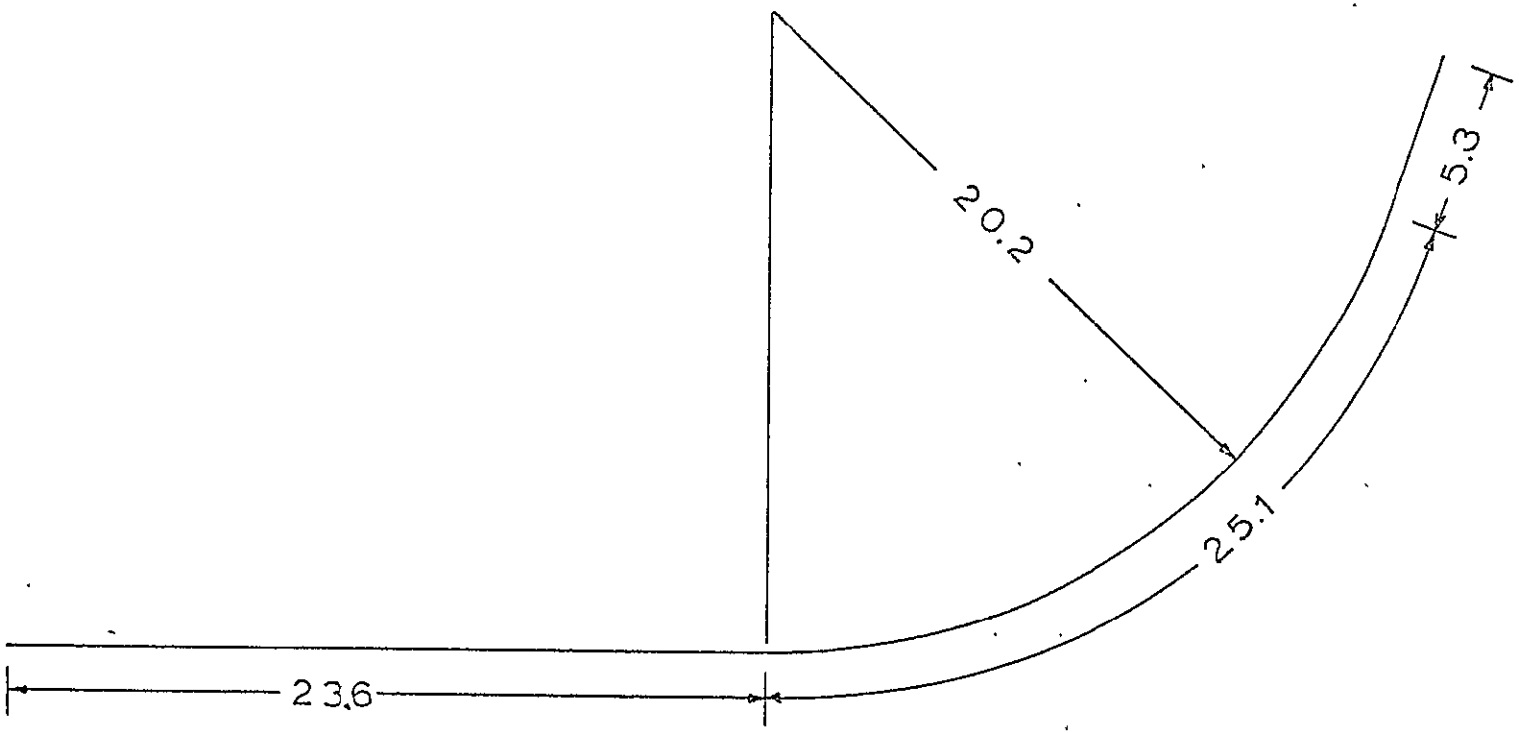

Figure 3.8 Wing-Flap Contour - Dimensions in Centimeters

are made for later analysis on the CDC. The computer was programmed using an FFT algorithm to provide power spectral densities and, from these, phase, coherence, and transfer functions from the cross-correlations. All spectral quantities (pressure fluctuations) are presented in decibel notation referenced to the dynamic pressure, q_j, at the exit. Coherence, which is similar to correlation but is frequency dependent, is plotted in dB where 0 dB corresponds to a perfect coherence of one. The transfer function amplitude is defined as one half the difference in decibels between two power spectral densities determined by different probes, the phase angle is the same as that of the cross-spectrum, while the coherence is the difference between twice the cross-spectrum and the sum of the two auto-spectra, also in decibels.

3.2.1 Pressure Sensor System

Pressures were monitored in the flow and on the wing surface with a variety of probes. Pressure fluctuations were transferred from the probes via 1/8 inch I.D. plastic tubing to 1/8 inch B&K Type 4148 condensor microphones powered by B&K Type 2619 Preamplifiers. Probe configurations used are divided into two major classifications: free probes and surface probes. Schroeder (ref. 1) devoted a large portion of his work to identifying transfer functions of the probes and developing an analytic expression for these transfer functions. The more important points of his work will be presented at appropriate points later in this work.

Free Probes

Two configurations of free probes, a total and static version, were used in this work. Both were constructed of

stainless steel tubing with dimensions as shown in Figure 3.9. The total probe was used only for average measurements and was found to be quite reliable for this type of measurement. The static probe used was studied by Schroeder (ref. 1) who met with limited success in determining the frequency response of this probe. His work indicated that significant attenuation of the signal did occur especially at the higher frequencies.

Schroeder's efforts were extended by the author in an attempt to develop at least a rough approximation of the probe frequency response. Two methods were used to accomplish this task. The first consisted of placing a static probe with 3.0 meters of plastic tubing next to a microphone in the exit plane of the facility. Pink noise was then introduced into the plenum chamber through a loudspeaker attached to the side. The resultant transfer function of the two signals which is shown in Figure 3.10 was due to the effects of the static probe and tubing. The erratic nature of this plot was due to the limitation in dynamic range of the correlator. The correlator is capable of following differences in signal amplitude of no greater than 27 dB. When signals exceed this difference, the output from the system is meaningless. In this particular situation this occurred at sporadic frequency points as a result of resonances in the plenum chamber-nozzle cavity. Consequently, this method was unreliable at a number of frequencies. To compensate for this the frequency response was determined for third octave bands where an average of the transfer function was determined for each band. For the lower frequencies where the third octave band widths are of the order of the frequency interval obtained in the PSD analyses, an alternate method was used where; instead of pink noise, pure tones from an audio signal generator

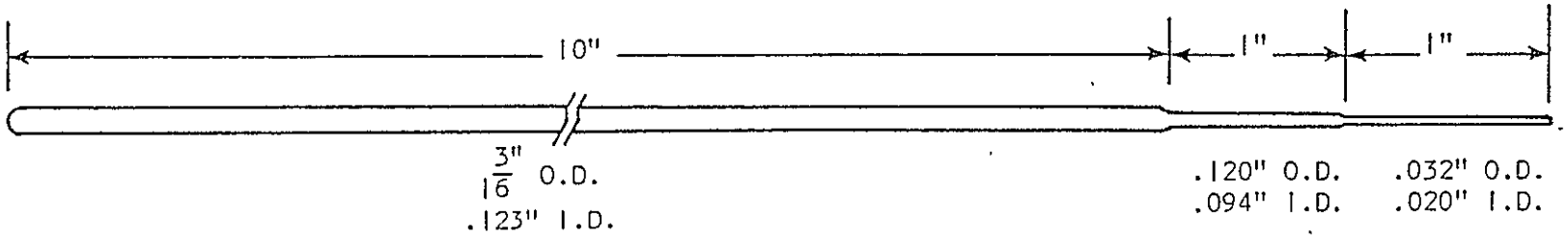

Total Pressure Probe

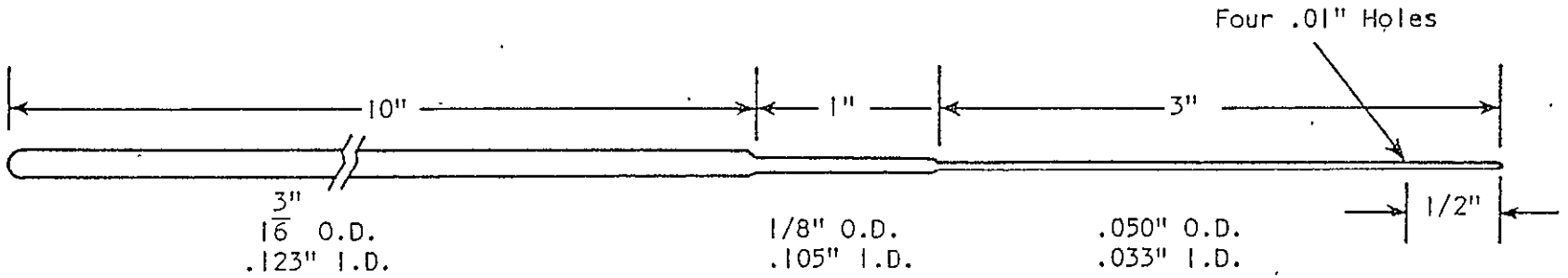

Static Pressure Probe

Figure 3.9 Pressure Probes

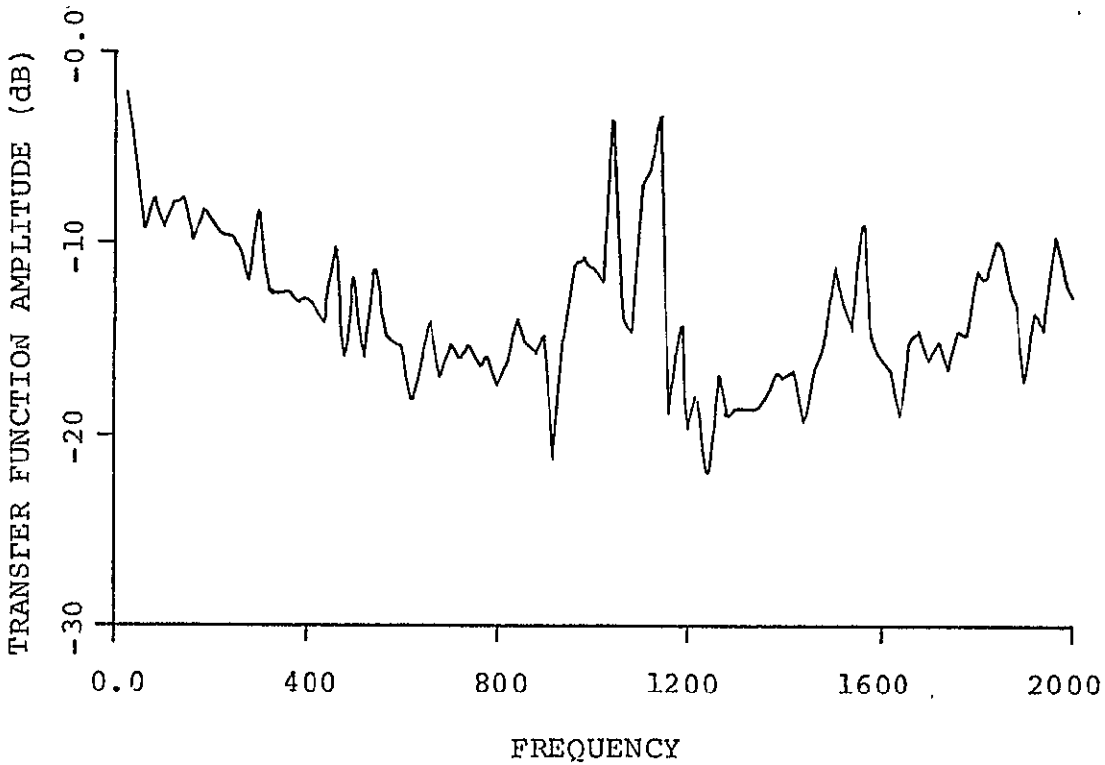

Figure 3.10 Transfer Function of Static Probe with Pink Noise

were used to drive the speaker in the plenum chamber. The response of the static probe was then compared to an adjacent microphone using a Mechanalysis Real Time Spectrum Analyzer at 10 Hertz intervals. The results of this low frequency calibration were compared with those obtained with the pink noise and are presented in Figure 3.11. The combination of these two methods enabled a first approximation of a correction curve for third octave spectra to be obtained which has been presented in Figure 3.12.

The frequency response of the probes was of interest only when single point measurements were being made. When two point measurements were made (i.e., cross-correlations), the frequency response of each probe was of little consequence provided the geometrical configuration of the two probes were adequately matched. That this was the case can be seen from Figure 3.13 which is the transfer function of two static probes at equal axial positions but separated by a small lateral distance (0.5 cm). Their position in the flow was such that convecting flow disturbances would reach each probe simultaneously which, if the probes were matched, would produce a transfer function that was a constant 0.0 dB.

However, failure to reproduce the transfer function of the static probes more accurately prompted the design of a new static probe which, at the time of this writing, is in an initial state of development with only preliminary results available. In this design, shown in Figure 3.14, the plastic tubing is eliminated by threading the inside of the end of the probe to be compatible with the 1/8 inch microphone. The response check made for the original probe with the Real Time Analyser was repeated for this new design and is presented in Figure 3.15. As can be seen this probe has a superior response as compared to the

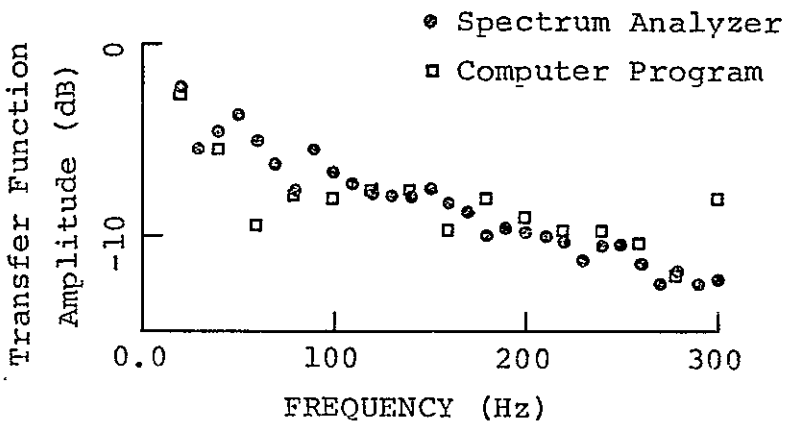

Figure 3.11 Static Probe Calibration Comparison

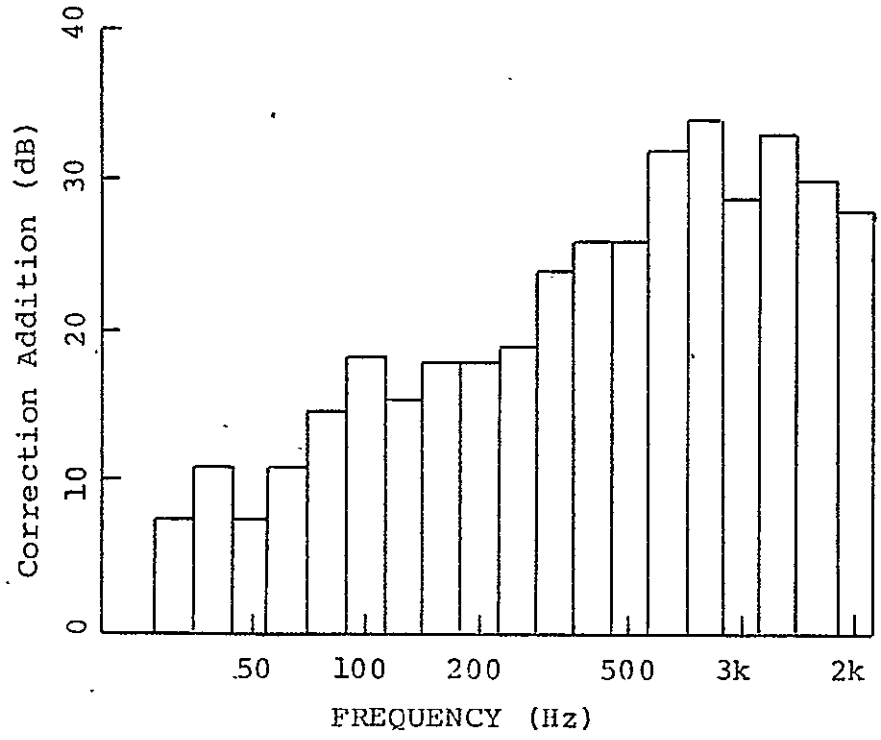

Figure 3.12 Static Probe Correction Curve

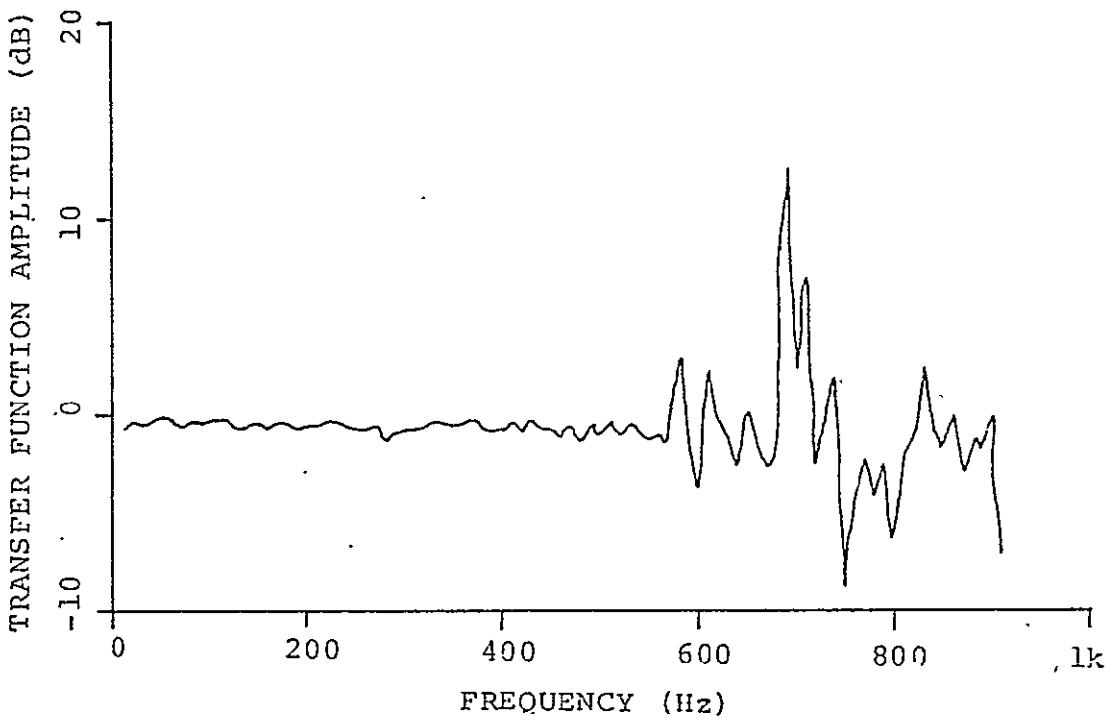

Figure 3.13 Transfer Function Between Matched Static Probes at Equal Downstream Locations

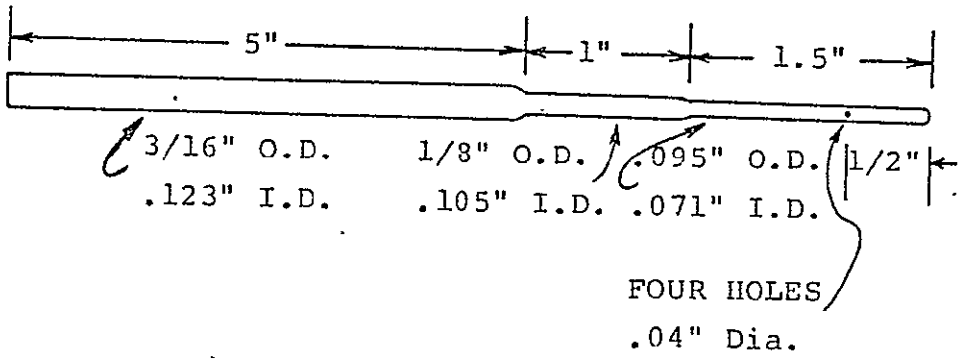

Figure 3.14 New Static Probe Dimensions

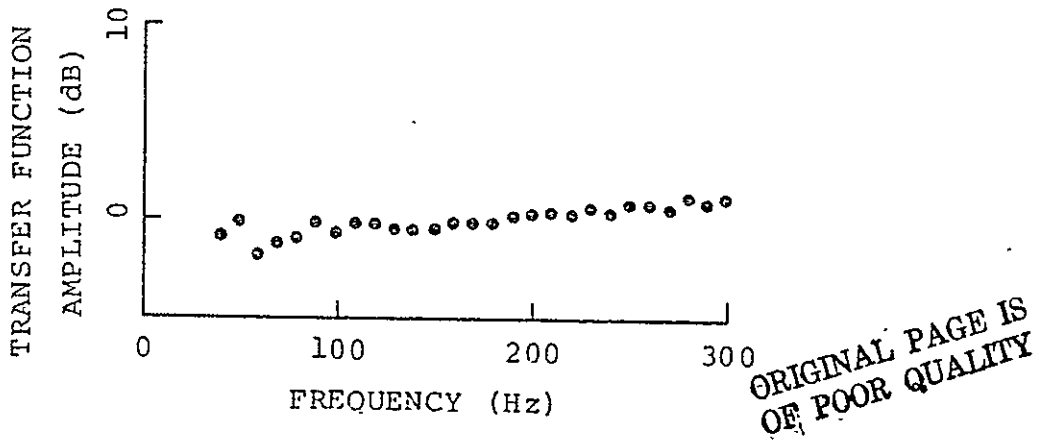

Figure 3.15 New Static Probe Transfer Function

original. However, when this probe is placed in a flow a noticeable "ringing" results. This was attributed to the adaptor on the microphone which provides a transition from the 1/8 inch diameter of the microphone to the 1/2 inch diameter of the preamplifier. The adaptor was known to be sensitive to vibrations, and it was felt that the "ringing" was caused by external excitation of the adaptor by the flow. Despite this drawback this probe is promising. Probes of similar configuration have appeared in the literature and seem to have been used successfully.

A final comment on the free probes is to indicate that their intended use was never that of a precision pressure sensor. They were meant to provide a rough approximation of pressure phenomenon in the flow field in so far as it may relate to pressure fluctuations experienced by surfaces subjected to that flow. Frequency response corrections and the degree of duplication achieved in probe configuration allows for reasonable indications of pressure spectra from single point measurements and phase and coherence from two point measurements in the flow field. In terms of developing scaling laws for fluctuations experienced by wing surfaces, it becomes difficult to justify an extensive development of free probes; and therefore, studies of the probes themselves were given a lower priority. Consequently, discussions as to the validity of static pressure measurements in turbulent flows have been omitted but can be found in several references (ref. 10-12).

Surface Probe

In order to measure the pressure fluctuations on the model wing surface aluminum pressure ports were inserted in the wing flush with the surface as shown in Figure 3.16. Connection to the microphone was made with 1 cm of plastic

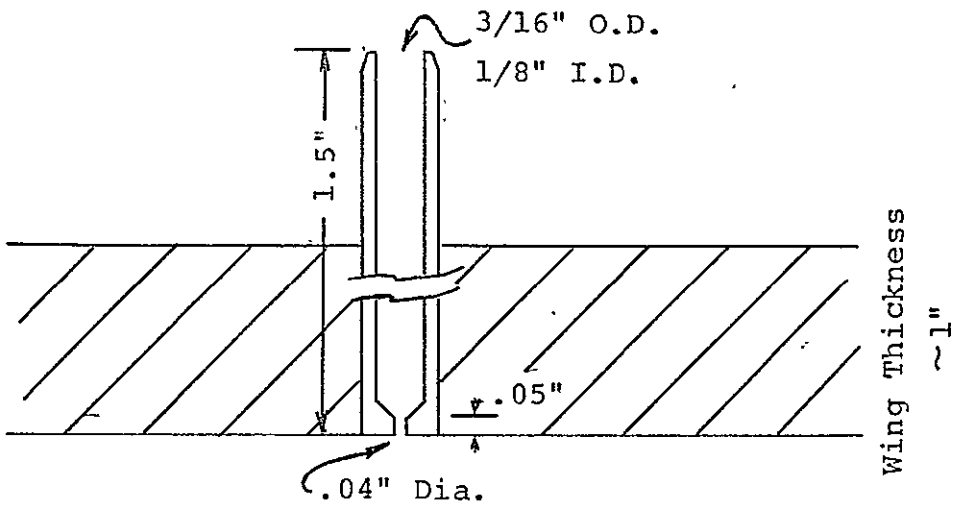

Figure 3.16 Surface Probe Configuration

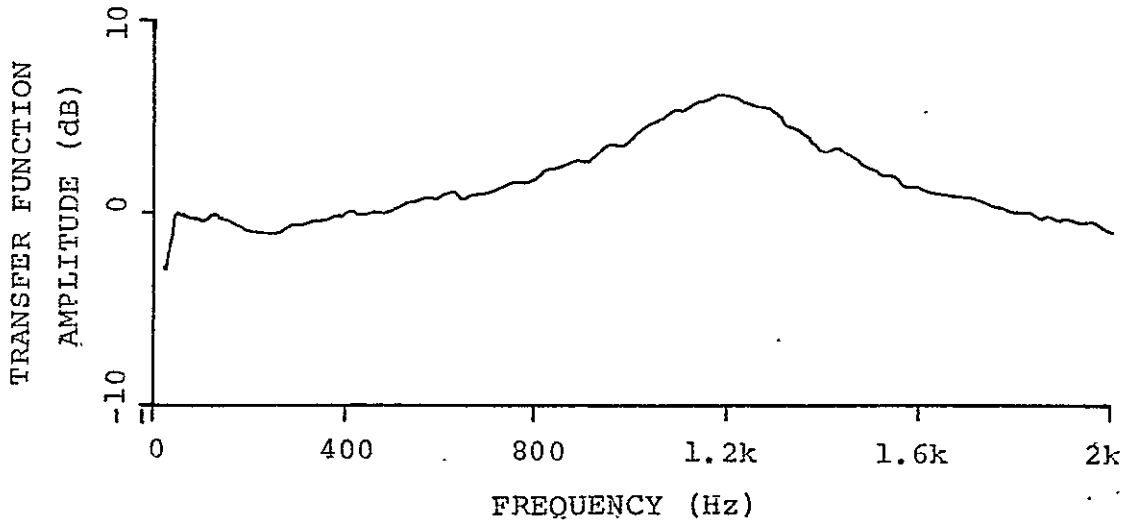

Figure 3.17 Surface Probe Transfer Function

tubing. Results reported by Schroeder (ref. 1) were used to select the diameter of the orifice, with selection guided by a desire to keep the size of this orifice as small as possible but large enough to prevent attenuation of the signal. The smaller the orifice, the better the resolution is; and, as reported by Willmarth and Roos, (ref. 13) minimizing the size of the orifice reduces error in the measured power spectrum. They reported that for a transducer of 1.6 mm diameter an error of 4.5% occurred in the rms pressure level. The diameter of the pressure port used in the present, work was 1.0 mm.

Since the pressure transducer was not mounted flush with the surface (this would have been impractical due to the large number of ports needed although provisions were made to flush mount two microphones), there existed a cavity between microphone and surface openings such that any frequencies near the resonant frequency of this cavity experienced an amplification in level. The magnitude of this amplication is not small as can be seen from Figure 3.17 which is the transfer function that results when comparing the probe signal to the signal from a flush mounted microphone. In order to correct for this error two alternatives, mechanical or electronic compensation, could be used, though neither were. Mechanical compensation could be obtained through damping by introducing some type of absorbing material such as cotton or steel wool (ref. 14 and 15). Alternatively, electronic compensation could be obtained via the computer. The transfer function of Figure 3.17 could be reproduced analytically in a manner similar to Schroeder's (ref. 1) approach or experimentally as was done with the free probes in the present study. This could then be programmed into the computer to provide the necessary corrections. Which of the above methods pro-

vide the more accurate compensation for probe transfer function was not determined.

The full array of pressure ports on the model wing surface is shown in Figure 3.18. This distribution was selected to duplicate measuring points on the full size wing section and to enable correlation and convection velocity studies to be made. In the present study, however, measurements were only made at four locations.

The limited number of measurements made on the wing were all third octave spectra which were cut off at a frequency of 630Hz. As will be seen later, frequencies above 630 Hz are of little interest for purposes of comparisons between full scale and model spectra due to scaling relations between full scale and model. In addition, probe response was essentially flat out to 630 Hz, with corrections, as determined by averaging the transfer function over third octave bands, being only 2.5 and 3.1 dB for the 500 and 630 Hz bands.

Probe Traverse and Coordinate System

A five degree of freedom traverse was constructed for the free probes where positions could be changed in three translational directions and rotations were possible in a vertical plane parallel to the longitudinal axis of the facility and in a horizontal plane. Figure 3.19 is a schematic representation of the probe traverse and coordinate system used while Figure 3.20 presents photographs of the traverse system and facility.

3.3 Muffler Design

The initial configuration, as described up to this point, was used for all of the preliminary survey of the flow field produced. Upon completion of this survey an

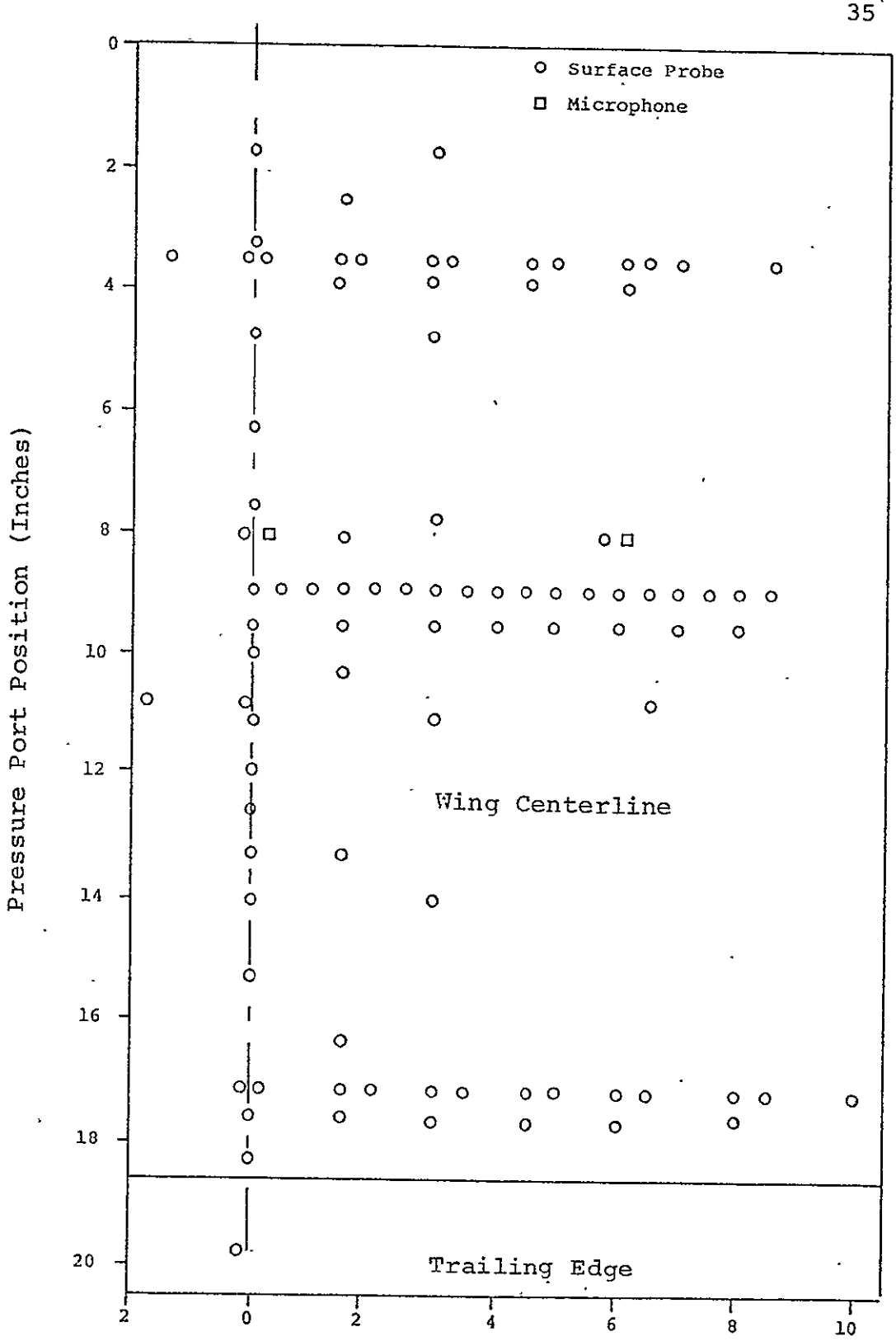

Figure 3.18 Wing Surface Pressure Port Distribution

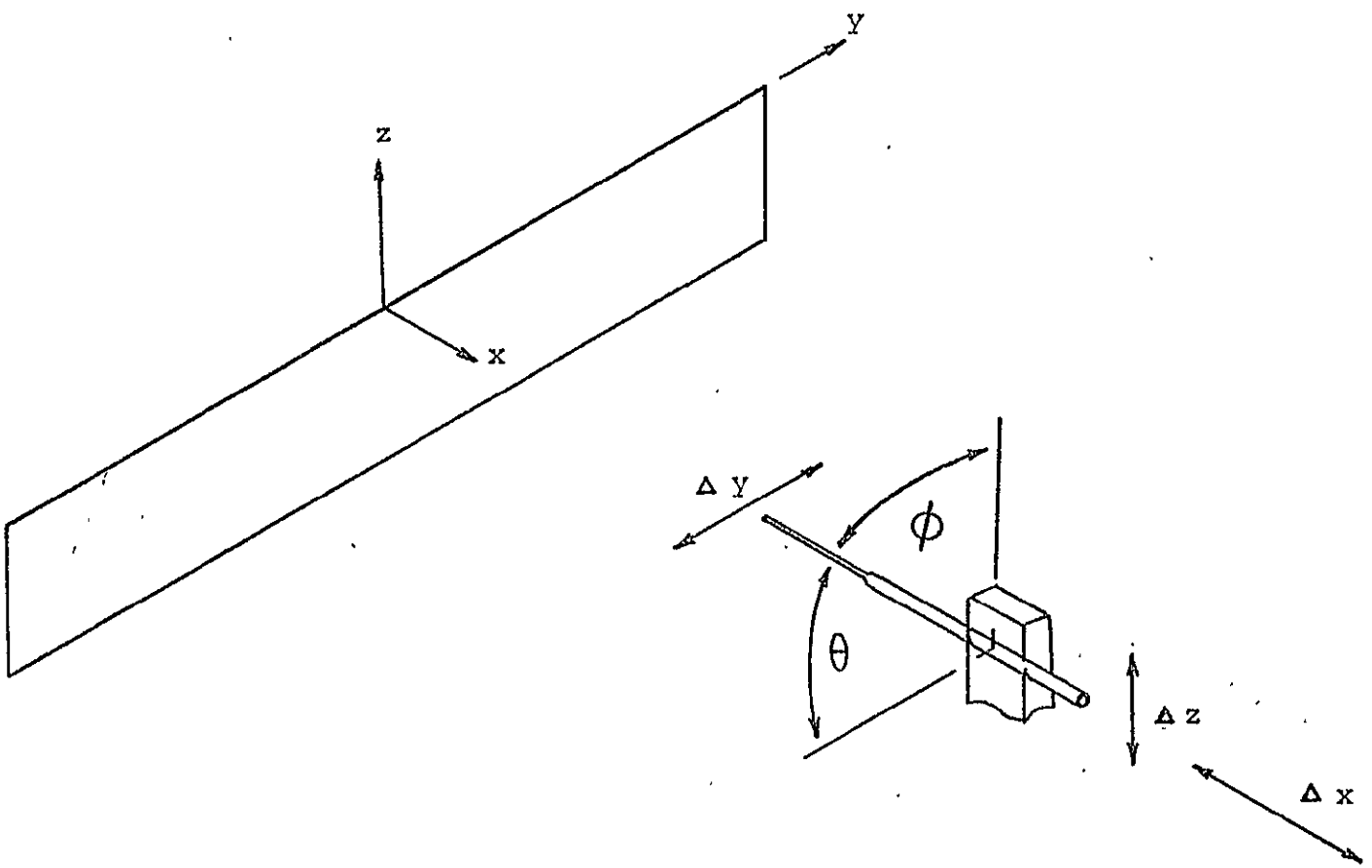

Figure 3.19 Coordinate System and Probe Traverse

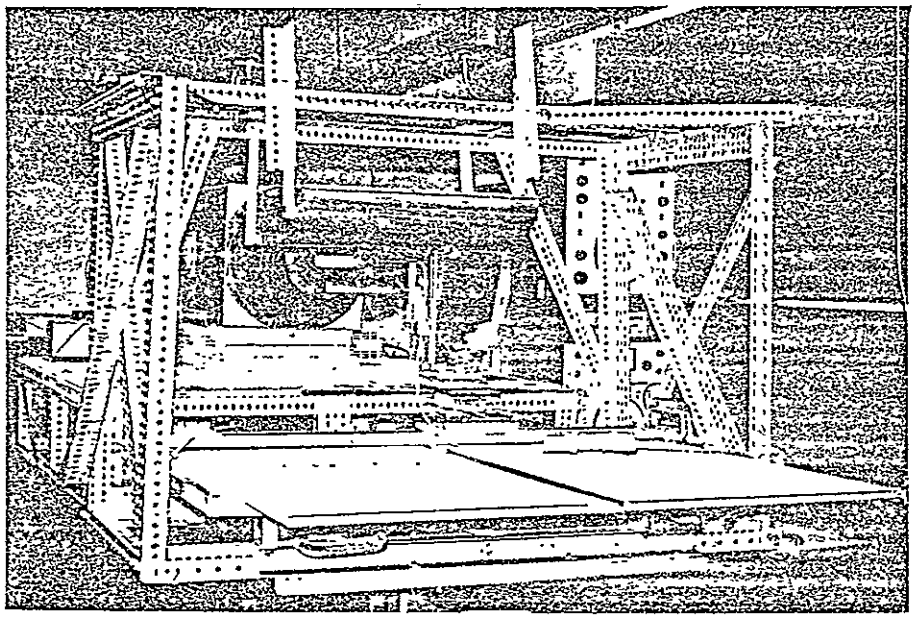

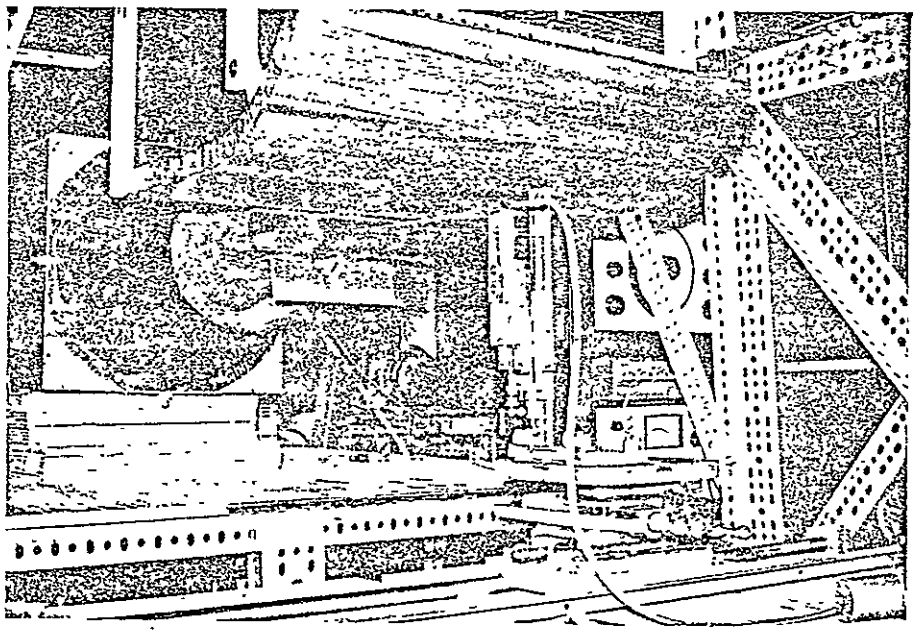

Figure 3.20 Upstream View of Facility Showing Probe Traverse

effort was made to eliminate a long standing problem in the facility, that of vibrations caused by the blowers, which were transmitted through the structure to the probes and to the microphones. Consequently, measurements in regions of low turbulence levels where microphone signals were small (for example, near the exit plane) had been very difficult. To alleviate the problem the blowers were removed from the plenum chamber and mounted on separate structures standing on the floor.

As part of an evaluation of these changes measurements were made to determine spectral content of acoustic levels in the plenum-nozzle cavity. In the light of Crow and Champagne's (ref. 5) work it was felt that noise from the blowers may have been effecting the flow. Figure 3.21 shows a third octave spectrum of one blower made with a free standing microphone. This figure is presented merely as an indication of the relative frequency content of blower noise. The indicated SPL is accurate for the particular position of the microphone but is not an indication of sound levels in the plenum chamber or nozzle exit plane.

Pressure ports were added to the adjustment cone near the plenum chamber to monitor acoustic levels. These ports were simply small holes drilled through the fiberglass with 3.0 m of plastic tubing connecting a microphone. Transfer functions were not determined for these ports. Therefore, these ports are only reliable as indicators of relative differences at the same point (i.e., on the adjustment cone) due to changes in the facility or to flow conditions. For example, reliable comparisons between spectra determined at the exit plane with a static probe and at the adjustment cone ports was not possible.

In spite of this, third octave spectra measured at the adjustment cone port did provide a rough indication of acoustic levels inside the nozzle-plenum cavity. Figure

3.22 is a spectrum taken with one blower on at full speed. The prominent peak in this spectrum at 200 Hz was cause for alarm. As can be seen from Figure 3.23 which shows the third octave spectra at several downstream positions along the centerline of the facility, there was also a pronounced peak at about 200 Hz. It appeared that the flow was being excited by internal acoustic signals as predicted by Crow and Champagne.

This result stimulated the development of resonant type mufflers. Two designs were used and are presented in Figure 3.24 as they were installed in the system. The first design was obtained from Beranek (ref. 16). The performance of this design can be appreciated from Figure 3.25. This is a simple before and after comparison where the values plotted are the differences in decibels of sound pressure levels in third octave bands as measured at the adjustment cone. Above a frequency of 50 Hz the effect of the muffler was quite pronounced. However, the levels below 40 Hz appeared to be amplified. This was believed to be a result of vortex formation off the edges of the ducts used. These were 0.152 m in diameter and represented 1.85 times the area of the exit plane. Assuming incompressible flow, this implied that with a 21.9 m/sec. exit velocity as was the case, the velocity in the duct was 11.8 m/sec. These ducts were essentially circular nozzles and could be expected to produce flow at their exits which would exhibit spectral peaks at Strouhal numbers (S_t=f d/Uj) of 0.3 which corresponds to a frequency of 23 Hz.

In an attempt to correct this drawback a second muffler was constructed. This was similar to the first design except the central duct was continuous but peppered with one inch holes over the region that was cut out in the first muffler. The results of the modification can be seen in

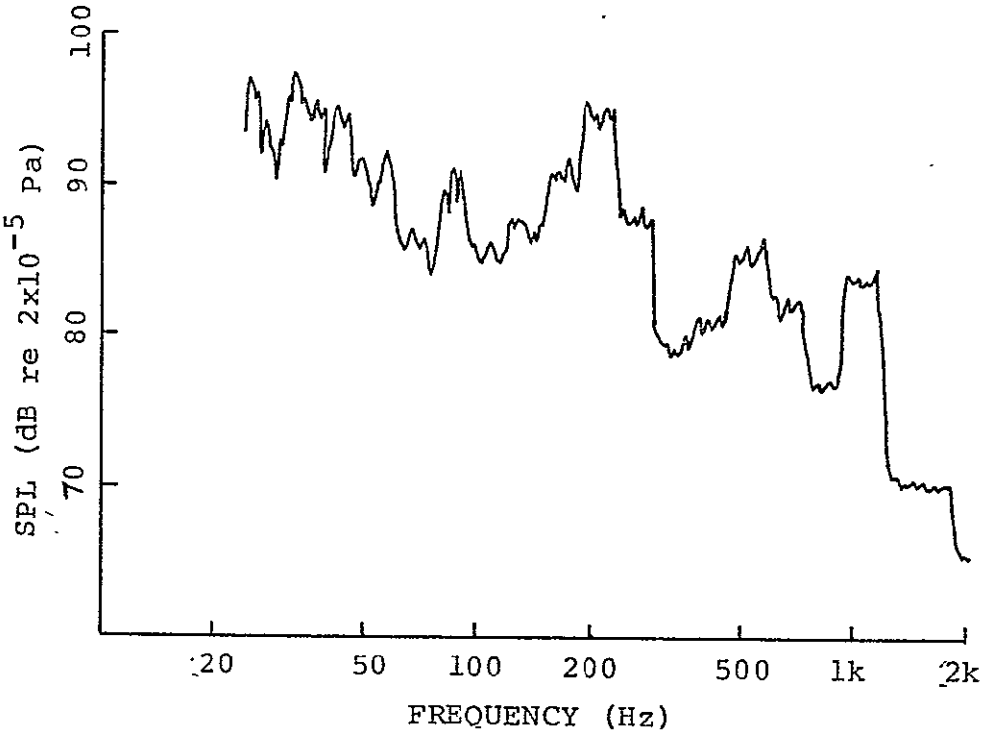

Figure 3.22 Adjustment Cone Spectrum with One Blower

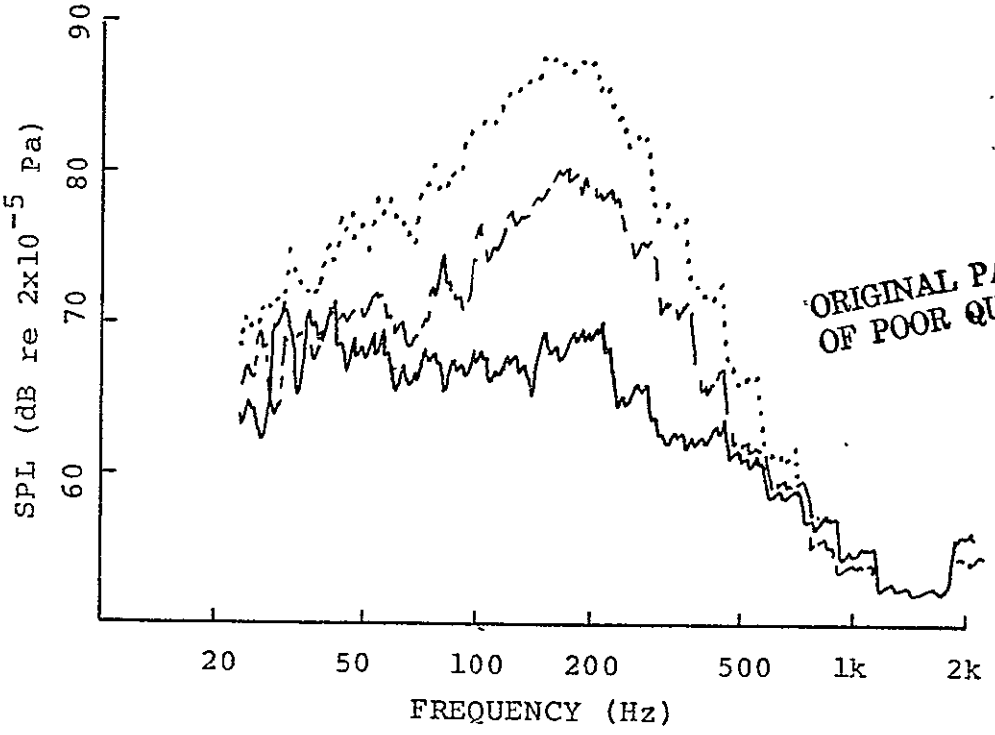

Figure 3.23 Centerplane Spectra with One Blower

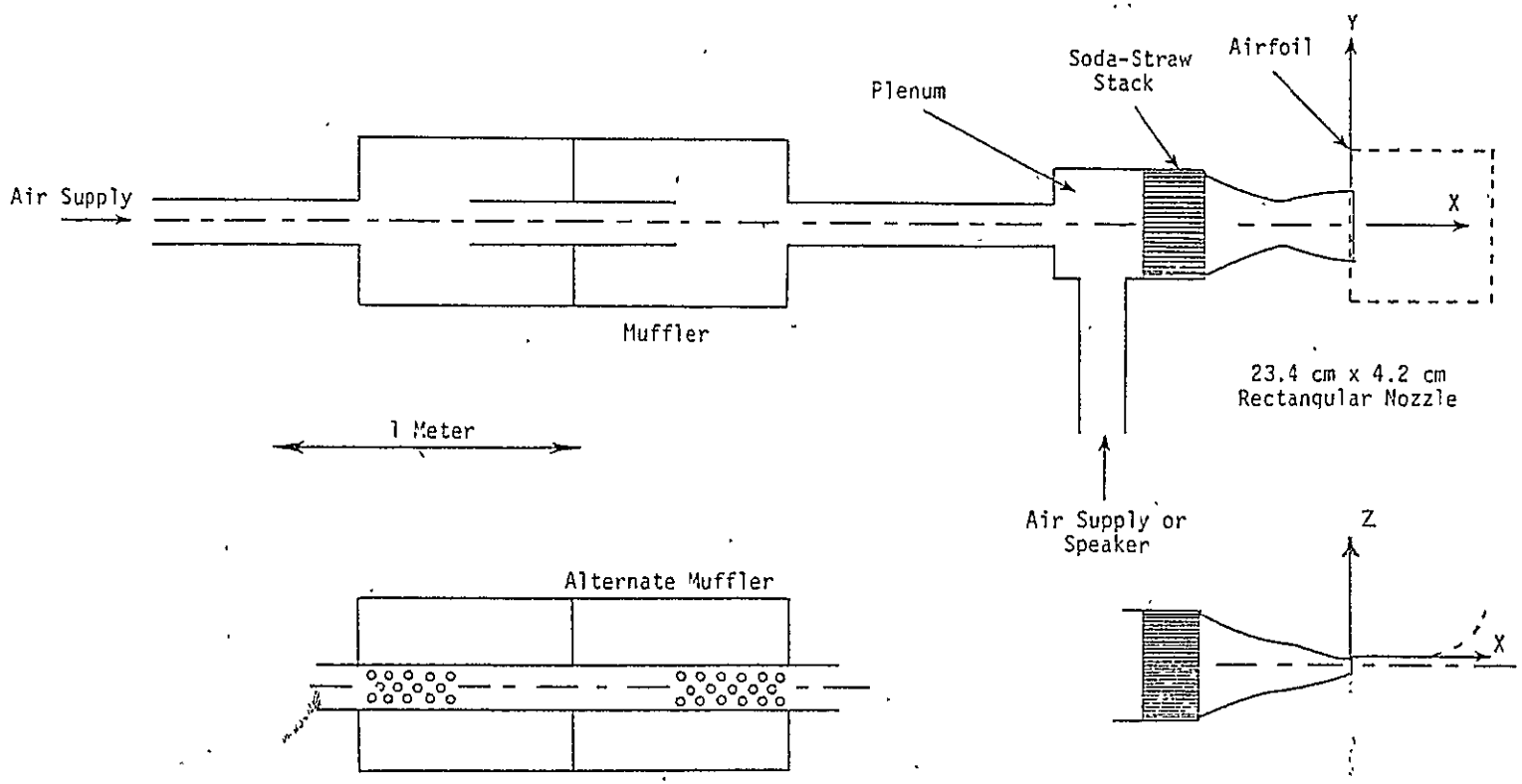

Figure 3.24 Final Configuration of Facility

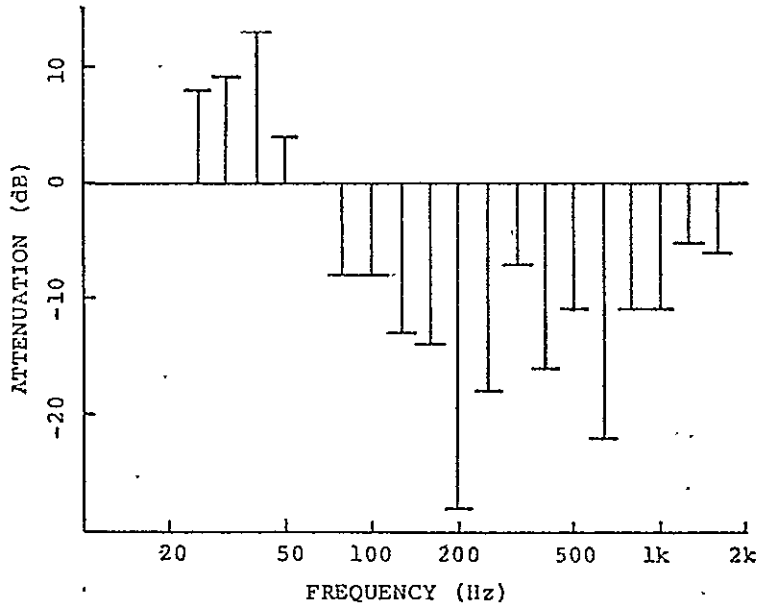

Figure 3.25 Performance of Muffler A

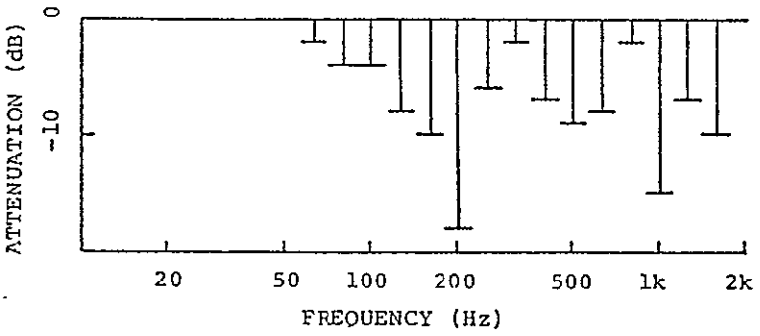

Figure 3.26 Performance of Muffler B (Alternate Muffler)

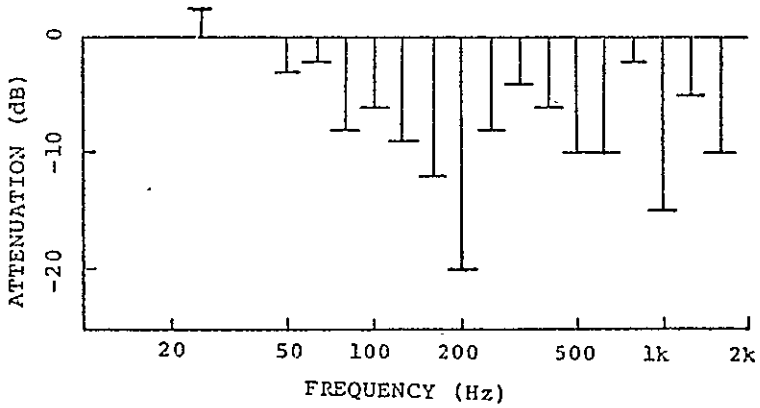

Figure 3.27 Performance of Muffler A and B

Figure 3.26. It is evident that the low frequency (20-40 Hz) was no longer produced, but that there was considerable deterioration in the high frequency performance.

The performance of both mufflers operating simultaneously was also checked and the results are presented in Figure 3.27. The effect of both mufflers together is approximately the same as the second muffler alone.

The addition of the mufflers completed the modifications of the facility to date. Figure 3.24 is a scaled drawing of the entire facility in its present form. Discussion of the effect of the mufflers on the flow field will be deferred until the next chapter.

Chapter 4. Initial Survey

A preliminary survey of the flow field behind the rectangular nozzle (without coaxial flow) with the jet free, and with the jet bounded by a wing, was performed to provide a general description of pressure fluctuations within this flow field. Where possible, comparisons were made to existing data or theories reported in the literature. The flow field simulated the condition of perfect mixing in a coaxial turbofan engine and in this regard did not accurately duplicate the exhaust flow of a turbofan engine.

Surveys are presented of average total pressure in the exit plane, unsteady rms static pressure, and third octave spectra. In addition to these single point measurements, two point cross-correlation measurements were made and were used to provide the correlation coefficients, phase lag, and coherence data which are also presented. Results of a brief investigation of the effect of background noise with several combinations of mufflers are reported. Finally a comparison is made between pressure spectra on the model and on the full-scale article, as measured on the "Beach" facility.

Rms static pressure has been referenced to 2×10^{-5} Pa for the pressure profile curves while sound pressure levels (SPL) are referenced to the dynamic pressure, q_j, at the exit plane

$$SPL = 10 \mathrm{Log}_{10} \left[(P_{rms})^2 / q^2_j \right] \text{ re. } q_j$$

All spatial locations referred to in the ensuing discussion are based on a right-hand coordinate system centered at the upper lip of the 4.2 X 23.4 cm nozzle with the positive x-axis directed downstream and aligned with the centerline of the set up (refer to Figure 3.19).

4.0 Investigation in Free Jet (with Wing Removed)

The average total pressure survey (not shown) indicates a uniform velocity distribution in the exit plane of the nozzle. The maximum difference between any two points in the exit plane is 0.3 m/sec. for a 30 m/sec. jet. The average total pressure drops off rapidly behind the lips of the nozzle.

RMS Static Pressure Survey

Figures 4.1 and 4.2 present several unsteady rms static pressure profiles for various downstream locations. The z or vertical position for each lateral profile (z and x were held fixed while y was varied) was chosen on the basis of its relative decibel level. That is, the point selected was the minimum rms level between the two peak rms points behind the nozzle lips. Thus, the profile at x = 2 cm is at a vertical position of z = -2.1 cm which is halfway between the upper and lower nozzle lips while at x = 40 cm, this minimum rms level point has shifted up to z = 0.0 cm. This shift results from the unsymmetric contour of the nozzle in the x-z plane. Also note the outward shift in the position of the "humps" in Figure 4.2 which is apparently due to the diverging planform of the nozzle.

Figures 4.3-4.7 are additional rms static pressure profiles (vertical: x and y fixed while z was varied) taken with the wing out. The variations in the exit plane profiles of Figure 4.1 and the irregular shape of the profiles at x = 2 cm in Figure 4.3 may have resulted from picking up vibrations in the system directly with microphones. The rms levels at these locations were near the lower end of the dynamic range of the pressure transducers. As a result, vibrations imparted to the probe and tubing were picked up by the microphone, thus increasing background levels. Minor reductions were obtained with padding

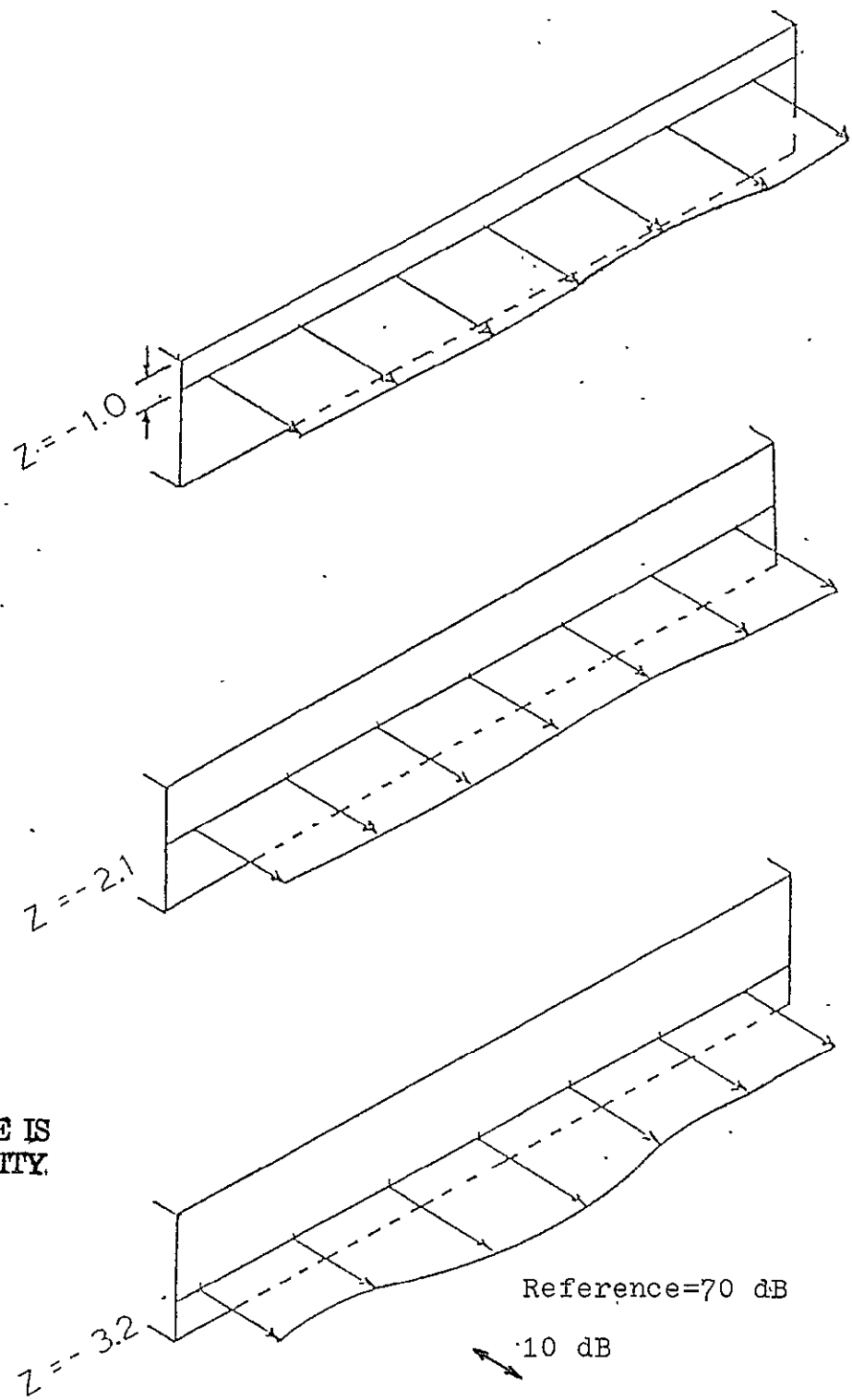

Figure 4.1 Exit Plane Rms Static Pressure Profiles-Wing Out

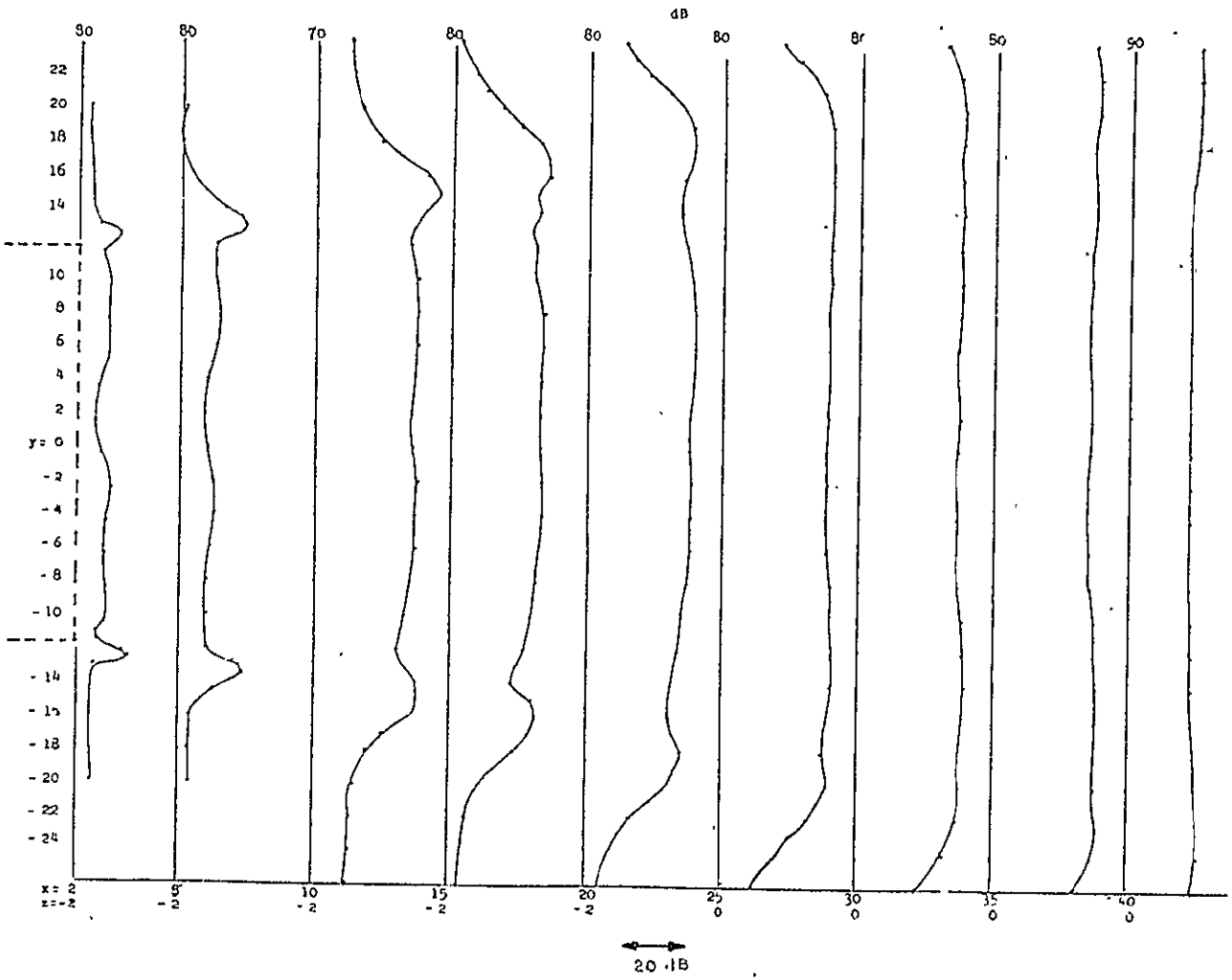

Figure 4.2 Lateral Rms Static Pressure Profiles-Wing Out

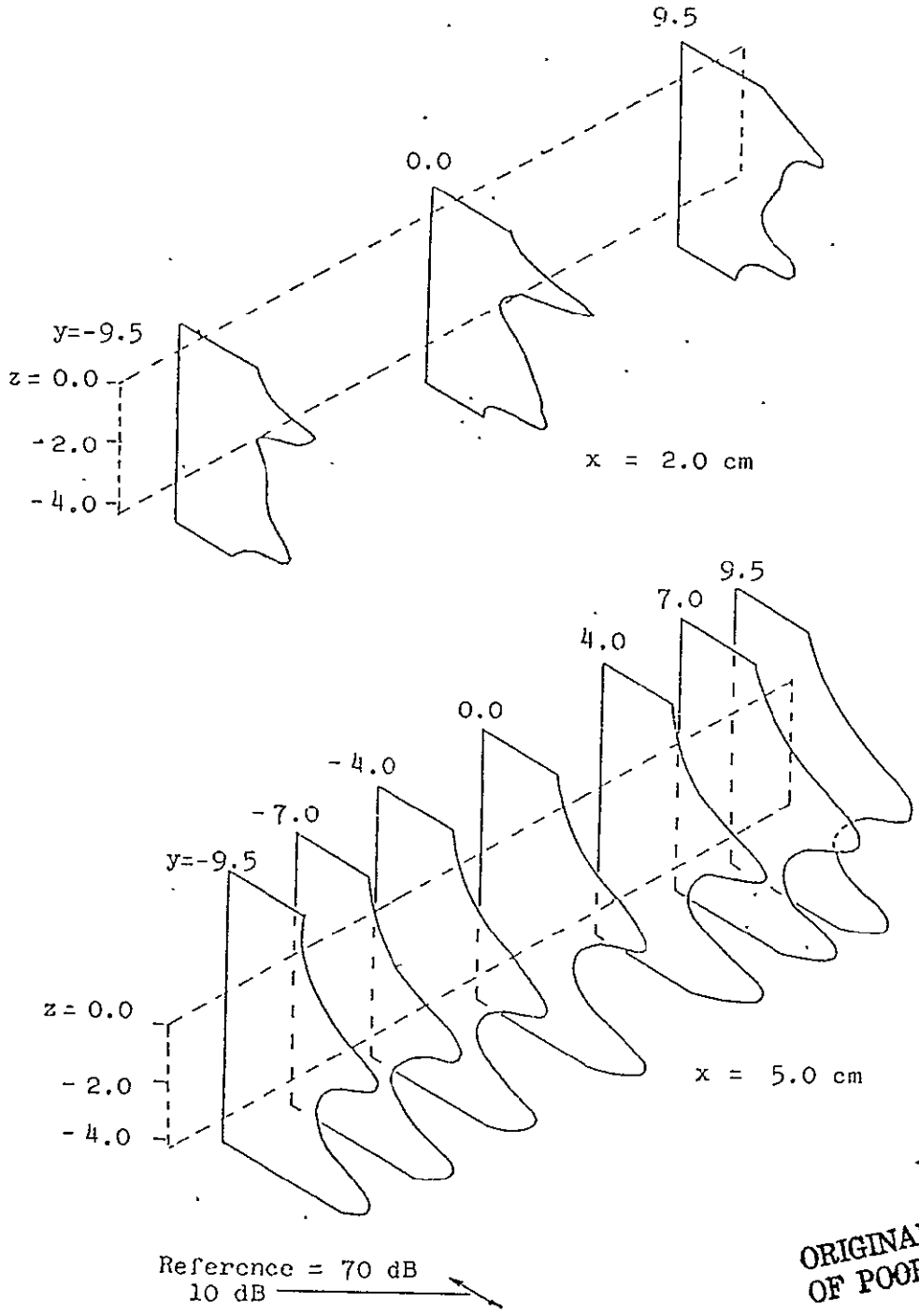

Figure 4.3 Rms Static Pressure Profiles-Wing Out

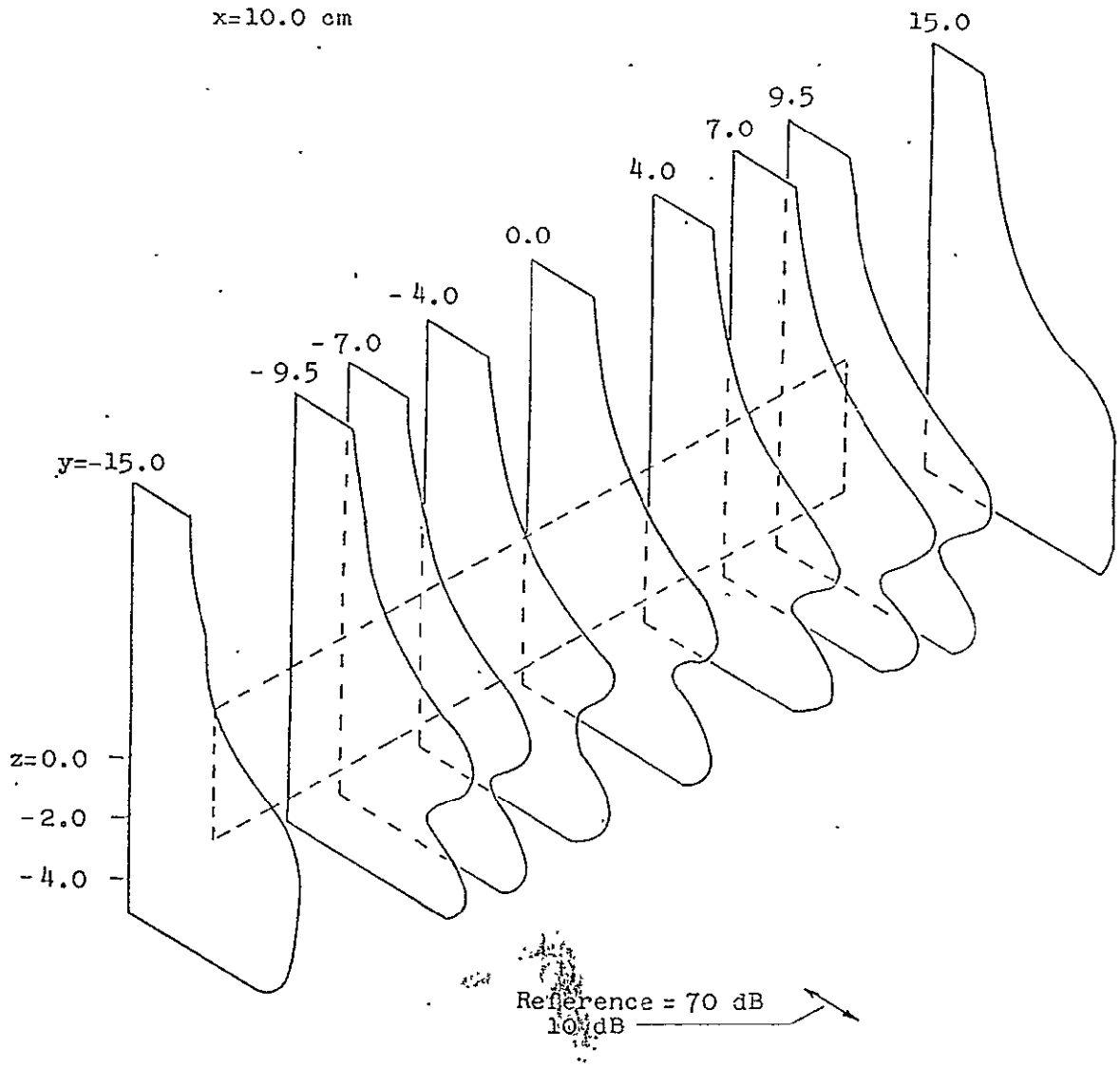

Figure 4.4 Rms Static Pressure Profiles-Wing Out

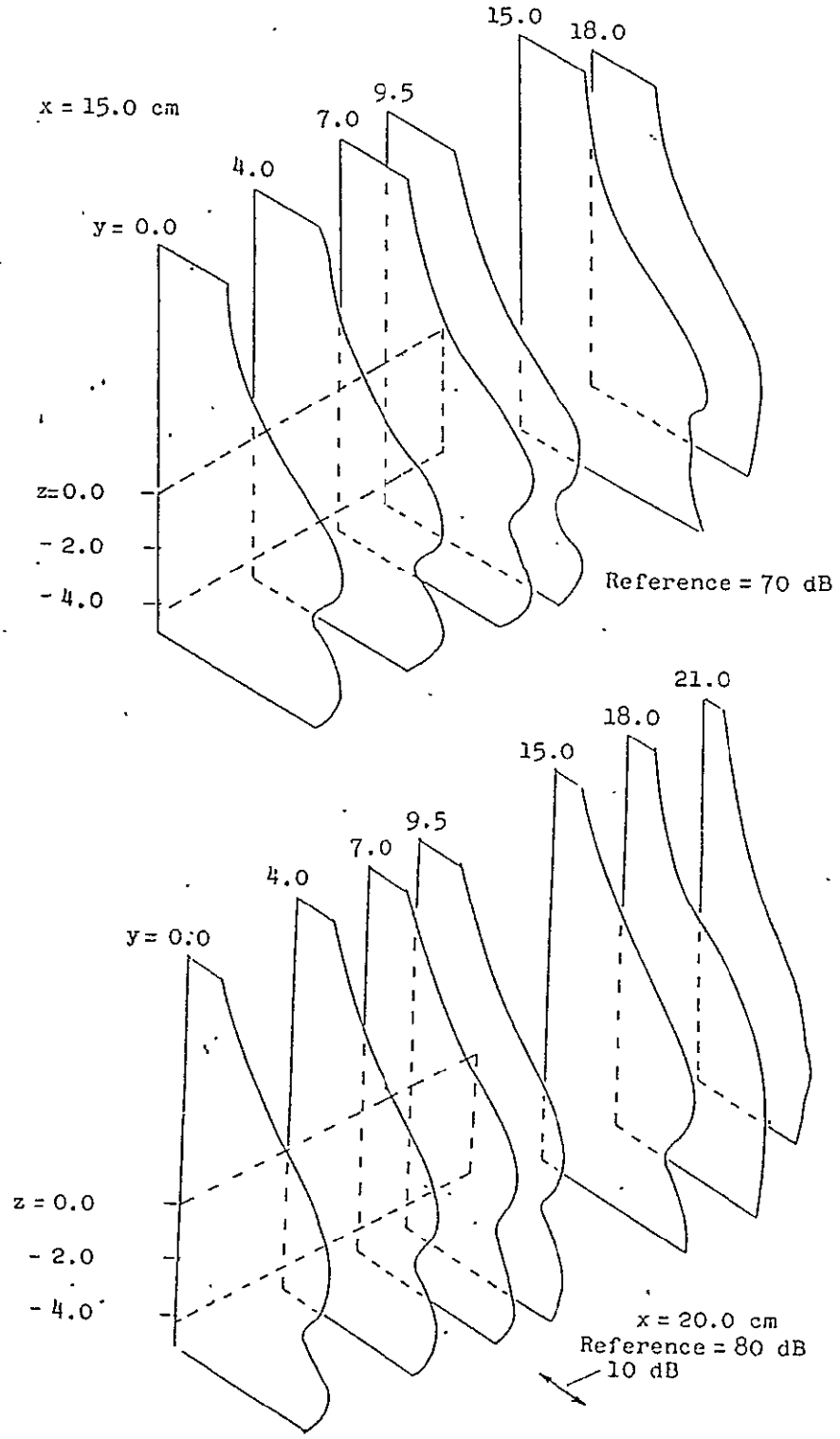

Figure 4.5 Rms Static Pressure Profiles-Wing Out

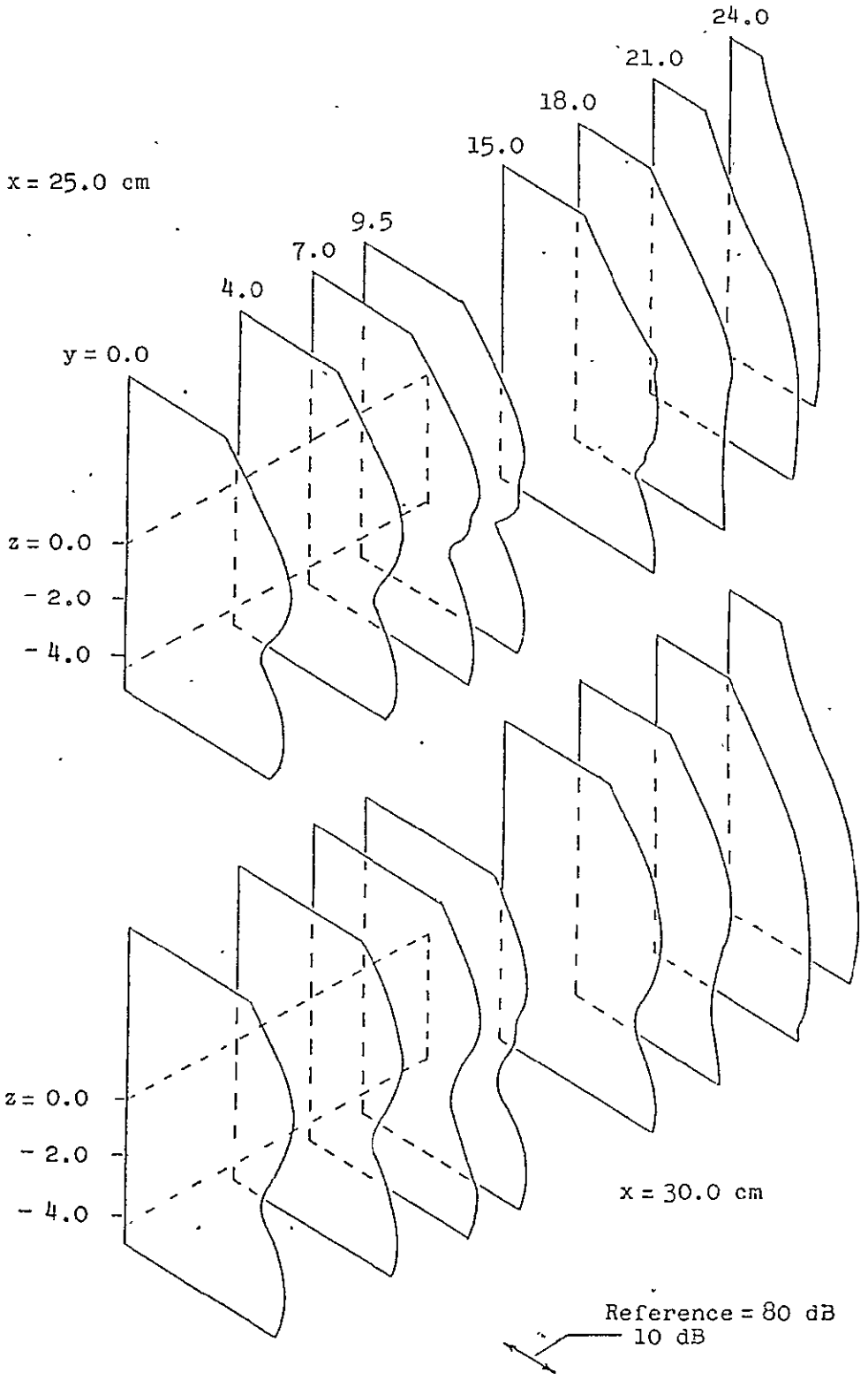

Figure 4.6 Rms Static Pressure Profiles-Wing Out

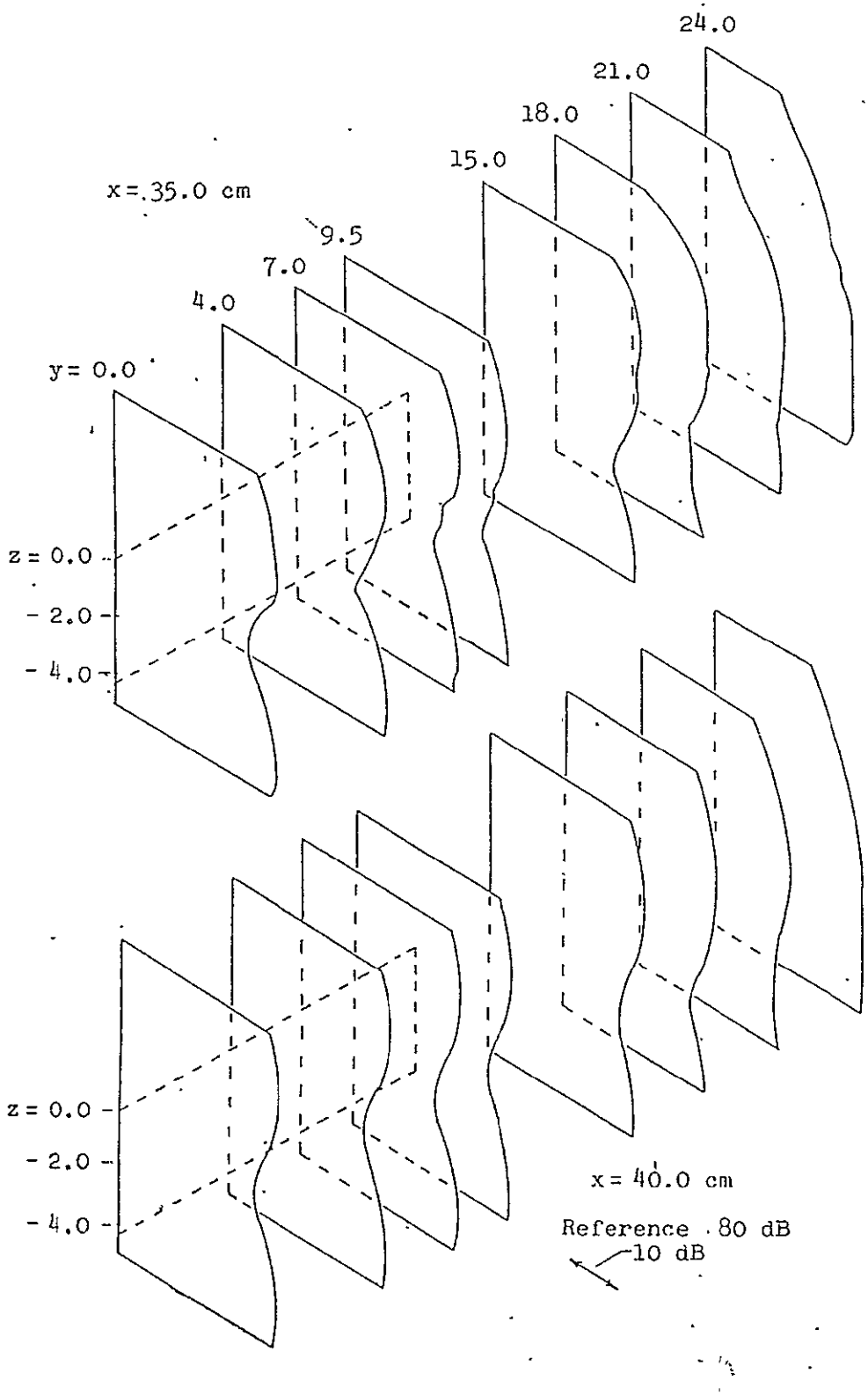

Figure 4.7 Rms Static Pressure Profiles-Wing Out

and careful placement of tubing but further reductions were not obtained until the blowers were isolated from the plenum chamber. Since difficulties in background levels were only encountered in a small region near the nozzle, it was decided that this change could be delayed. From these profiles, it is apparent that the peak pressure fluctuations occur behind the nozzle lip but that the upper peaks shift upward as one moves downstream. This upward shift amounts to approximately 4° which again was attributed to the contour of the nozzle.

The validity of these measurements as indications of absolute pressure levels is certainly to be questioned. Correction of rms pressure measurements as made with an analog type instrument such as the B & K 2113 was not possible. However, the rms static pressure measurements are quite meaningful as indications of relative rms pressure which was their intended use.

Third - Octave Survey

The spatial locations of the majority of third-octave measurements made in the free jet are shown in Figure 4.8. The numbers in this figure represent the peak frequencies in the spectrum at each position. There is a general shift in the frequency peaks from 315 Hz near the exit plane ($x < 15$ cm) to 100 Hz at $x = 40$ cm along the centerline. Notice also how the outer flow regions ($y > 15$) precede the centerline flow in this shift to lower frequencies. Spectral peaks in the outer region appear to be a rough prediction of developments along the centerline. If this is so, then the indication is that the centerline spectral peaks will eventually shift to 40 Hz at some point beyond $x = 40$ cm (measurements were made only out to this downstream location). Assuming a spectral peak at a Strouhal

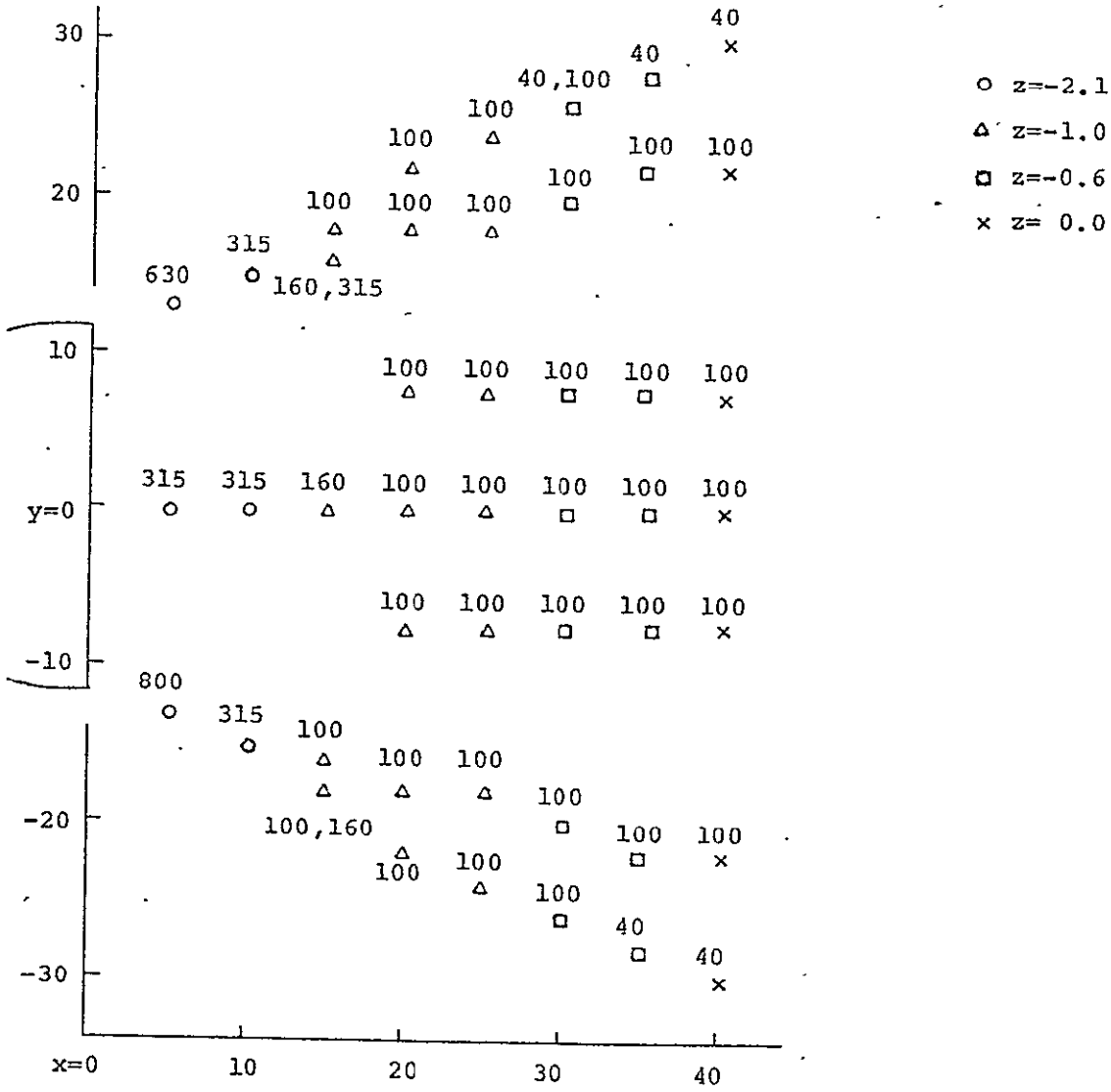

Figure 4.8 Third Octave Survey of Peak Frequencies (Hz)- Wing Out

number ($St = fd/U_j$) of 0.3 (typical of peaks in circular nozzles) with a 30 m/sec. jet, the dimensions associated with the frequencies presented in Figure 4.8 are listed in Table 4.1 below.

Table 4.1
Frequency Peaks and Associated Dimensions

Frequency	Dimension
315 Hz	2.9 cm
200 Hz	4.6 cm
100 Hz	9.2 cm
40 Hz	23.2 cm

For comparison, the jet exit dimensions are 4.2 cm x 23.4 cm.

It is also interesting to note that the Strouhal number corresponding to a frequency of 315 Hz from a 30 m/sec. jet with a dimension of 4.2 cm is 0.44 which is well within the range of Strouhal numbers at which Crow and Champagne (ref. 5) were able to force their circular jet. The point is that the spectral peak observed at 315 Hz may have resulted from background noise whereas, in the absence of this noise, the peak might have occurred at a lower frequency corresponding to a Strouhal number of 0.3.

Figures 4.9 - 4.12 are third - octave spectra taken at several key points shown in Figure 4.8. They illustrate respectively the downstream spectral evolution along the centerplane, the downstream spectral evolution in the outer flow region, and cross-stream comparisons at two downstream locations. Notice the frequencies at which peaks were observed in the exit plane spectrum. Pressure levels in the exit plane are a measure of background noise due to

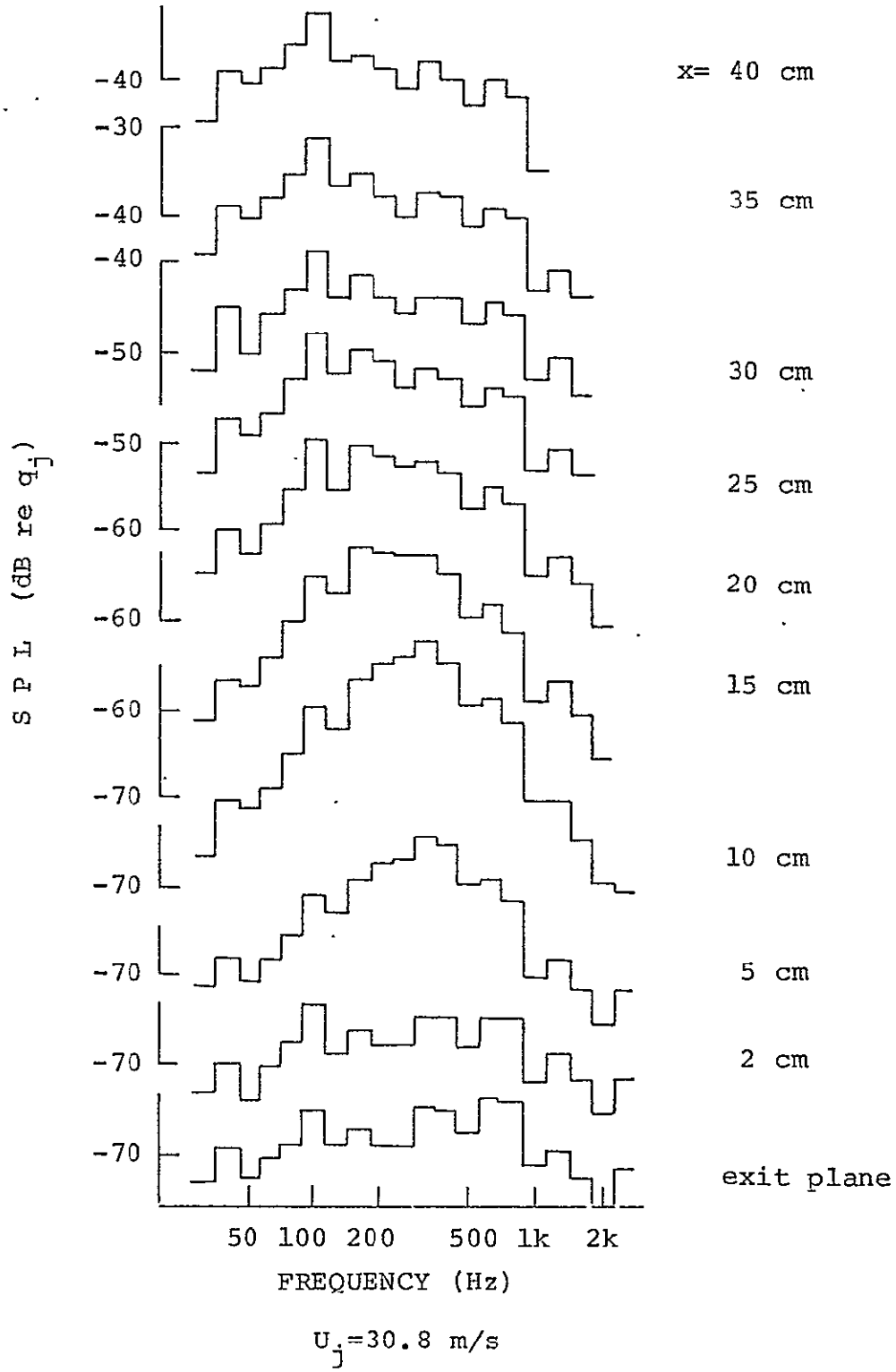

Figure 4.9 Downstream Evolution of Centerplane Spectra

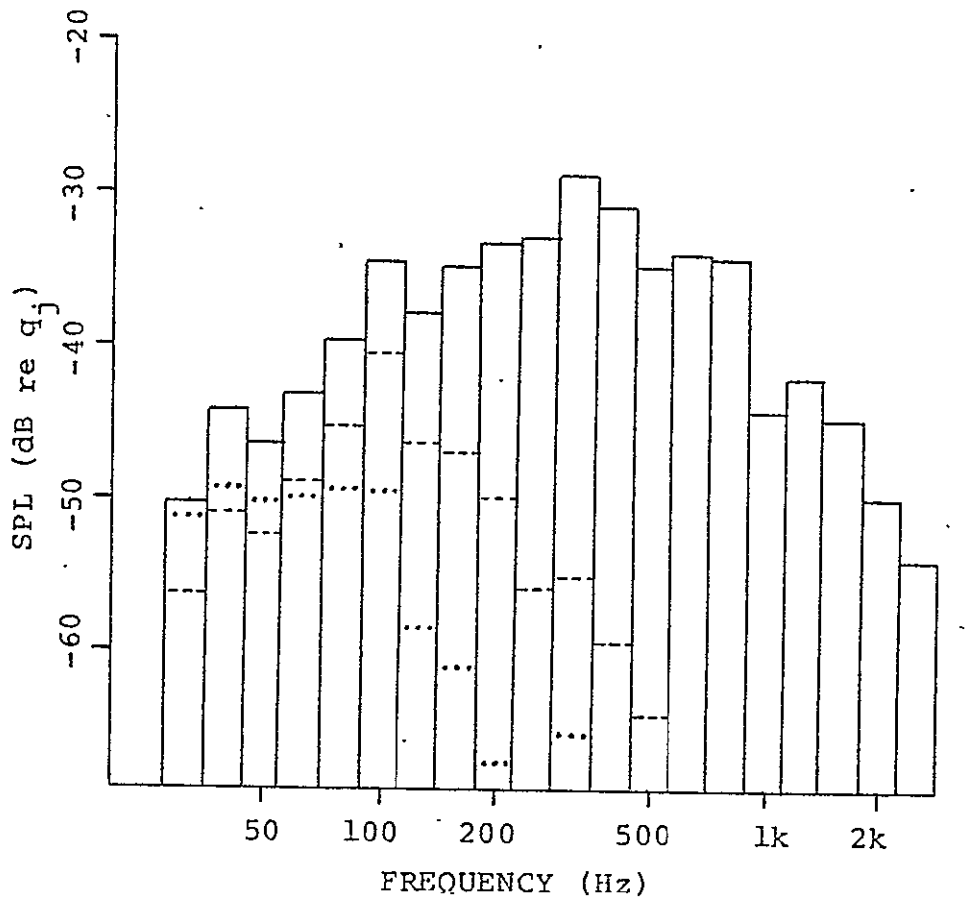

—— x=10, y=15, z=-2.1 cm

--- x=20, y=22, z=-1.0 cm

··· x=40, y=30, z= 0.0 cm

U_j=30.8 m/s

Figure 4.10 Outer Flow Downstream Spectral Evolution

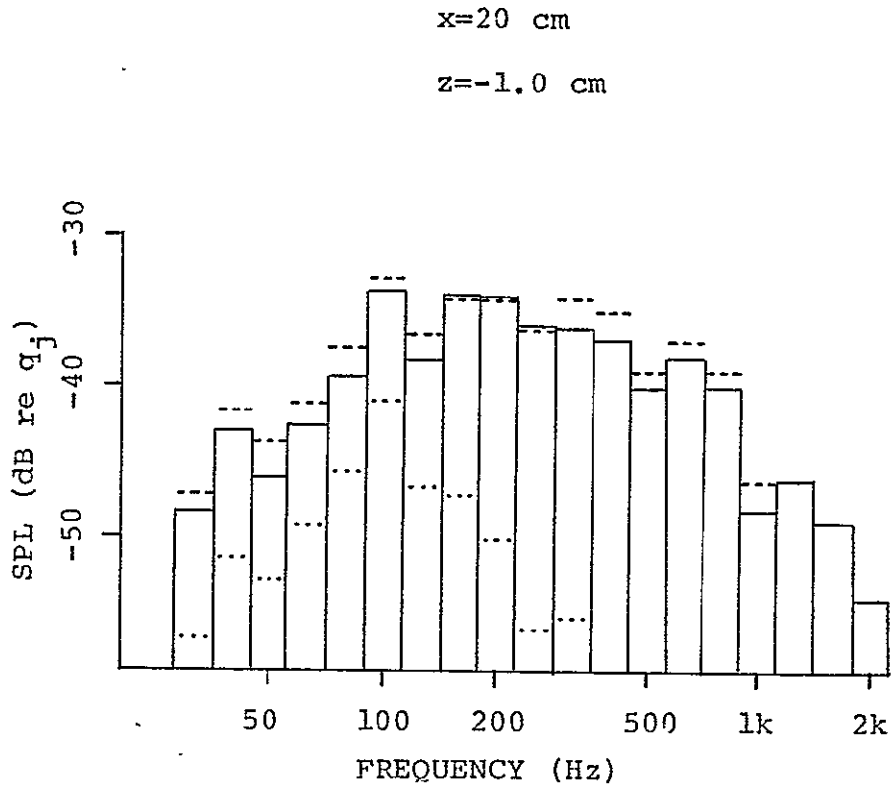

Figure 4.11 Cross-stream Spectral Comparison

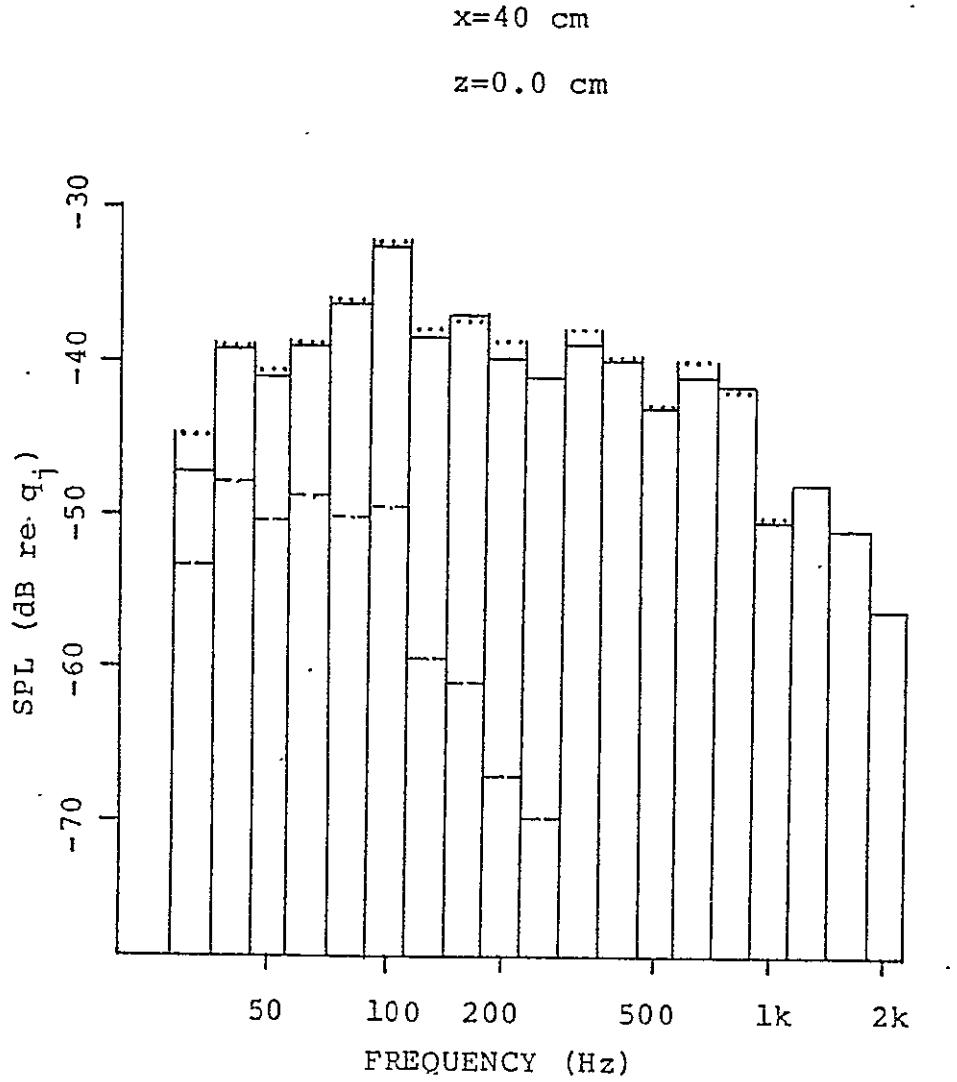

Figure 4.12 Cross-stream Spectral Comparison

blowers and their influence on the flow is strongly suggested by Figure 4.9. This will be discussed in greater detail at a later point in the paper. It is reasonable to assume that the acoustic background did not influence the overall structure of the flow. Rather, as in circular jets where the coherent structure will exist with or without acoustic forcing, the frequencies associated with a jet structure will be effected within certain ranges (i.e., coherent structures can be induced at frequencies other than those corresponding to a Strouhal number of 0.3 which is the preferred frequency of circular jets) (ref. 5). With this in mind, a possible explanation for observations of multiple peaks is that the jet may have a multiple structure. In the case of a circular jet, as was mentioned earlier, a vortex structure develops that scales with the diameter of the jet nozzle. It could be expected then that the rectangular nozzle would impose at least two length scales on the flow resulting in the formation of coherent eddies of different sizes which would interact in some manner that may produce a third eddy size which scales on an effective diameter of the nozzle. The effective diameter as suggested by Stone (ref. 9) of the nozzle used is 9.3 cm which compares closely with the dimension associated with spectral peaks at 100 Hz (St. no. = 0.3). In the flow region examined this appears to have been one of three prominent frequencies where 315 Hz and, to a lesser extent, 40 Hz were the other two. Work done on circular jets indicates that the major influence of coherent eddies is experienced between 1-5 nozzle diameters downstream of the exit plane. Applying this to the rectangular jet, it could be expected that the smaller eddies would develop and decay at different downstream distances depending on the size of the eddy. Thus one

would expect eddies associated with the narrow dimension of the nozzle to diminish by about x = 20 cm (recall that nozzle dimensions are 4.2 x 23.4 cm) while the intermediate sized eddy would predominate in the flow out to about x = 45 cm at which point the large eddy would dominate. At overlapping regions of influence two eddies may coexist with each exerting varied degrees of predominance. It is difficult to describe this development with a model similar to the vortex model for circular jets since, if several different sized eddies do exist, there is likely to be a complex interaction between them.

Correlation Measurements

Correlation measurements were taken at three downstream locations (x = 8.3 cm, x = 17 cm, x = 22 cm) to determine correlation coefficients and convection velocities for various lateral (Δy) and vertical (Δz) probe separations. One probe (M Probe) was held fixed at the centerplane positions of x = 8.3, 17, and 22 cm, y = 0.0 cm, and z = -1.0 cm, while the other probe (L probe) was varied in either a lateral (x and z constant) or vertical (x and y constant) direction to determine correlation coefficients and coherence relations.

Table 4.2 lists the cross-correlation coefficients obtained for various lateral and vertical separations. The coefficients, ρ_{12}, were determined using the digital output from the correlator. The formula for ρ_{12} is given by

$$\frac{R_{12}(t)}{\left[R_{11}(0)R_{22}(0)\right]^{\frac{1}{2}}} = \rho_{12}$$

where $R_{12}(t)$, $R_{11}(0)$, and $R_{22}(0)$ are, respectively, the peak value of the cross-correlation function and the values of the auto-correlation functions at zero time delay. For

Table 4.2

Cross - Correlation Coefficients

in Free Jet (Wing Removed)

ρ_{12}

y Separation	x = 8.3 cm	x = 17 cm	x = 22 cm
0.3 cm	.92		
0.5 cm	.86	.90	.88
5.0 cm	.21	.26	.26
11.7 cm	.014	.044	.066
17.1 cm	.012	.024	.026
20.6 cm		.035	.021
z Separation			
1.1 cm	.63	.53	.72
3.2 cm	.23	.38	.60
5.0 cm	.34		
6.0 cm		.35	.50

horizontal separations the cross-correlation coefficient decays rather rapidly with increasing separations with little difference between corresponding separations at the farther two downstream positions while between downstream positions of x = 8.3 and 17 cm the cross-correlation coefficient increases. The most noteworthy point with vertical separation is the higher coefficients obtained over those from equivalent horizontal separations.

Coherence plots, some of which have been presented in Figure 4.13, determined for the above positions reinforce the cross-correlation results while adding information on frequency. For lateral separations greater than 5 cm the coherence deteriorated rapidly while for a vertical separation of 5 cm the coherence was at least 5 dB higher than the associated horizontal coherence. Table 4.3 lists the peak value of coherence and the frequency of the peak for vertical and lateral separations of 5 cm for each downstream position. There is a tendency for the coherence to recover slightly when the measuring point is beyond the lip of the nozzle (nozzle lip: $\Delta z = -3.2$ cm) which is in agreement with correlation measurements made in circular jets (ref. 1).

Convection velocities, U_c, were determined at several points for the three downstream positions using probes separated laterally (Δy) 1.0 cm and longitudinally (Δx) 1.0 cm (unless otherwise noted). The phase plots (shown in Figure 4.14) resulting from cross-correlations taken of the two probe signals were used to obtain convection velocities through application of the following formula

$$U_c = -360 \Delta x \frac{f}{\omega} ,$$

where ω is in degrees. Table 4.4 presents the convection velocities found nondimensionalized by the jet exit velocity

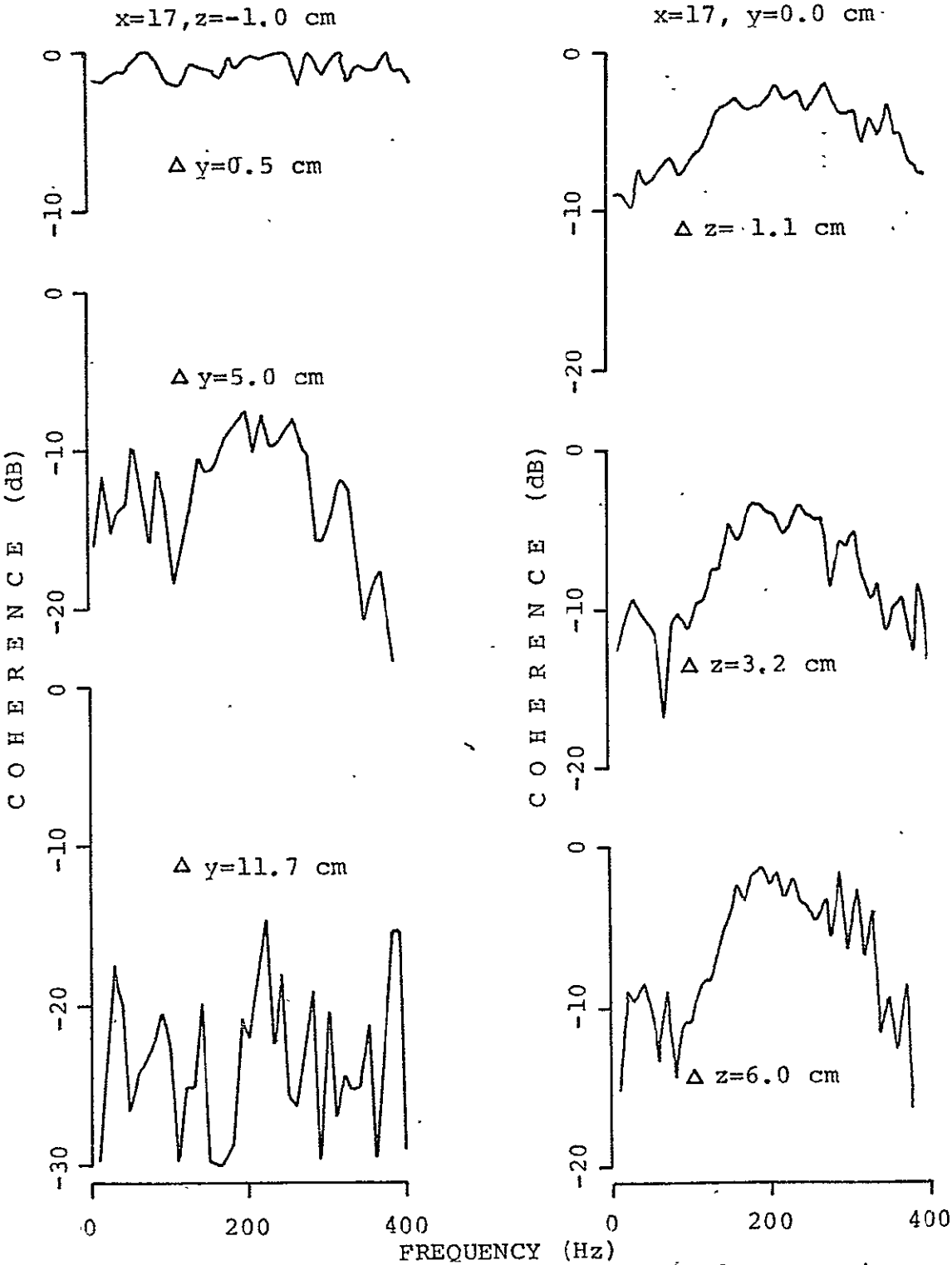

Horizontal Separation Vertical Separation

Figure 4.13 Coherence for Several Separations with One Probe Fixed at x=17,y=0.0,z=-1.0 cm

Table 4.3
Peak Coherence and Frequency

Position	Coherence	Frequency
x=8.3, z=-1.0, y=0-5.0 cm	-8.3 dB	250 Hz
x=8.3, z=-1.0 - -2.1, y=0 - 0.5 cm	-1.9 dB	220 Hz
x=8.3, z=-1.0 - -4.2, y=0 - 0.5 cm	-5.9 dB	280 Hz
x=8.3, z=-1.0 - -6.0, y=0 - 0.5 cm	-3.1 dB	240 Hz
x=17.0, z=-1.0, y=0 - 5.0 cm	-7.3 dB	200 Hz
x=17.0, z=-1.0 - -2.1, y=0 - 0.5 cm	-1.9 dB	210 Hz
x=17.0, z=-1.0 - -4.2, y=0 - 0.5 cm	-3.3 dB	190 Hz
x=17.0, z=-1.0 - -7.0, y=0 - 0.5 cm	-1.3 dB	190 Hz
x=22.0, z=-1.0, y=0.0 - 5.0 cm	-9.2 dB	100 Hz
x=22.0, z=-1.0 - -2.1, y=0.0 - 0.5 cm	-0.6 dB	180 Hz
x=22.0, z=-1.0 - -4.2, y=0.0 - 0.5 cm	-1.4 dB	100&160 Hz
x=22.0, z=-1.0 - -7.0, y=0.0 - 0.5 cm	-1.2 dB	190 Hz

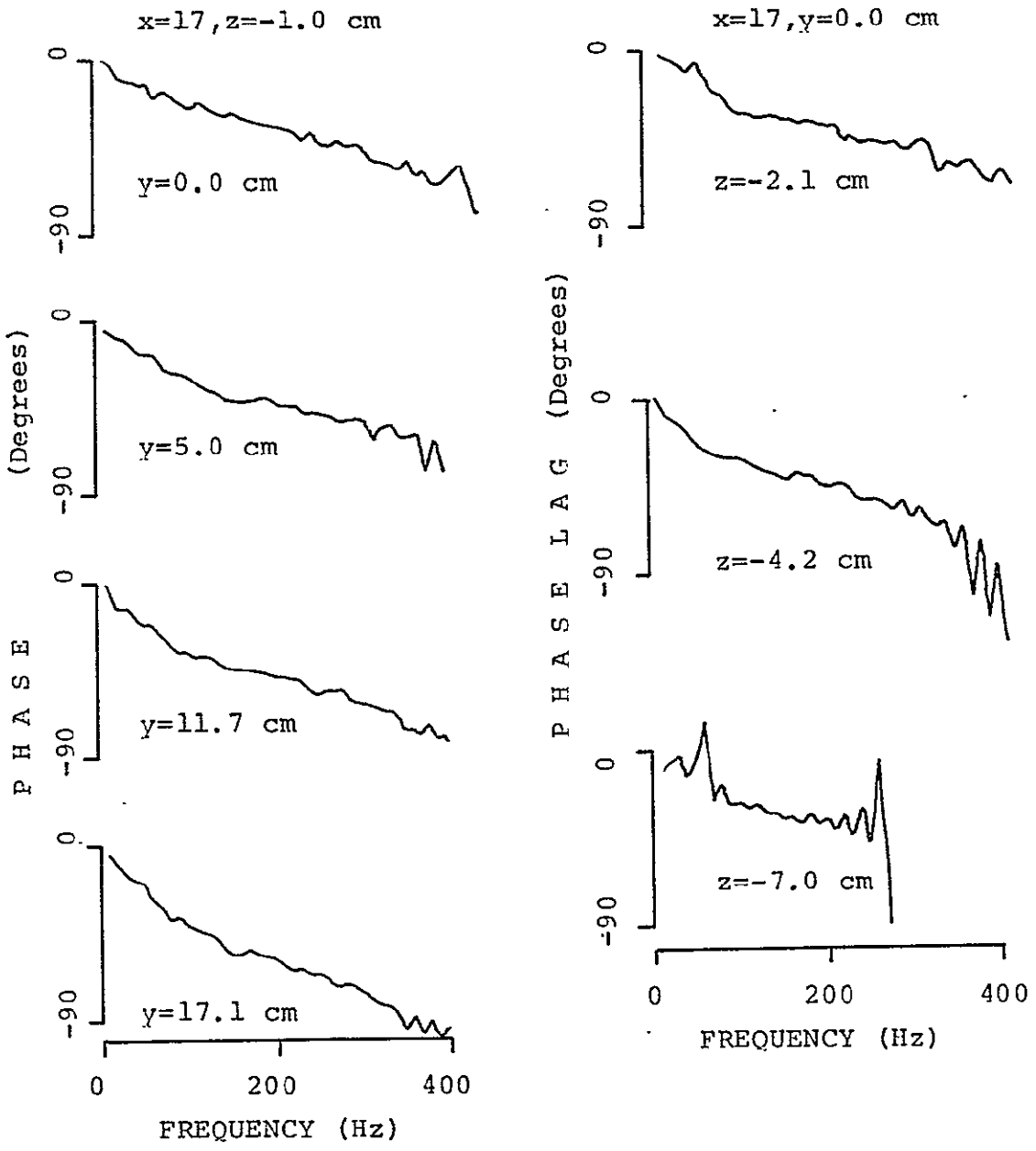

Figure 4.14 Phase Lag Curves used for Convection Velocity

Table 4.4
Convection Velocities (Wing Out)

Position	U_c/U_j Low freq.	Med. freq.
x=8.3 cm, z=-1.0 cm, y=0.0 cm	.33	.56
x=8.3 cm, z=-1.0 cm, y=5.0 cm	.34	.52
x=8.3 cm, z=-1.0 cm, y=11.7 cm	.23	.54
x=8.3 cm, z=-1.0 cm, y=17.1 cm	.29	.49
x=8.3 cm, z=-2.1 cm, y=0.0 cm	.58	
x=8.3 cm, z=-4.2 cm, y=0.0 cm	.38	.61
x=17.0 cm, z=-1.0 cm, y=o.o cm	.58	.7
x=17.0 cm, z=-1.0 cm, y=5.0	.42	.61
x=17.0 cm, z=-1.0 cm, y=11.7 cm	.3	.54
x=17.0 cm, z=-1.0 cm, y=17.1 cm	.31	.44
x=17.0 cm, z=-2.1 cm, y=0.0 cm	.44	.7
x=17.0 cm, z=-4.2 cm, y=0.0 cm	.33	.54
x=17.0 cm, z=-7.0 cm, y=0.0 cm	.49	
x=22.0 cm, z=-1.0 cm, y=0.0 cm	.38	.61
x=22.0 cm, z=-1.0 cm, y=5.0 cm	.35	.54
x=22.0 cm, z=-1.0 cm, y=11.7 cm	.35	.58
x=22.0 cm, z=-1.0 cm, y=17.1 cm	.24	.44
x=22.0 cm, z=-2.1 cm, y=0.0 cm	.41	.56
x=22.0 cm, z=-4.2 cm, y=0.0 cm	.41	.49
x=22.0 cm, z=-7.0 cm, y=0.0 cm	.38	

(32.7 m/s). For many positions two convection velocities were found and are presented as low frequency (less than 100 Hz) and medium frequency (greater than 200 Hz).

The coexistence of more than one average convection velocity at the same spatial location hints at the presence of multiple vortex structures. The fact that constant convection velocities less than the velocity of the jet were observed over specified frequency ranges can be explained in terms of vortex structures. Results from circular jets indicate vortices convect downstream at approximately 0.6 the jet velocity depending on the size of the eddy (ref. 17 and 18). Smaller eddies move faster because their dimensions are such that they are more completely contained in the region near the axis of the jet (where the flow is fast) while the larger structures are more in the outer flow regions where slower velocities are encountered. With this in mind, the existence of two or more coherent vortex structures of different sizes would produce convection velocities constant over frequency ranges that would depend on the characteristics of the vortex structure. The larger the structure presumably the lower its frequency and convection velocity would be. The stronger and more coherent the vortex is the greater its influence would be on neighboring frequencies resulting in constant convection velocities over larger frequency bands.

4.1 Investigation in Bounded Jet (with Wing in Place)

Measurements made in the bounded jet, with the wing in place, were restricted to downstream distances of 25 cm or less which corresponds to the flat portion of the wing. Using symmetry arguments, testing was limited to the left side of the centerline of the facility. As was the case with the wing removed, the average total pressure in the

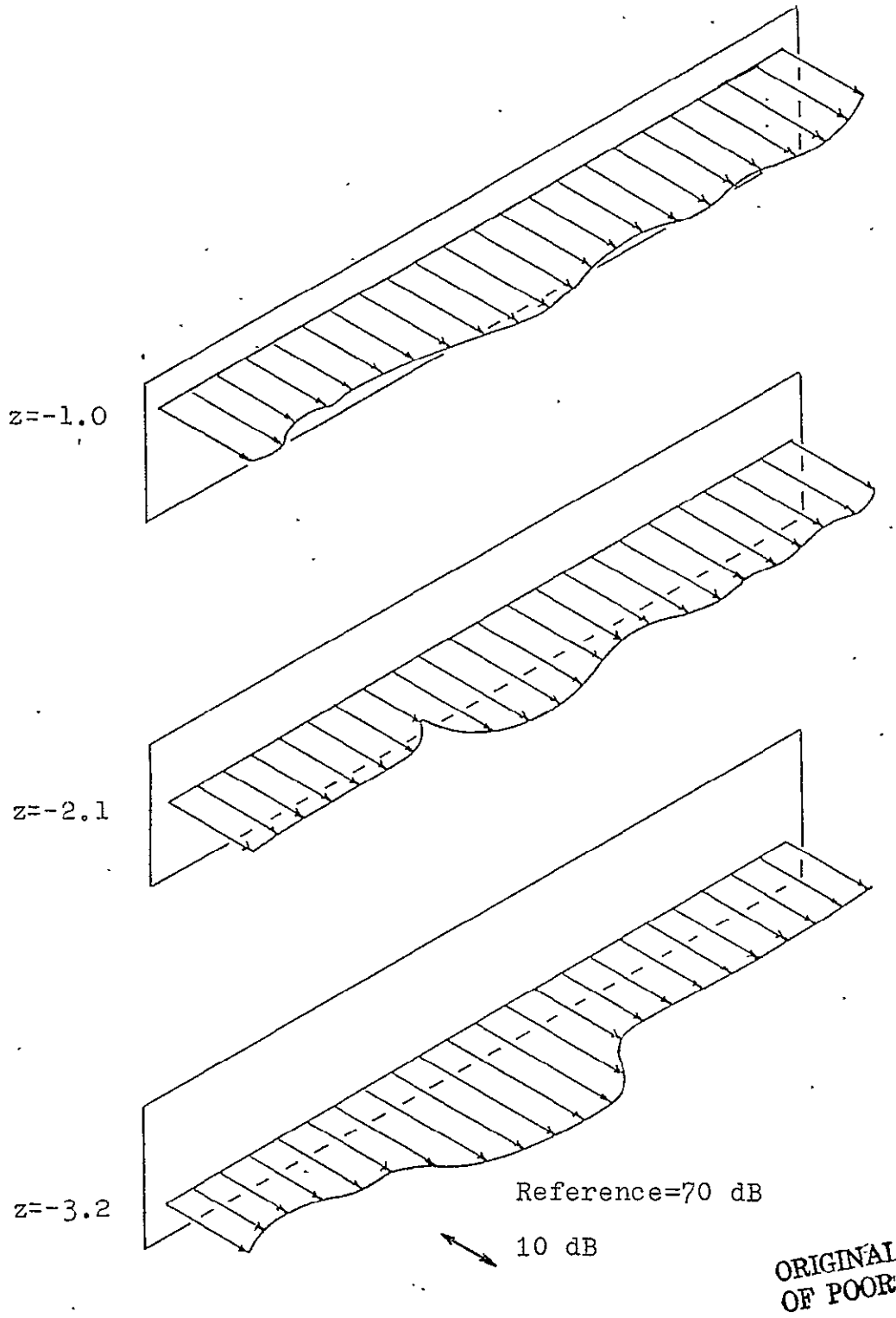

Figure 4.15 Exit Plane Rms Static Pressure Profiles-Wing In

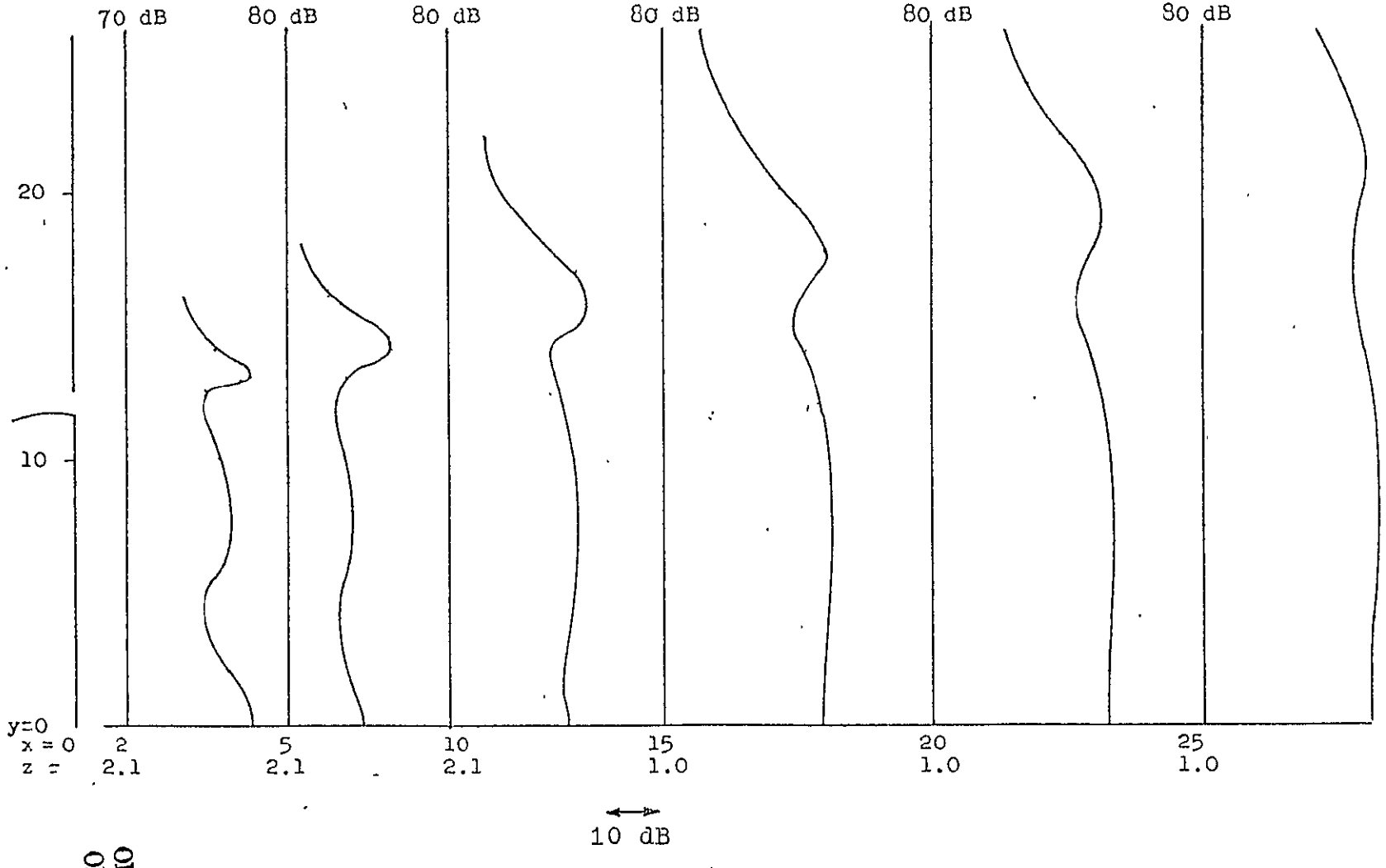

Figure 4.16 Lateral Rms Static Pressure Profiles-Wing In

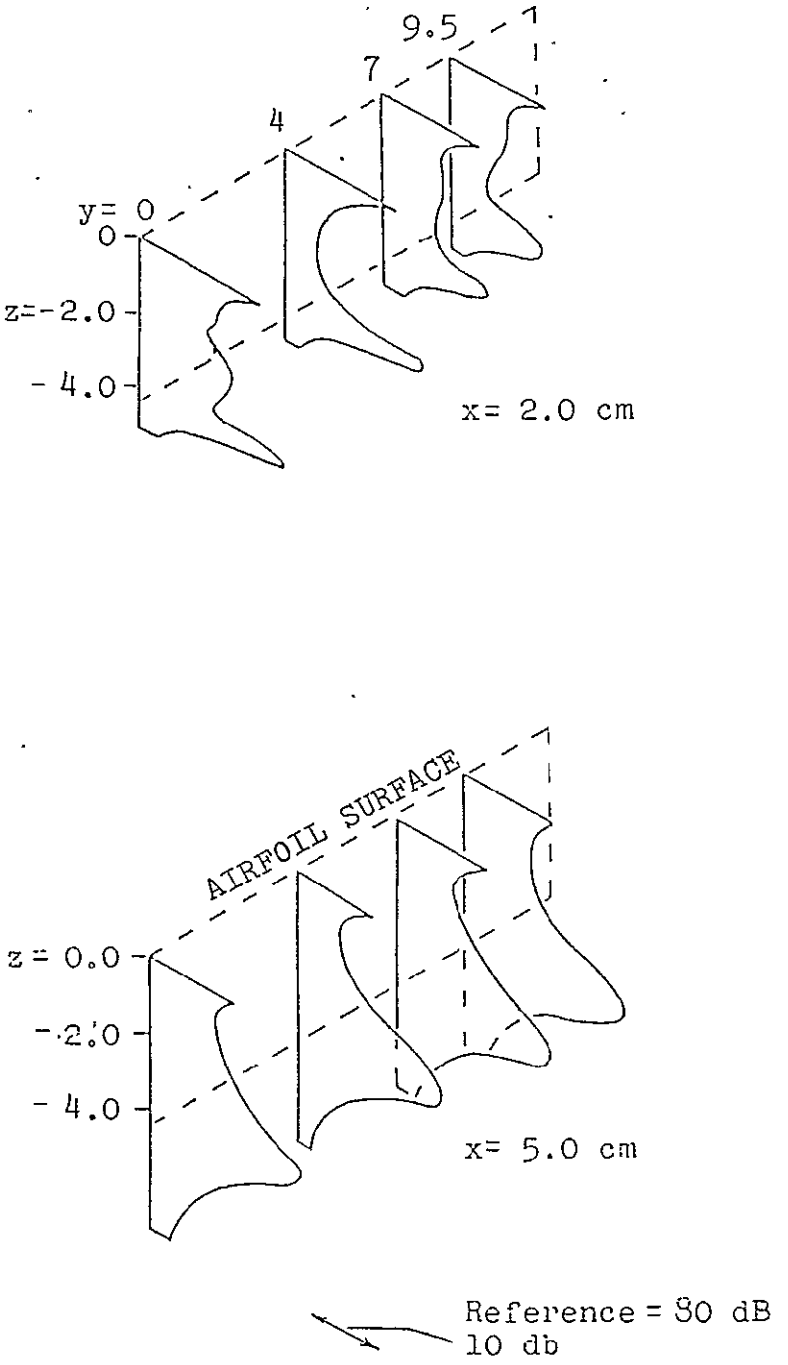

Figure 4.17 Rms Static Pressure Profiles-Wing In

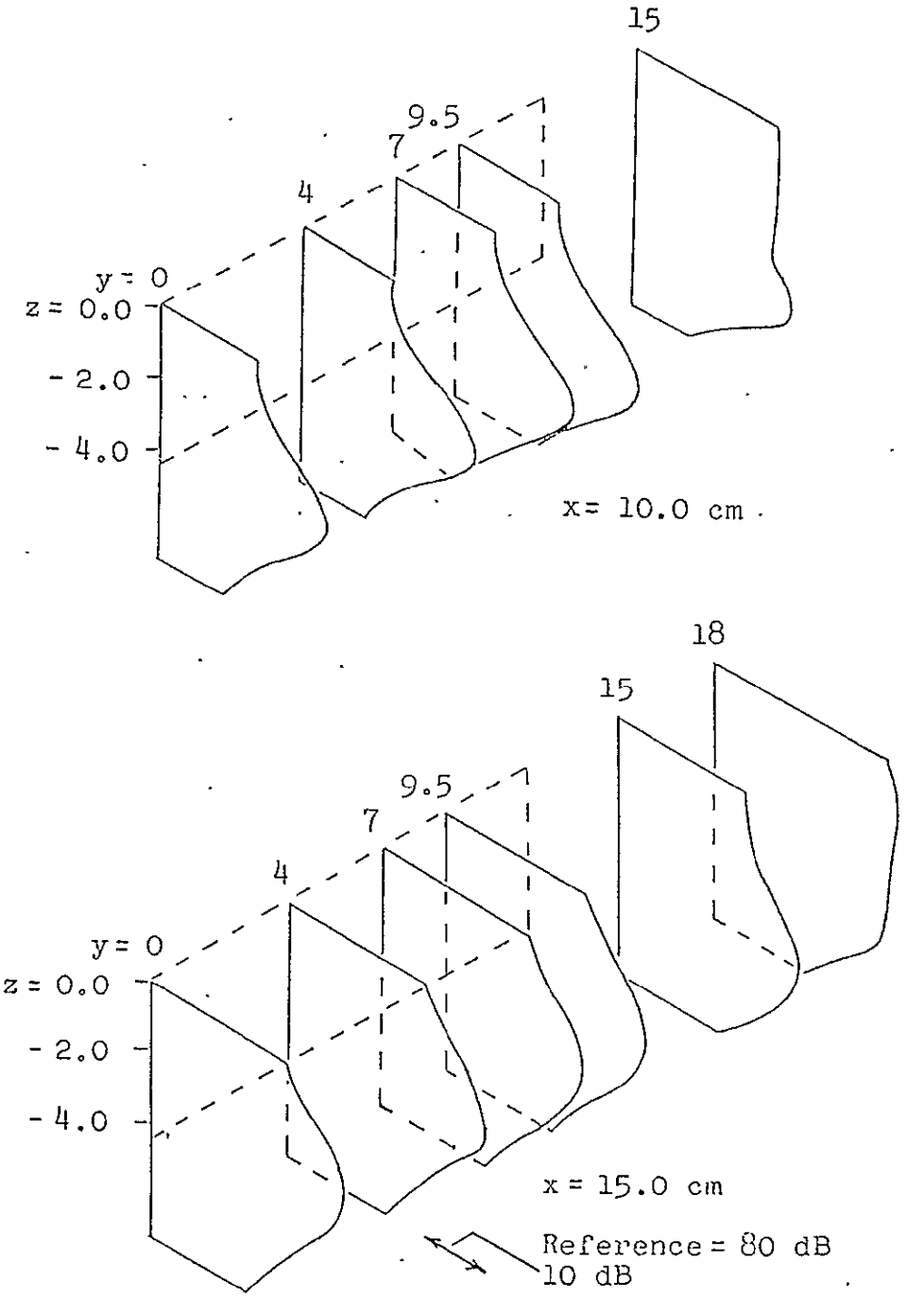

Figure 4.18 Rms Static Pressure Profiles-Wing In

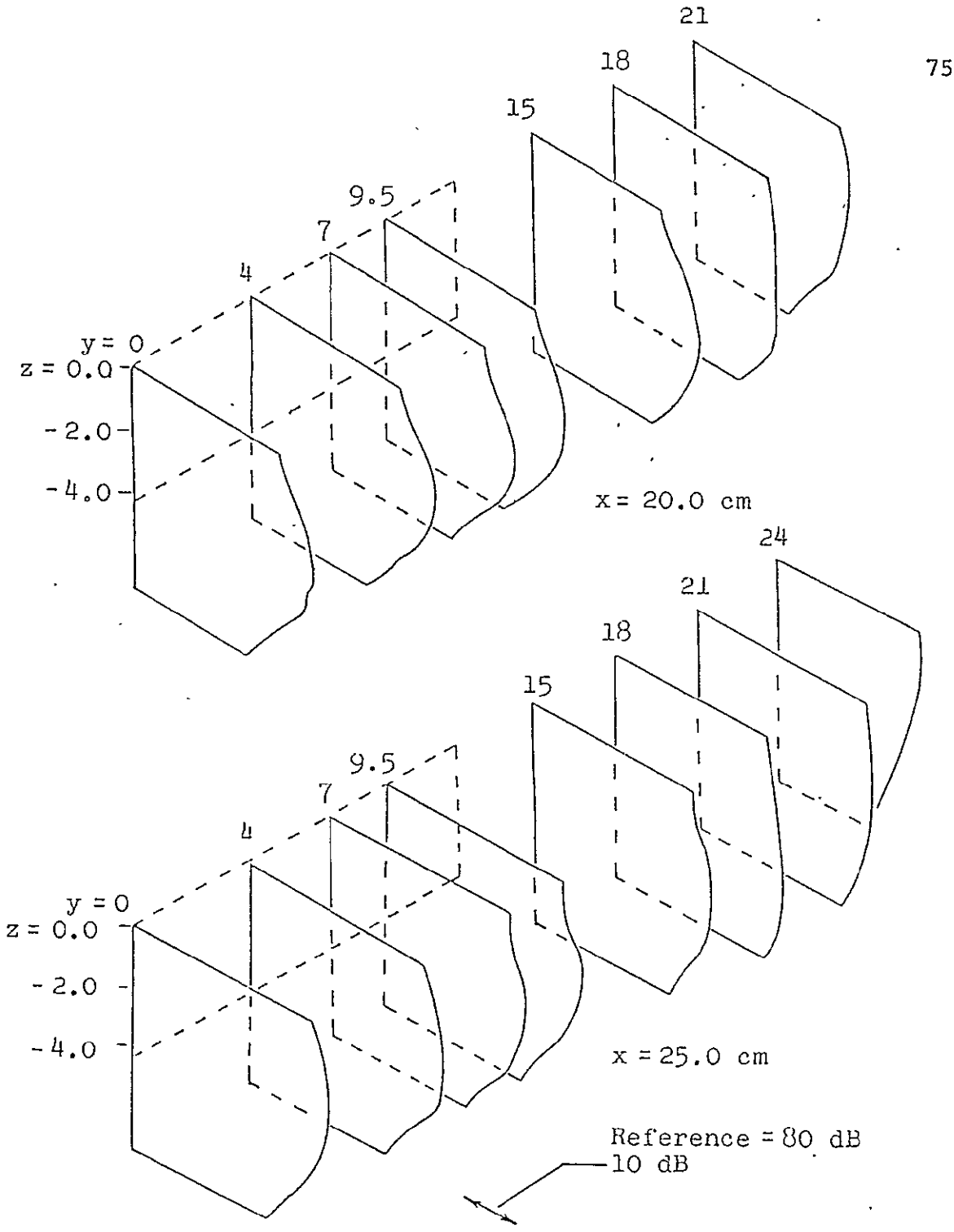

Figure 4.19 Rms Static Pressure Profiles-Wing In

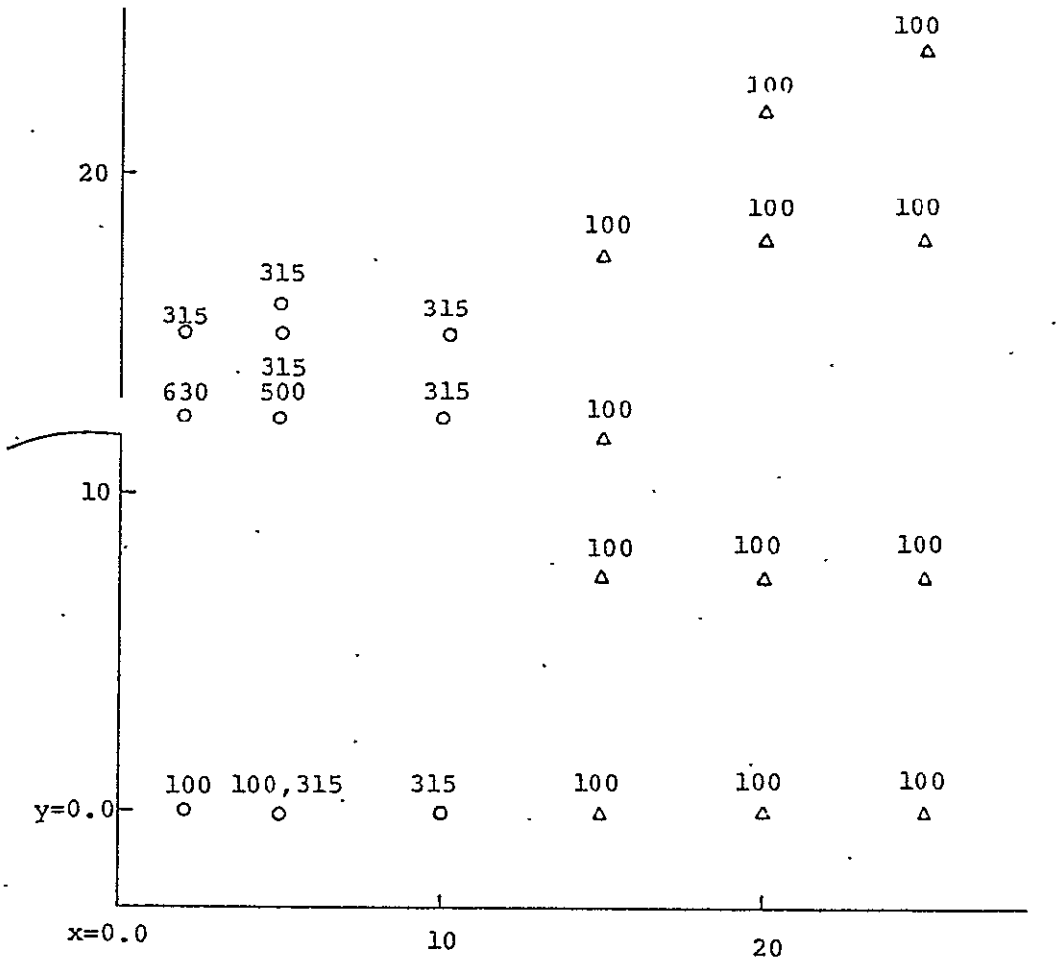

Figure 4.20 Third Octave Survey of Peak Frequencies (Hz)- Wing In

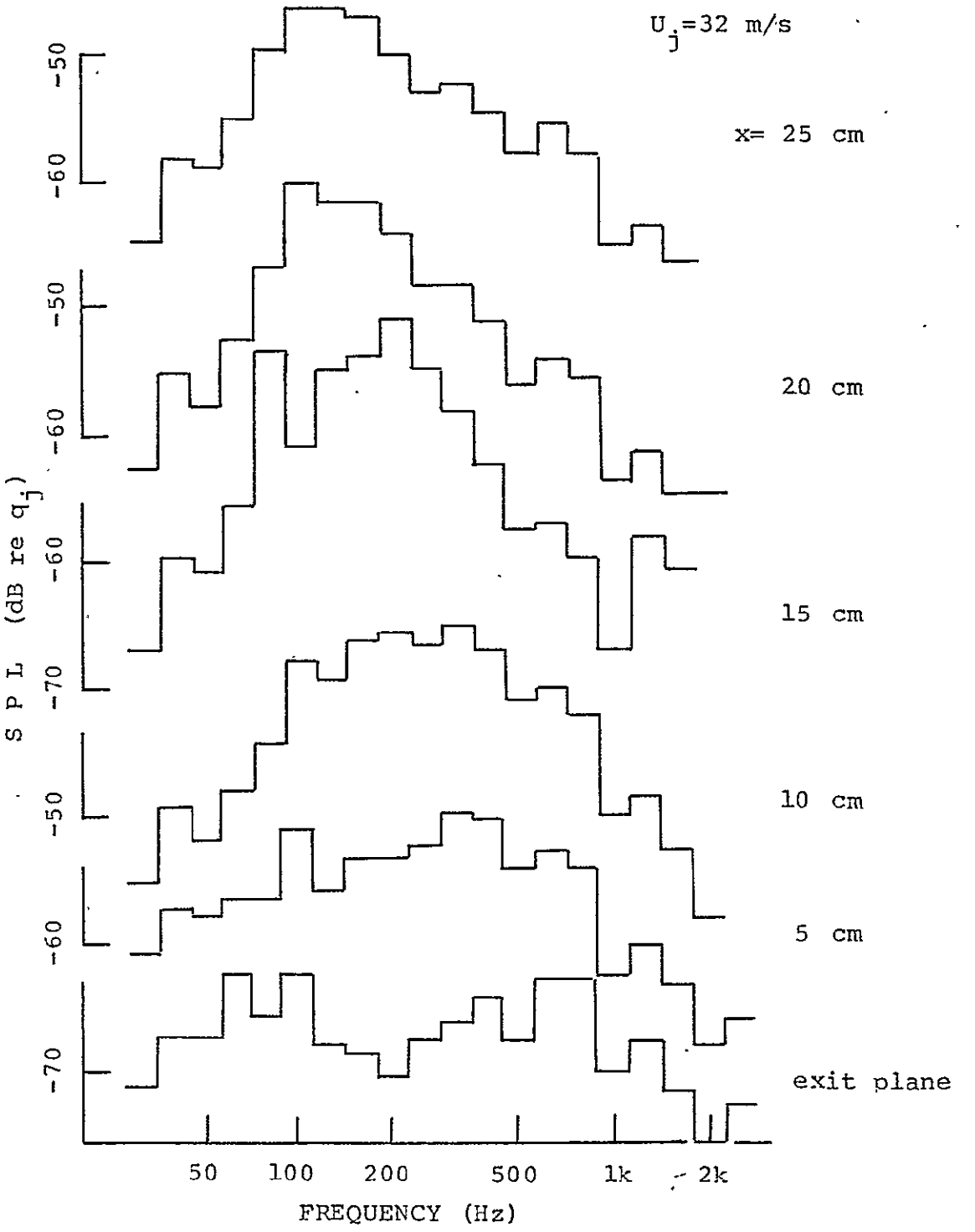

Figure 4.21 Downstream Centerplane Spectral Evolution

close to the nozzle are relatively unchanged. The outer flow spectra shown in Figure 4.22 and the cross stream comparison in Figure 4.23 compares closely in shape with those obtained with the wing removed although the 100 Hz frequency peak again was accentuated with the wing in place.

Correlation Measurements

Correlation measurements made with the wing removed were repeated with the wing in place except at the downstream position of x = 8.3 cm. Table 4.5 lists the correlation coefficients obtained at the downstream positions of x = 17 and 22 cm for various lateral and vertical probe separations. Two differences between the wing in and wing out cases are apparent. The first is that close agreement between the x = 17 and 22 cm axial positions are obtained in the bounded jet where this is not true in the free jet. Second, higher correlation coefficients and less rapid decay of the spatial correlation curve were observed in the bounded jet than in the free jet. These points are emphasized by Figure 4.24 which compares the two flow conditions.

Convection velocities determined in the bounded jet are listed in Table 4.6. The same procedures as were used in calculating convection velocities in the free jet were used for the bounded jet. As can be seen from Tables 4.4 and 4.6 convection velocities in the bounded jet were slightly lower than in the free jet. In addition, in both the bounded and free jet flows there was a tendency for convection velocities to decrease with increasing lateral distance from the jet centerplane, this effect being more pronounced in the bounded jet. This decrease could be the result of jet spreading which, as mentioned earlier, was greater in the bounded jet. Vortices in the flow field may have had a lateral component of convection velocity such

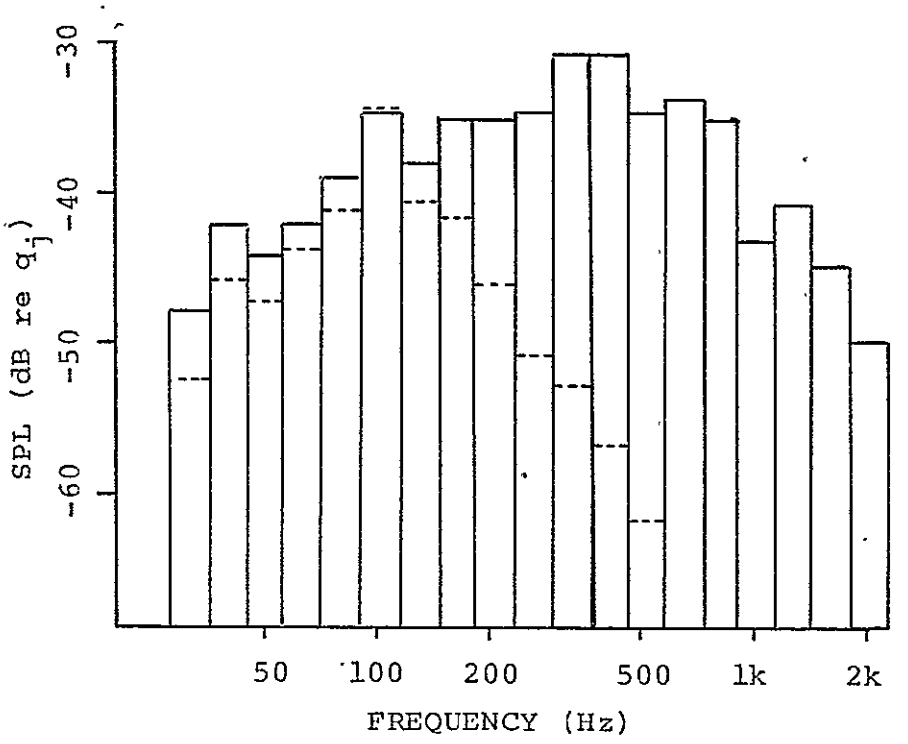

Figure 4.22 Outer Flow Downstream Spectral Evolution-Wing In

x=20 cm
z=-1.0 cm

--- y=0.0 cm
—— y=7.5 cm
••• y=22 cm

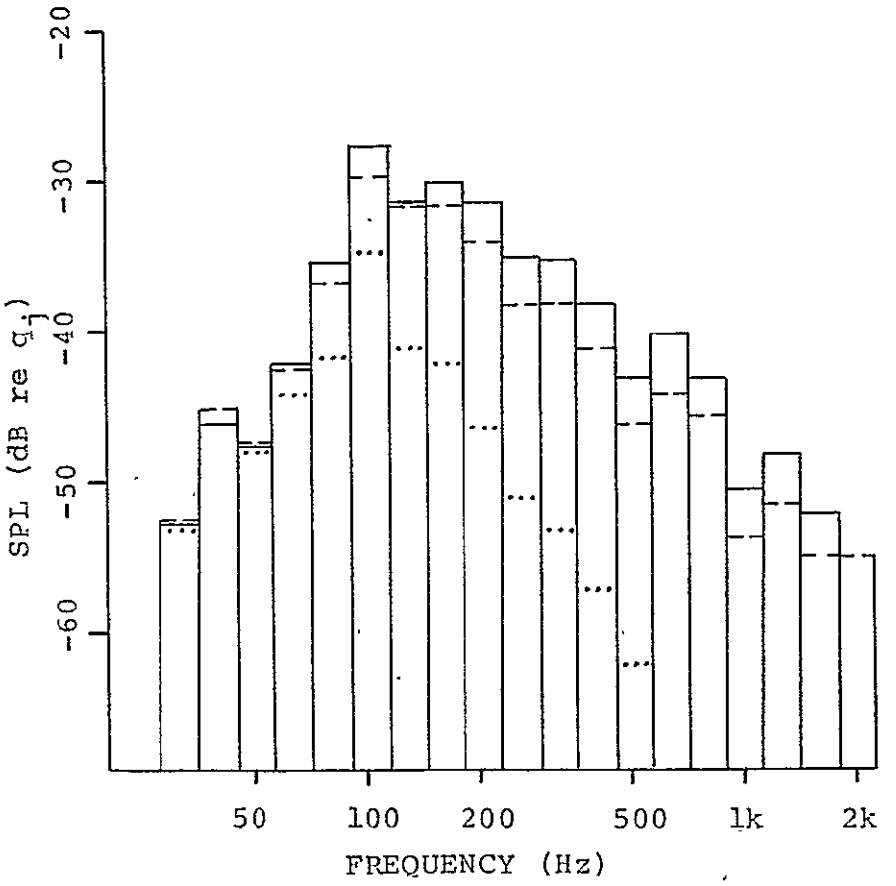

U_j=32 m/s

Figure 4.23 Cross-stream Spectral Comparison-Wing In

Table 4.5

Cross - correlation Coefficients in Bounded Jet (Wing In)

	ρ_{12}	
y Separation	x = .7 cm	x = 22 cm
0.3 cm	1.0	
0.5 cm	.97	.97
5.0 cm	.54	.50
11.7 cm	.14	.15
17.1 cm	.07	.07
20.6 cm	.04	.05
z Separation		
1.1 cm	.91	.90
3.2 cm	.73	.77
6.0 cm	.81	.82

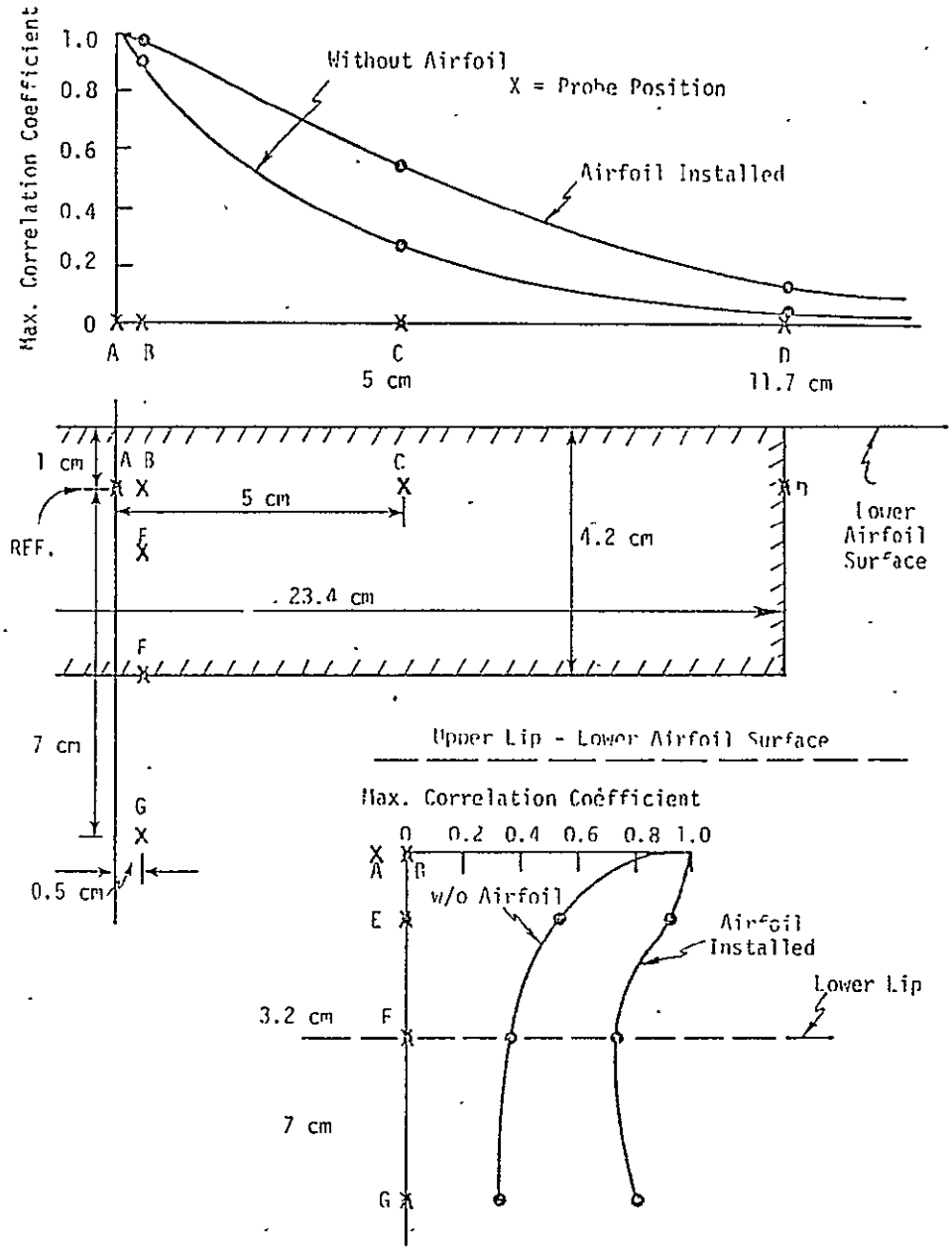

Figure 4.24 Comparison of Correlation Measurements-
Wing In vs. Wing Out

Table 4.6
Convection Velocities (Wing In)

Position	U_c/U_j Low freq.	Med. freq.
x=17.0 cm, z=-1.0 cm, y=0.0 cm	.29	.41
x=17.0 cm, z=-1.0 cm, y=5.0 cm	.26	.41
x=17.0 cm, z=-2.1 cm, y=0.0 cm	.62	
x=17.0 cm, z=-4.2 cm, y=0.0 cm	.35	.49
x=17.0 cm, z=-7.0 cm, y=0.0 cm	.38	.49
x=22.0 cm, z=-1.0 cm, y=0.0 cm	.38	.54
x=22.0 cm, z=-1.0 cm, y=5.0 cm	.24	.54
x=22.0 cm, z=-1.0 cm, y=11.7 cm	.24	.47
x=22.0 cm, z=-1.0 cm, y=17.1 cm	.27	.35
x=22.0 cm, z=-1.0 cm, y=20.6 cm	.15	.35
x=22.0 cm, z=-2.1 cm, y=0.0 cm	.40	.61
x=22.0 cm, z=-4.2 cm, y=0.0 cm	.54	.65
x=22.0 cm, z=-7.0 cm, y=0.0 cm	.61	

that a pair of probes set up to measure axial convection velocities would only measure one component of the actual convection velocity. Thus it would have appeared that convection velocities decreased with increasing lateral position. As a result of the above trends instrumentation was provided on the wing surface by which two components of convection velocities can be determined (on the wing surface). These measurements, when completed, should provide additional insight into the nature of coherent structures within the bounded flow.

4.2 Investigation of High Frequency Peak

Third-octave measurements made with a static probe indicated the presence of a high frequency secondary peak. This peak was observed at positions close to the exit plane opposite the upper and lower nozzle lips at a frequency of 1.6 to 2.0k Hz. Figure 4.25 illustrates the rapid decay of this peak with increasing distance downstream. The spatial distribution of this disturbance in the vertical direction was even more restricted where its influence was limited to no more than one centimeter bands centered on the upper and lower nozzle lips. Evidence of a high frequency peak was not found at positions adjacent to the right and left nozzle lips. The presence of the wing had no effect on this peak but the frequency of the peak was found to be velocity dependent as can be seen from Figure 4.26. Changes in the thickness of the nozzle lip resulted in no changes in the frequency of the peak. This disturbance did not appear to be in the boundary layer of the internal flow as it did not show up in spectra made from the adjustment cone port (see Figure 3.22). Convection velocity measurements indicated that the disturbance was not acoustic as is evidenced by Figure 4.27 which is a phase lag

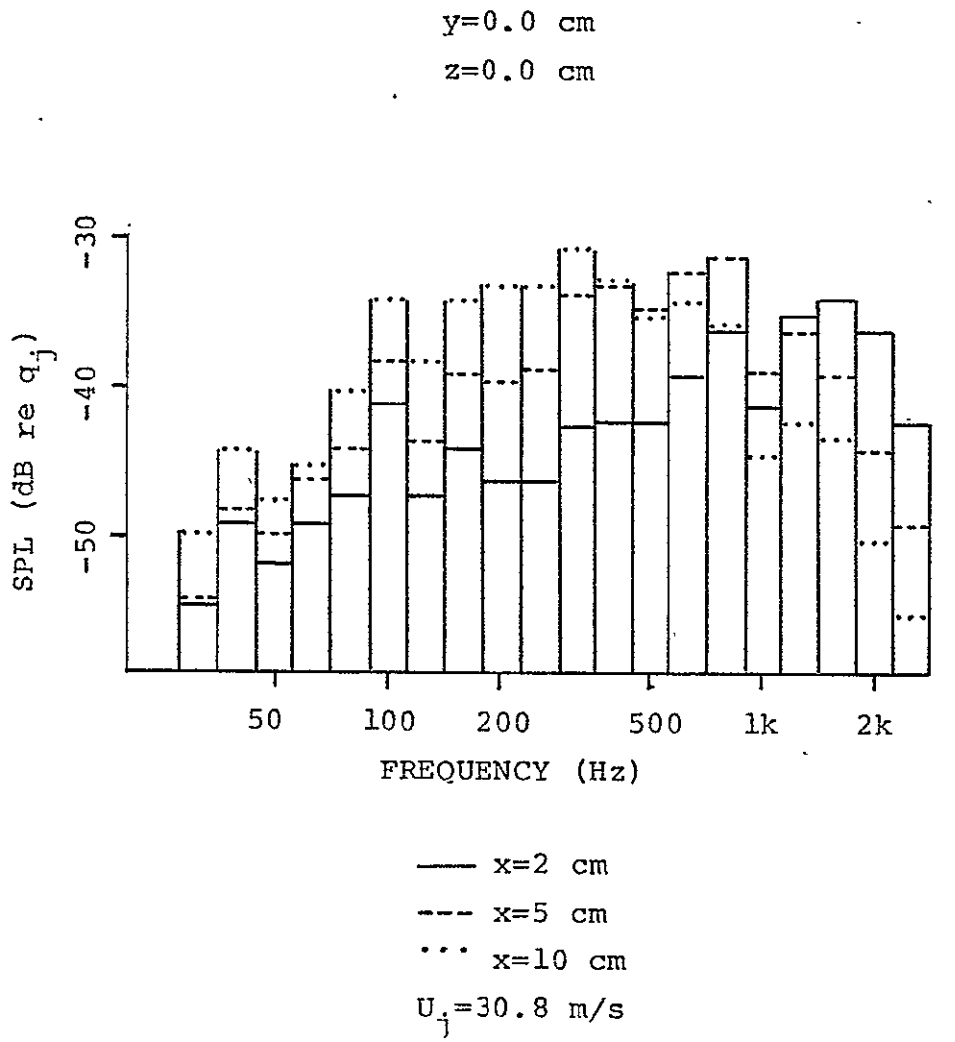

Figure 4.25 Downstream Decay of High Frequency Peak

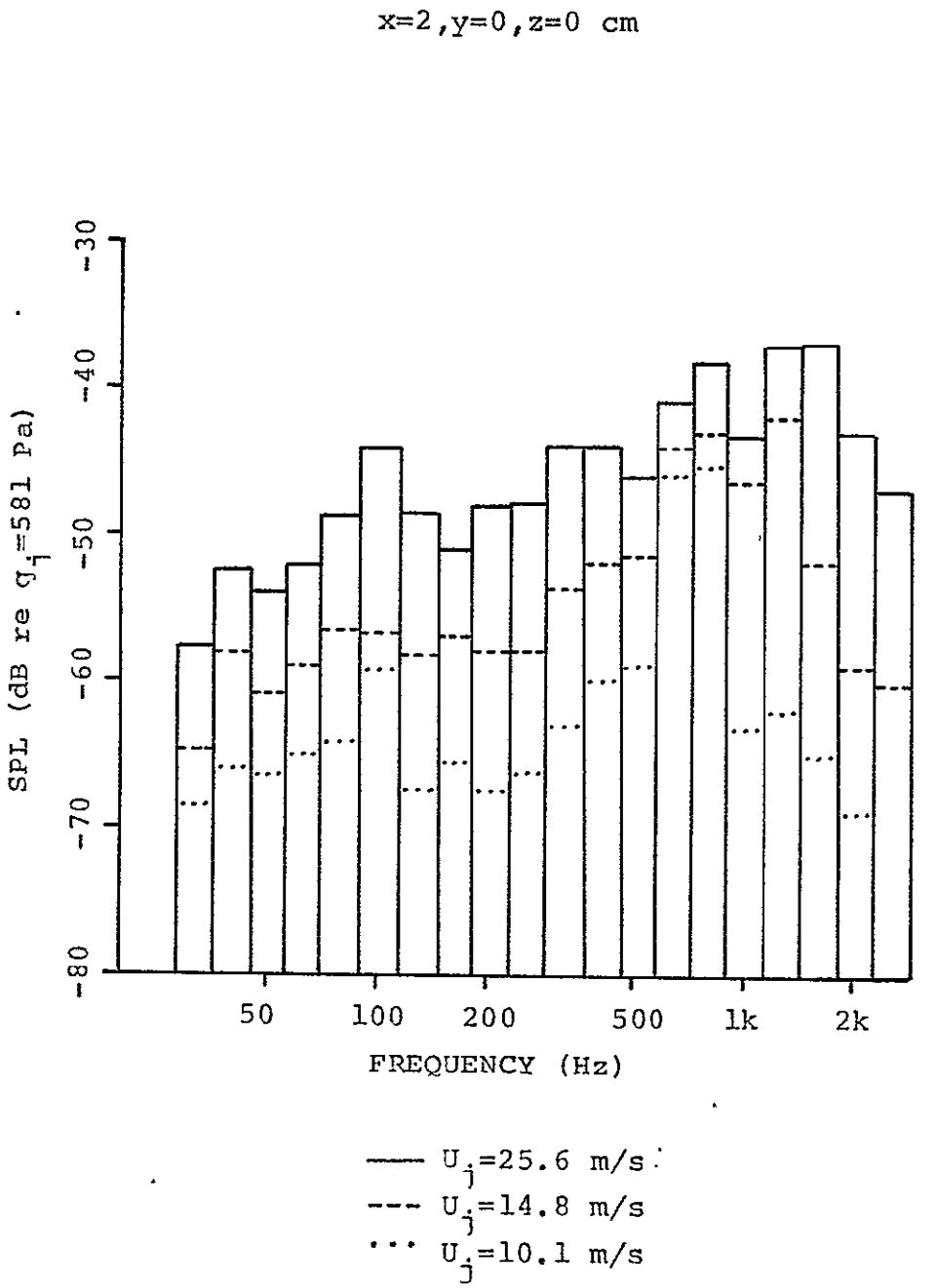

Figure 4.26 Velocity Dependence of High Frequency Peak

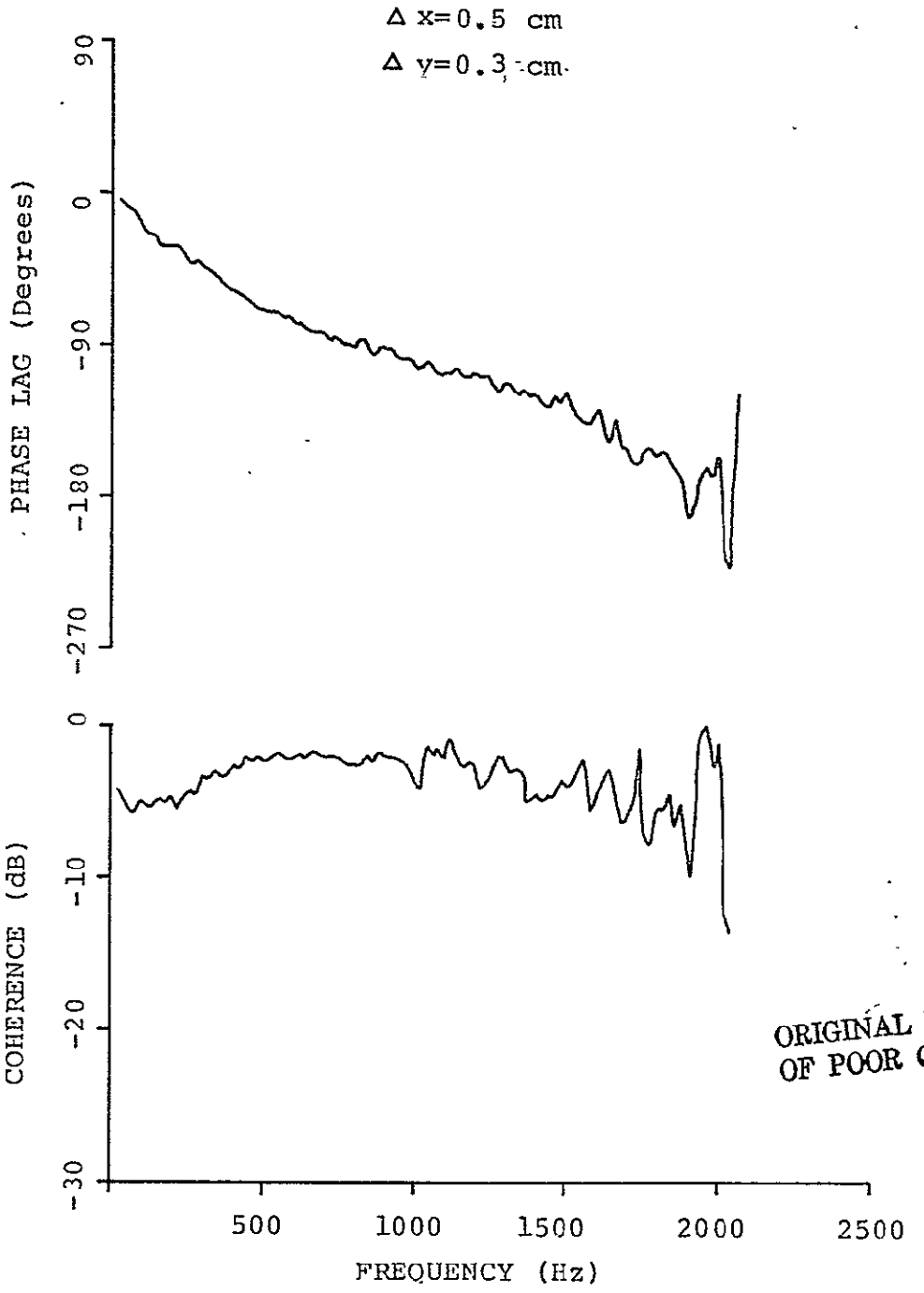

Figure 4.27 Phase and Coherence for Convection Velocity Determination of High Frequency Peak: x=2,y=0.0,z=-4.2 cm

plot measured adjacent the lower lip. The convection velocity measured was approximately 0.6 the jet exit velocity.

Crow and Champagne (ref. 5) discussed a high frequency structure in their paper on circular jets which appears to be similar to the disturbance observed in the present work. As indicated earlier, Crow and Champagne found that the high frequency structure, found only near the nozzle adjacent the lip, scales on the thickness of the laminar boundary layer leaving the nozzle lip. If the boundary layer is tripped producing a turbulent boundary layer, they reported that the high frequency structure disappears. They also found that the disturbance had a phase velocity of about 0.5 the jet exit velocity. An attempt to trip the boundary layer in the nozzle of the present study, which would have provided a further clue as to the nature of the high frequency peak, was not made.

4.3 Influence of Jet Boundary Conditions

As described earlier, mufflers were installed in the system to provide a greater degree of control over the boundary conditions of the jet in the exit plane of the nozzle. It was suspected that acoustic noise from the air supply may have excited the flow causing the development of coherent structures associated with frequencies which depend on the frequency of excitation. This phenomenon has been well documented for circular jets by Crow and Champagne (ref. 5) but has yet to be demonstrated in rectangular jets. The results of the present study indicate the presence of similar effects in rectangular jets.

It has already been established that significant noise levels are present in the nozzle cavity with no mufflers and that these levels are reduced by the mufflers. However, the effect of these changes on the flow is uncertain, as

can be appreciated by examination of Figure 4.28.

Only muffler A exerted any desirable influence on pressure levels in the exit plane by bringing the levels down to the limits of the sensitivity of the microphone with the exception of the 31.5 and 40 Hz bands. Thus at these levels an accurate determination of the pressure levels in the exit plane was not possible with the 1/8 inch microphone which meant only a maximum value could be assigned, so that, the levels may be less but are no greater than those presented in Figure 4.28 for muffler A. The results for muffler B indicate poor performance as a muffler but it did provide a background level different from muffler A and from no-muffler conditions by which to judge the effects of different exit plane levels on the flow. The differences between spectra 5 cm downstream are relatively small, particularly the magnitude and frequency of the peak. The effects of pressure levels in this range in the exit plane on the flow 5 cm downstream are negligible except at the low frequencies.

Though there are several possible explanations for these observations, it was believed that the most likely explanation is that the pressure levels were too small to excite the flow. A quick experiment was performed in an attempt to establish this more firmly. Sinusoidal signals were fed into the plenum chamber at several different frequencies. These single frequency excitations produced peaks at the corresponding frequencies that were well above the pressure levels of neighboring frequencies. From Figure 4.29, which is a third octave spectrum at x = 5 cm along the centerline of the facility (z = -2.1, y = 0.0), it can be seen that the peaking was much more pronounced than spectra measured without acoustic stimulus. That the peak measured in the flow was not acoustic is demonstrated by Figure 4.30 which

C-2

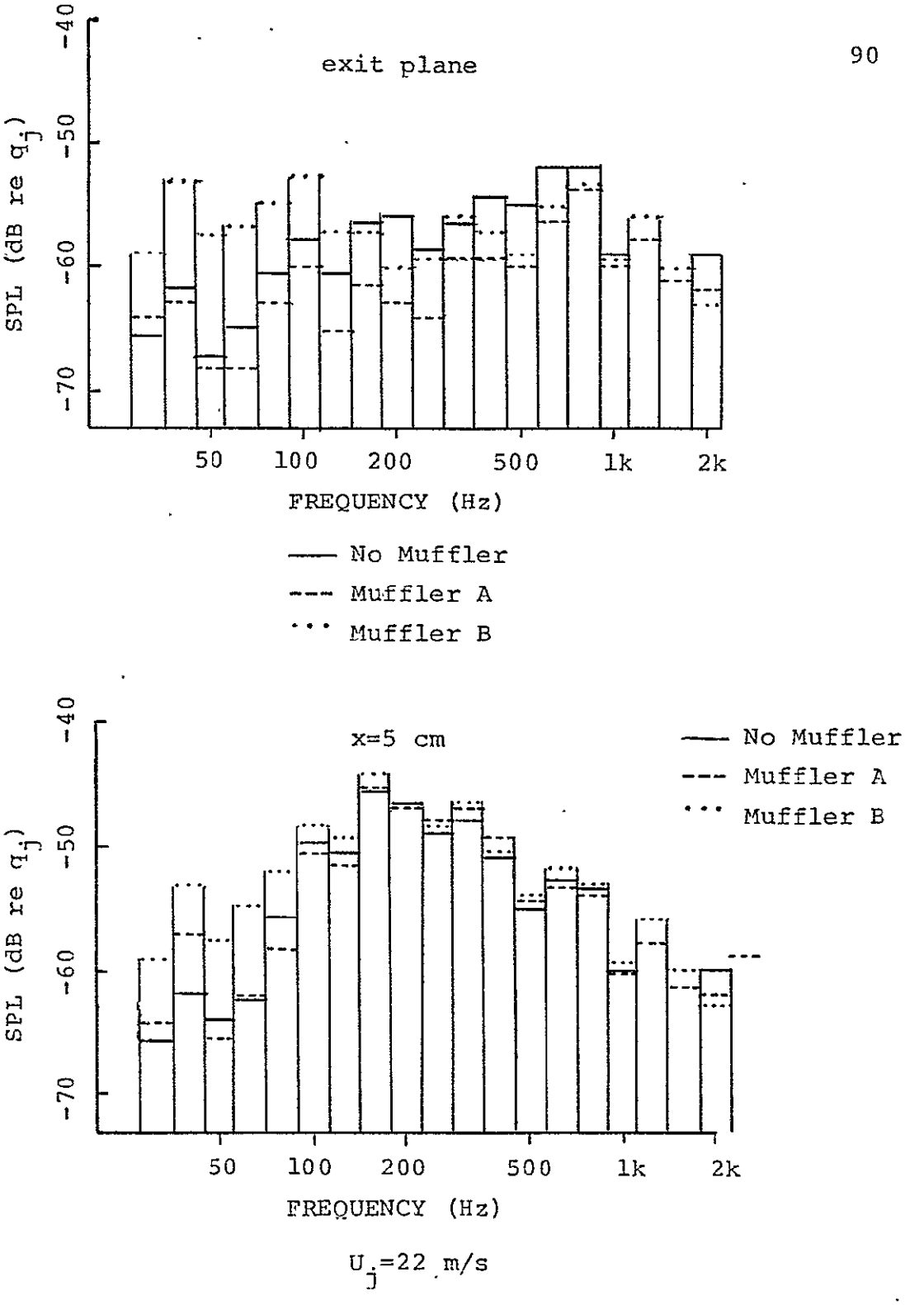

Figure 4.28 Influence of Muffler on Flow: y=0.0, z=-2.1

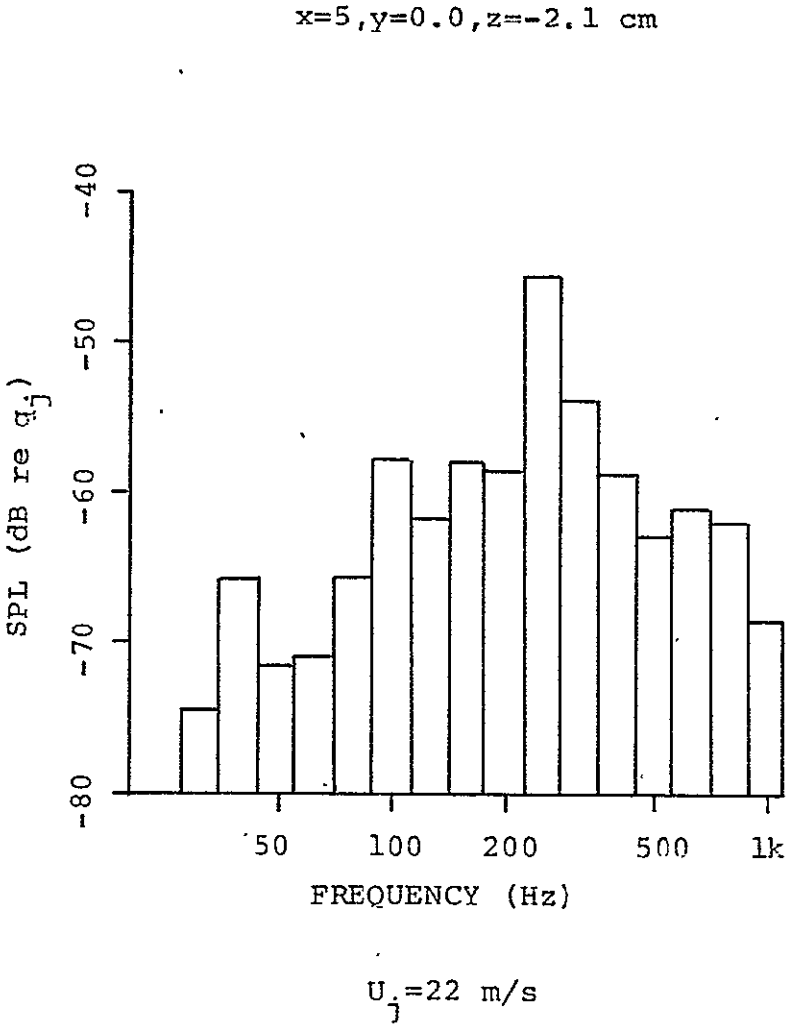

Figure 4.29 Third Octave Spectrum with 250 Hz Excitation

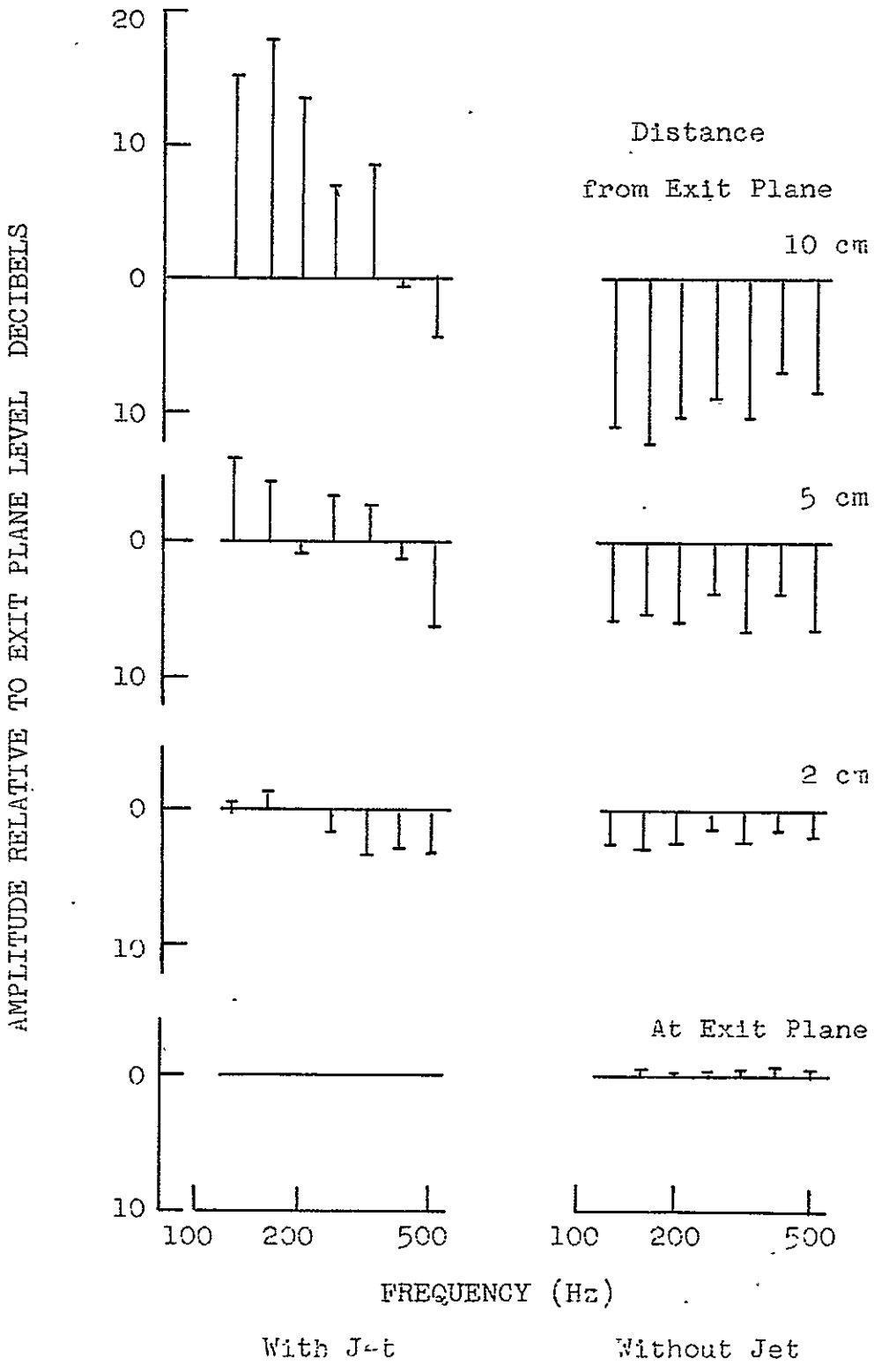

Figure 4.30 Jet Response to Acoustic Excitation in Exit Plane

is third - octave pressure levels with and without air flowing referenced to levels at the exit plane with air flowing. The increase in pressure level for a particular frequency with increasing distance downstream with air flowing and the decrease in pressure level with increasing distance downstream with no air flowing indicate the disturbance tripped in the flow was not acoustic, and therefore was presumably due to a vortex structure. Although this experiment was brief, it demonstrates that it is possible to excite the flow in a rectangular jet producing spectral peaks in a range of frequencies. It is interesting to note that at the downstream locations monitored the frequency which produced the greatest response in the flow was 160 Hz. For the jet speed used (22 m/sec) and assuming a peak at a Strouhal number of 0.3, the 160 Hz peak corresponds to a dimension of 4.1 cm which is the minor dimension of the rectangular nozzle.

4.4 Surface Pressure Measurements

Surface pressure measurements were made at four locations along the centerline of the model wing for comparison with power spectral densities measured on the full scale wing in the "Beach" facility at NASA Langley. Measurements on the model consisted of sound pressure levels (SPL) in third - octave bands that were corrected for probe response converted to power spectral densities, (PSD), and then non-dimensionalized for comparison to full scale data. The third - octave to power spectral density conversion is given by

$$P.S.D. = (10)^{\frac{SPL - 94}{10}} \times \frac{1}{B.W.} ,$$

where B.W. refers to third - octave band widths. Both

model and full scale power spectral densities were non-dimensionalized by referencing to the square of the jet dynamic pressure divided by frequency, q_j^2/f. Frequencies were nondimensionalized by Strouhal number, fd/U_j, where the effective diameter of the nozzles, d_{eff}, were used (d_{eff} = 9.3 cm for model and d_{eff} = 35.7 cm). Full scale and model flow conditions are listed in Table 4.7 below.

Table 4.7
Model and Full Scale Flow Conditions

	U_j	Temperature	Mach No.
Full Scale	277.4 m/s	610 k	0.56
Model	21.6 m/s	294 k	0.06

Figure 4.31 presents the comparison between model and full scale spectra. Agreement between full scale and model is relatively good except at the P3 position. This lack of agreement at P3 could be the result of any one or a combination of several reasons. The impingement angle of the model wing did not duplicate the full scale angle. The separation between wing surface and inside nozzle surface was not properly scaled due to construction limitations on the model (the nozzle lips were about the same thickness on model and full scale). Rather than having the wing overlap the nozzle exit plane as was done the wing surface could be mounted flush with the inside nozzle surface. Installation of the core nozzle may be necessary to increase accuracy, or introduction of acoustic noise in the plenum to simulate turbofan engine noise may be required. It is within the capacity of the facility to study the effect of changes in these variables, which should be done.

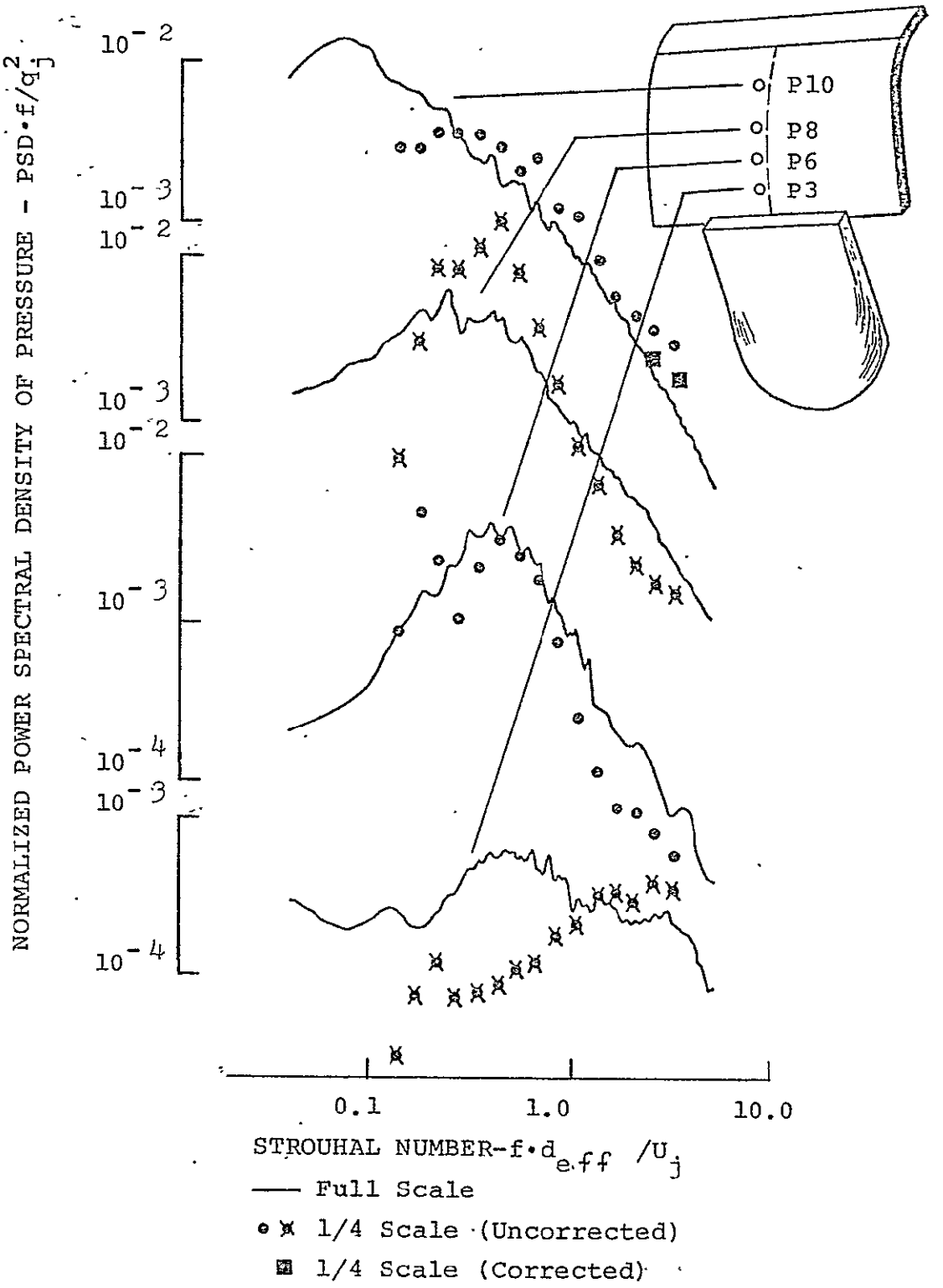

Figure 4.31 Comparison of Model and Full Scale Spectra

One limitation of the facility is evident from the P10 curves. Without the installation of additional filters, third - octave analysis cannot measure low enough frequencies to simulate the low frequencies in the full scale set-up due to the large difference in velocities ($f_{F.S.}/f_m$=2.12). The low frequencies can be handled using correlation techniques but the advantage of making real time measurements and the capability of controlling the averaging time while maintaining fixed bandwidths is lost. However, further study may indicate that repeatability for the low frequencies is poor (less than 30 Hz) requiring the avoidance of these frequencies. If the requirement to scale the full scale low frequencies is strong, either high velocities or a smaller scale in the model would change the frequency scaling such that the very low frequencies could be avoided.

A final comment on scaling from the model facility concerns the mufflers. Muffler A was in place during the wing surface measurements and its effect is evident in the curves for P6. The low frequency peak in the PSD curve from the model corresponds to the 40 Hz third - octave band which has been shown to be influenced by muffler A. Thus additional work on the mufflers is required to improve the scaling accuracy of the facility.

Chapter 5 Concluding Remarks

It was the goal of this study to develop a model jet facility characteristic of a jet STOL propulsive lift configuration and to demonstrate its feasibilities as an investigative tool for the study of scaling laws involved in dynamic pressure loadings on wing surfaces in such configurations. The initial results were encouraging as evidenced by comparison of model and full scale pressure spectra measured on wing surfaces. Based on these results it is felt that further development and study of the model facility and its flow field is warranted.

Results from the initial survey have indicated that the concept of coherent structures in circular jets is applicable to rectangular jets. However, whereas in circular jets these structures scale on a single dimension, the nozzle diameter, in rectangular jets there appear to be three relevant dimensions, the major and minor dimensions of the rectangular nozzle and an effective diameter as proposed by Stone (ref. 9). The influence of vortices associated with these dimensions varies depending on the location in the flow. The smaller vortices develop and decay at smaller downstream distances than the larger vortices. The installation of a wing surface in the flow had a marked effect on the area of influence of the vortices, with this area increasing when the wing was in place.

Of primary concern for effective use of the facility is the establishment of probe transfer functions. Mechanical compensation would be desirable in that it would allow analog measurements such as third - octave spectra to be made without the need for time consuming corrections which must be done by hand. Should mechanical compensation prove to be impractical, digital data processing lends itself to

correction by electronic means after the transfer function has been determined analytically or experimentally.

Initial indications were that establishment of a reliable surface probe will be straight forward while the development of a free static probe will be more difficult. Although it can be argued that for the purpose of studying fluctuating loads on wing surfaces free probes may not be needed, it is felt that a reliable free probe would sufficiently enhance the capabilities of the facility to justify its development. A reliable free probe would not only allow more detailed studies of the free flow but pressure correlations between free and surface probes could be made to further understand mechanisms producing fluctuating wing loads. Therefore work should continue on the free probe but on a lower priority basis.

Assuming firm establishment of both free and surface probe transfer functions has been made, the versatility of the model facility could then be exploited. The particular studies made with the facility would depend to a certain degree on the aims of the project. Within the structure of the current research project, whose goal is the development of scaling laws for fluctuating pressure loads, studies should be initiated into the effects of changes in several variables on scaling wing pressure spectra. These variables would include wing impingement angles, nozzle flow deflectors, and acoustic levels in the exit plane. If this fails to produce satisfactory scaling then the assumption of perfect mixing should be relaxed requiring the installation of a core nozzle which would provide coaxial flow.

With the core nozzle in place effects of changes of the above variables should be rechecked. If satisfactory pressure scaling still has not been achieved, then a hot jet facility would be required. With a hot facility all full

scale flow variables could be scaled such as Mach numbers, dynamic pressure ratios, and mass flow ratios.

Assuming satisfactory pressure scaling is obtained with the cold facility, a more detailed investigation of pressure fluctuations on the wing surface should be made. The wing has been instrumented such that correlations can be measured with lateral (Δy), longitudinal (Δx) and, with a free probe, vertical (Δz) separations. Two components (lateral and longitudinal) of convection velocities can be determined at various locations.

Techniques for the construction of nozzles have been established so that various geometric nozzle configurations can be installed, such as a "D" shaped nozzle. Thus a family of nozzles and their associated scaling laws can be studied.

Further investigation of the free flow should be initiated. More detailed correlation studies of lateral and vertical probe separations (large longitudinal probe separations are not practical with free probes due to probe interference), as well as convection velocity investigations, with pressure surges imposed on jet background conditions using the loudspeaker arrangement would provide added insight into the nature of coherent structures in rectangular jets. Comparison with bounded jet measurements may help to further understand these structures and their interaction with wing surfaces.

REFERENCES

1. Schroeder, J.C., "Development of Experimental Techniques for Investigation of Unsteady Pressures behind a Cold Model Jet", M.S. Thesis, The University of Virginia, 1976.

2. Catalano, G.D., "An Experimental Investigation of an Axisymmetric Jet in a Coflowing Airstream", M.S. Thesis, The University of Virginia, 1975.

3. Lau, J.C., M.J. Fisher and H.V. Fuchs, "The Intrinsic Structure of Turbulent Jets", J. Sound and Vibration, 1972.

4. Davies, P.O.A.L., "Structure of Turbulence", J. Sound and Vibration, 1973.

5. Crow, S.C. and F.H. Champagne, "Orderly Structure in Jet Turbulence", J. Fluid Mechanics, 1971.

6. Mixon, J.S., J.A. Schoenster and C.M. Willis, AIAA Paper 75-472, 1975.

7. Schoenster, J.A., "Acoustic Loads on an Externally Blown Flap System due to Impingement of TF-34 Jet Engine Exhaust", NASA Report TM X-71950, 1973.

8. Shivers, J.P. and C.C. Smith, Jr., "Static Tests of a Simulated Upper - Surface Blown Jet - Flap Configuration Utilizing a Full - Size Turbofan Engine", NASA TN D-7816, 1975.

9. Stone, J.R., "Interim Prediction Method for Jet Noise", NASA TM X-71618, 1974.

10. Fuchs, H.V., "Measurement of Pressure Fluctuations Within Subsonic Turbulent Jets", J. Sound and Vibration, 1972.

11. Siddon, T.E., "On the Response of Pressure Measuring Instrumentation in Unsteady Flows", UTIAS Report No. 136, 1969.

12. Strausberg, M., "Measurements of the Fluctuating Static and Total - Head Pressures in a Turbulent Wake", Research and Development Report, Dept. of the Navy, 1963.

13. Willmarth, W.W. and F.W. Roos, "Resolution and Structure of the Wall Pressure Field beneath a Turbulent Boundary Layer", J. Fluid Mechanics, 1965.

14. Meecham, W.C. and D.R. Regan, AIAA Paper 75-505, 1975.

15. Miller, David R. and Edward W. Comings, "Static Pressure Distribution in the Free Turbulent Jet", J. Fluid Mechanics, 1957.

16. Beranek, Leo L., Noise and Vibration Control, McGraw-Hill, Inc., New York, New York, 1971.

17. Davies, P.O.A.L., "Coherent Structures in Turbulence", Seminar, Joint Institute for Acoustics and Flight Sciences, NASA - Langley, October 9, 1974.

18. Davies, P.O.A.L., "Viscous Vortex Rings", Seminar, Joint Institute for Acoustics and Flight Sciences, NASA - Langley, October 16, 1974.

DISTRIBUTION LIST

Copy No.	
1 - 2	NASA Scientific and Technical Information Facility P. O. Box 8757 Baltimore/Washington International Airport Maryland 21240
3 - 5	Mr. James Schoenster M/A 463 Building 1208 A.N.R.D. - Structural Acoustics Section Langley Research Center Hampton, Virginia 23365
6	Dr. John Mixson M/S 463 Building 1208 A.N.R.D. - Structural Acoustics Section Langley Reserach Center Hampton, Virginia 23365
7 - 8	J. K. Haviland
9 - 10	J. B. Morton
11	L. S. Fletcher
12	I. A. Fischer OSP
13 - 14	E. H. Pancake Clark Hall
15	RLES Files

UNIVERSITY OF VIRGINIA

School of Engineering and Applied Science

The University of Virginia's School of Engineering and Applied Science has an undergraduate enrollment of approximately 1,000 students with a graduate enrollment of 350. There are approximately 120 faculty members, a majority of whom conduct research in addition to teaching.

Research is an integral part of the educational program and interests parallel academic specialties. These range from the classical engineering departments of Chemical, Civil, Electrical, and Mechanical to departments of Biomedical Engineering, Engineering Science and Systems, Materials Science, Nuclear Engineering, and Applied Mathematics and Computer Science. In addition to these departments, there are interdepartmental groups in the areas of Automatic Controls and Applied Mechanics. All departments offer the doctorate; the Biomedical and Materials Science Departments grant only graduate degrees.

The School of Engineering and Applied Science is an integral part of the University (approximately 1,400 full-time faculty with a total enrollment of about 14,000 full-time students), which also has professional schools of Architecture, Law, Medicine, Commerce, and Business Administration. In addition, the College of Arts and Sciences houses departments of Mathematics, Physics, Chemistry and others relevant to the engineering research program. This University community provides opportunities for interdisciplinary work in pursuit of the basic goals of education, research, and public service.